GEAP-22201
UC-78
September 1982

GEAP--22201

DE83 003103

FLOW-INDUCED VIBRATION CHARACTERISTICS OF BWR/6-238 JET PUMPS

J. F. Schardt

Reviewed: M. R. Torres
M. R. Torres, Manager
FIV Experiments

Reviewed: C. H. Solanas
C. H. Solanas, Manager
Hydrodynamic and Mechanical
Components

Approved: E. Kiss
E. Kiss, Manager
Applied Mechanics

Prepared for the
U.S. Department of Energy
Prime Contract DE-AC02-77ET34209-~~25~~

NUCLEAR ENGINEERING DIVISION • GENERAL ELECTRIC COMPANY
SAN JOSE, CALIFORNIA 95125

GENERAL ELECTRIC

CONTENTS

ILLUSTRATIONS

ILLUSTATIONS (Continued)

ILLUSTATIONS (Continued)

ILLUSTATIONS (Continued)

ABSTRACT

Four prototype BWR/6-238 jet pumps (two jet pump pairs) were tested to determine their flow-induced vibration (FIV) characteristics in the High Flow Hydraulic Facility, $(HF)^2$, over the period June to September 1978. Tests consisted of operating the jet pumps, which were heavily instrumented with accelerometers, pressure transducers and strain gages, at the design operating condition, as well as at numerous off-design drive flows and M-ratios, and at temperatures between 70°F and 180°F and at 455 psig. Results were combined with those from past jet pump tests to predict the response at reactor temperature (533°F). Major conclusions reached related to the BWR/6-238 jet pump are:

- The FIV response at design operating conditions is well within the BWR/6-238 preoperational and startup vibration criteria. Consequently, design margin has been confirmed.

- The FIV response increases with increasing drive flow (related to the drive flow squared) and with decreasing M-ratio.

- The FIV response typically increases with increasing fluid temperature.

ACKNOWLEDGMENTS

I would like to express my appreciation to those who worked with me to make this test program a success:

- Larry Dorfman, for managing the acquisition of much of the test data.

- Bill Weed, Mike Stone and Carroll Brekke, for their initiative, persistence and quality workmanship in preparing the hardware and conducting the test.

- Ray Manyik, Mike Racick and John Feeney, for their patience and dilligence in supporting the $(HF)^2$ computer system.

- Mark DeCoster and Martin Torres, for their counsel and support.

1. INTRODUCTION

The jet pump assembly (Figure 1-1) is part of the boiling water reactor (BWR) recirculation system. Its purpose is to circulate the required coolant through the reactor core. Having no moving parts, it is composed of three components: (1) a riser (one per two jet pumps); (2) a mixer which is mechanically attached to the riser; and (3) a diffuser which mates with the mixer at a thermal expansion slip-fit joint. Approximately one-third of the core flow is taken from the vessel, pumped through a piping-manifold system and returned to the vessel via the risers, where it is discharged from the jet pump nozzles at high velocity into the jet pump mixer throat. Through a process of momentum exchange, the nozzle flow entrains surrounding water into the jet pump mixer throat, where the two flows mix and then diffuse, to be discharged into the lower core plenum.

The jet pump assembly was first incorporated in the Dresden 2 (BWR/2) plant design, which began operation in 1970 and since has been a standard part of the General Electric BWR. Design changes have been minor, generally aimed at improving hydraulic efficiency, and the jet pump remains relatively unchanged in appearance. The assembly possesses several mechanical-hydraulic features which are known to be potential sources of high-level flow-induced vibration (FIV) (e.g., high velocity flow within pipes, high velocity jets into a confined region, mixing of a high velocity fluid and entrained surrounding fluid, and slip-joint leakage flow). Because of the extreme complexity of these characteristics, with associated forces which are, in some instances, highly nonlinear, it has been virtually impossible to predict the FIV response of the jet pumps using available state-of-the-art analytical techniques or even scale model tests. Consequently, General Electric has elected to evaluate each new jet pump design by first performing an extensive series of FIV tests of a full-size prototype in a special test facility, followed by in-reactor monitoring of the assembly during initial plant startup. Besides qualifying the design, these tests have contributed to an ever-increasing understanding of the key parameters which govern the FIV response of jet pumps.

Much has been learned about the character of the jet pump FIV as a result of the past nine years of testing, and this knowledge is being applied to insure its reliable operation in the reactor. Results have shown the response to be governed primarily by the jet pump's flexibility, the mixer-diffuser

slip-joint geometry and the leakage flow rate out of the slip joint. For most designs under normal installation and operating conditions, the response is low-level random, well within the vibration criteria. However, when the jet pumps are improperly installed (causing the structural flexibility to increase) or when they are operating at conditions which result in high differential pressure across the slip joint (and consequent high leakage flow), the response can increase dramatically, generally taking a purely sinusoidal character. The most effective means known of preventing high-level vibrations are: (1) to insure proper installation; (2) in some instances, to avoid certain atypical operating conditions; and (3) if necessary, reduce leakage flow through the slip joint by use of some type of flow restriction, such as a labyrinth seal or piston ring.

FIV tests were conducted on the BWR/6-238 jet pump over the period June through September 1978 in the new General Electric High Flow Hydraulic Facility, $(HF)^2$. This facility, the largest in the world dedicated to FIV, was primarily constructed to support the design verification and licensing of BWR/6. It has, as one of its two test stands, a 60^{o} sector, full-size model of a BWR/6-238, including two prototypical jet pump pairs. It provides a structural and flow environment almost identical to that found in a reactor, a condition not attainable in previous jet pump FIV test programs in GE's Steam-Water Test Facility at Moss Landing, California, where space limitations precluded the testing of more than one jet pump at a time.

The primary goals of the BWR/6-238 jet pump test program at $(HF)^2$ were to (1) confirm its design adequacy and operating margin and (2) support and supplement the BWR/6 preoperational and startup vibration test program. The strategy followed to reach these goals was to:

(1) perform extensive shake tests to identify the modal characteristics of the jet pumps;

(2) compare the test results from (1) with predicted frequencies and mode shapes from the finite element computer models used by the Reactor Vibration Analysis Unit of the Reactor Design Section and evaluate/verify the BWR/6 vibration model/criteria; and

(3) perform flow tests over a wide range of drive flow, M-ratio, and temperature conditions to identify the FIV response characteristics of the jet pumps. The BWR/6 vibration criteria were applied to the flow test data to establish the design's adequacy, as well as to assess and/or confirm the criteria's methodology.

This report documents the flow test results (item 3 above). Shake test results (items 1 and 2 above) were documented in NEDE-24198, "Modal Characteristics of a BWR/6-238 Jet Pump".

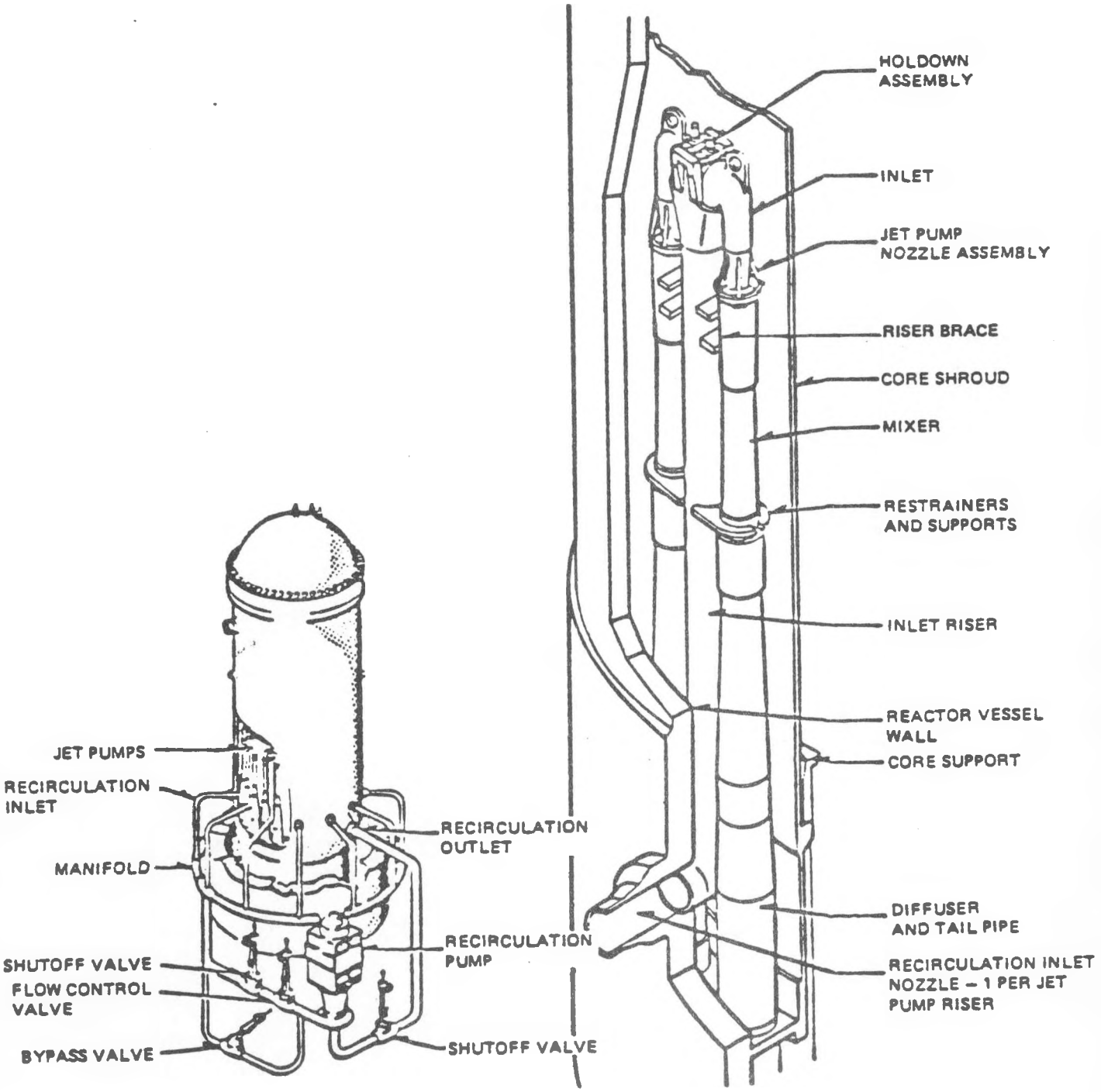

Figure 1-1. Jet Pump Recirculation System

2. TEST DESCRIPTION

The flow test program consisted of exercising the jet pumps over a wide range of hydraulic conditions while monitoring and recording key vibration parameters, such as accelerations, strains and dynamic wall pressures. The hydraulic conditions which were varied include drive flow, M-ratio (suction-to-drive flow ratio) and temperature. Drive flow and M-ratio were varied, since these are known to have a direct effect on the vibration intensity of the jet pump and are typically used to establish its vibration characteristics. The water temperature was varied to determine its effect on the vibration response, providing a means of assessing the validity of performing jet pump FIV tests at 180°F, the maximum capability of $(HF)^2$, as opposed to the 533°F at reactor operating conditions.

The test points covered are listed in Tables A-1 and A-2, Table A-1 describing the first phase of the test program and Table A-2 the second. The two phases, each covering essentially the same hydraulic range, were required because the number of vibration sensors (210) exceeded the $(HF)^2$ data acquisition capacity (160). Phase A1 contains many more test points, since it was during this period that $(HF)^2$ underwent its initial shakedown, with various test facility problems surfacing which made the repeat of some tests necessary. The ranges of hydraulic conditions investigated were as follows:

(1) $0.5 < \text{M-ratio} < 2.9$;

(2) $25\% \leq \text{Drive Flow} \leq 125\%$ (of Design Operating); and

(3) $70^{\circ}\text{F} \leq \text{Water Temperature} \leq 180^{\circ}\text{F}$.

2.1 TEST CONFIGURATION

2.1.1 Jet Pump Hardware

The flow tests were performed on prototypical BWR/6-238 jet pumps in the $(HF)^2$ 60° sector model (Figure 2-1). The jet pump assemblies had been modified to allow bolting (rather than welding) of the diffusers, riser braces and risers to the simulated reactor vessel so they could be removed and

instrumented prior to testing. These modifications were carefully designed and analyzed to insure they adequately simulate in-plant prototypical conditions.

2.1.2 Jet Pump Installation

The jet pumps were installed to comply with the BWR/6 installation specifications outlined in Drawing 762E835 (Installation Kit Jet Pump). This includes the establishing of a 2-mil minimum gap between mixer and diffuser at the slip-joint interface, 3-point contact at the mixer belly band, and a 30,500-lb preload on the beam bolt. The installation procedure followed, with minor exceptions, is the CBIN S-CN508 Jet Pump Assembly Instructions (GE Document VPF 5228-003-3). Supervision and verification of the diffuser installations were provided by CBIN reactor component installation personnel. Mixers were installed and verified by NTD Test Operations personnel. The bolts holding the diffusers, risers and riser braces in place were carefully preloaded to prescribed levels to simulate welded conditions.

The as-installed mixer-diffuser slip-joint gap configuration for each jet pump is shown in Figure 2-2. The average gap was approximately 5 mils and the minimum was 3 mils. It should be noted that for Jet Pumps 1 and 2, these gaps were established prior to shake tests and were lost in the radial direction during the shake test program (Jet Pumps 3 and 4 were not involved in shake tests). No adjustments were made upon the completion of the shake tests, so Jet Pumps 1 and 2 began the flow tests with no slip-joint radial gap.

One deviation from the normal installation procedure which should be noted is that the adjusting screws, which, along with the wedge, hold the mixer in position relative to the riser, were not tack welded to the riser bracket to prevent their backing out. Rather, to accommodate jet pump disassembly, they were held in place by rods welded to the set screw head as well as to the bracket (Figure 2-3). This greatly facilitated removal of the jet pumps but also introduced less constraint to the backing off of the set screws.

2.2 FLOW TEST ASSEMBLY

The hydraulic loop assembly for $(HF)^2$ is shown in Figure 2-4. Six multistage vertical turbine pumps, connected to 1250 hp vertical induction motors by variable speed drives, supply water to two headers which connect to the two risers (each header feeds one jet pump pair). Each pump is individually controlled, allowing for a wide range of drive flow conditions. For this program, header flows in excess of 10,500 gpm were achieved (approximately 125% of design operating conditions).

The facility can be operated at temperatures between 40°F and 180°F. The pump work is used to heat the water (vessel and piping are heavily insulated to prevent heat loss) and evaporative cooling towers are used to cool it. A constant temperature is maintained by continuously extracting, cooling and reinjecting a slipstream from the main return header. For this program, tests were performed at 70°F, 125°F and 180°F.

To prevent cavitation, the loop was pressurized to 455 psi.

2.3 DATA ACQUISITION AND ANALYSIS

The system used to measure, store and analyze the FIV data is outlined in Figure 2-5. Each of the elements is described below.

2.3.1 Vibration Sensors

The vibration sensors utilized in this test program include accelerometers, pressure transducers and strain gages. Their selection and mounting were based on the following criteria:

(1) match the instrumentation planned for the BWR/6 preoperational and startup vibration program;

(2) identify the predominant mode shapes of a jet pump pair;

(3) characterize the wall pressure fluctuations (forces) in a jet pump; and

(4) Identify the FIV responses of the jet pumps pairs as a function of flow conditions.

Details related to each sensor type are described below.

2.3.1.1 Accelerometers

Accelerometers were installed on the two jet pump pairs at the locations shown in Figures 2-6 and 2-7. The purpose of the large number of accelerometers on Jet Pumps 1 and 2 was to identify radial, tangential and axial modes during the shake test segment of the test program. These locations were selected based on the mode shapes reported in NEDE-23840 ("Vibration Analysis for the Reactor Internals of BWR/6-238 Plants"), which were generated by Reactor Design to establish plant criteria. The accelerometers on Jet Pumps 3 and 4 were located to monitor the maximum radial and tangential responses of the jet pumps, as well as the relative motion between the mixer and diffuser at the slip joint.

The accelerometers used are uniaxial, biaxial and triaxial piezoresistive devices manufactured by Entran Devices, Inc. The measuring element is a cantilever beam with four strain gages mounted on it to measure beam bending in a Wheatstone bridge electrical configuration. In general, the sensors are damped to 70% of critical. They are designed to measure accelerations between 0.01 and 200g's over a frequency range of DC to 1000 Hz. They are hermetically sealed and the leads are protected by 0.125-in.-diameter stainless steel hardline casings, which are capacitance welded to the jet pumps with stainless steel straps as they are routed to the vessel instrument parts.

2.3.1.2 Pressure Transducers

Dynamic pressure transducers were installed on all four jet pumps at the locations shown in Figures 2-8, 2-9, and 2-10. The philosophy behind this instrument plan is provided below:

(1) Jet Pump 2 was heavily instrumented with pressure sensors to measure the pressure fluctuations applied to the inner surface of the mixer and diffuser due to the combined drive and suction flows. The transducers are located on the mixer at distances 0.5 D_M, D_M, 2 D_M, 3 D_M,

5 D_M and 8 D_M from the suction flow inlet (D_M = mixer inlet I.D.) and on the diffuser at the distances D_d and 4 D_d from the top of the diffuser, just below the collar (D_d = I.D. at top of diffuser). The greatest concentration of sensors is located just downstream from the mixer inlet. It is here that the most unsteady mixing between suction and drive flow occurs, resulting in high turbulence intensities and consequent time-varying pressure forces on the mixer wall. Further down stream (approximately five mixer diameters from the mixer inlet), the fluctuating pressures are expected to be more homogeneous and much less intense.

At each axial position chosen for pressure measurements, four pressure sensors were mounted flush with the inner wall: two diametrically opposite to each other in the radial direction and two diametrically opposite in the tangential direction. By subtracting signals from diametrically opposite sensors, the far field noise is removed. In addition, it provides information useful in estimating the net radial or tangential force being applied at that axial location.

(2) Jet Pump 3's mixer and diffuser were instrumented with an array of pressure sensors (Figure 2-9) in order to examine the spatial correlation of the presssure field both axially and circumferentially. Sensor locations were chosen to determine the spatial correlation at distances of 1D, 2D, 4D and 8D, both axially and circumferentially. A value of D equal to 0.75 in. was chosen as the smallest practical distance, considering the physical size of the pressure sensors themselves. The spatial correlation was expected to be significant only at separation distances less than jet pump inlet diameter (6.4 in.).

(3) All four jet pumps were instrumented with pressure transducers on the diffusers at the mixer-diffuser slip joint. The objective was to better understand and to characterize the pressures in the slip-joint region as the jet pumps make the transition from low-level to high-level vibration intensities (i.e., as the M-ratio is decreased to induce high-level vibrations).

The dynamic pressure fluctuation measurements were made with hermetically sealed flush-mounted integrated circuit piezoelectric pressure sensors manufactured by PCB Piezotronics, Inc. The sensing element is a high-sensitivity multiplate quartz crystal. A low-noise amplifier within the sensor converts the charge produced by the crystal to a low impedence analog output signal proportional to the measurand compatible with most readout instruments. The sensor is capable of measuring pressure fluctuations from 0.01 to 100 psi over a frequency range of 3 to 1000 Hz. The sensor leads are enclosed in 0.125-in. O.D. stainless steel tubes to insure watertight integrity.

2.3.1.3 Strain Gages

The two jet pump pairs were instrumented with strain gages as shown in Figure 2-11 to match the sensor location planned for the BWR/6 Startup/Preoperational Vibration Measurement Program (General Electric Document No. 22A4660). This includes gages on the diffuser tailpipe, as well as on the upper leaves of the riser brace. In addition, the riser brace for Riser A1 was instrumented to match the strain gage sensor location for many of the BWR/4 and BWR/5 plants.

The strain gages used in this test program are Models MG 128-09H-20 and SG 128-01-30 from Ailtech. These gages are fabricated with the strain-sensing element encapsulated in mineral oxide and sheathed with a stainless steel flange. The flange is capacitive welded to the jet pump. Two sizes of strain gage were used: 0.500 in. and 1.093 in. The active gage length for the two are 3/16 in. and 3/4 in., respectively, and the gage factor for both is approximately 2.

2.3.2 Loop Hydraulic Measurements

Five key hydraulic parameters were determined for each test point: (1) jet pump drive flow; (2) M-ratio; (3) water temperature; (4) slip-joint differential pressure; and (5) system pressure. They were displayed on a CRT at the beginning of the test for use in setting the test conditions, recorded during the test on the "Housekeeping" data acquisition recording tracks, and printed out in "Hard-copy" form at the completion of the test.

The M-ratio calculation was performed in the same manner as is done in operating reactors. That is, the drive flow (Q, in CFS) and the pressure differential across the diffuser pressure taps (Δp in psi) were measured and then used in the following formula:

$$M = \frac{2Q_T}{Q_1} - 1 \qquad (2\text{-}1)$$

where the total flow (Q_T) is

$$Q_T = 21.4579 \sqrt{\frac{\Delta p}{k\gamma}} \qquad (2\text{-}2)$$

and

$$K = C_1 + C_2 M + C_3 M^2 + C_4 Q_1 \qquad (2\text{-}3)$$

$$C_1 = 1.93341 \times 10^{-1}$$
$$C_2 = -1.59533 \times 10^{-2}$$
$$C_3 = 3.53583 \times 10^{-3}$$
$$C_4 = -1.95 \times 10^{-4}$$

Equation 2-3 is simply a polynomial fit to an empirically derived relationship between K and M-ratio (General Electric report NEDC-21687) and is valid only in the range of M-ratios from approximately 1.2 to 2.6. For M-ratios outside this range, the values of K at M = 1.2 or M = 2.6 were used (i.e., for $M < 1.2$, K is calculated based on M = 1.2; for $M > 2.6$, K is calculated based on M = 2.6). This does not introduce a significant error, since K is relatively constant in these regions.

2.3.3 Data Acquisition System (DAS)

Vibration signals were stored on magnetic tape for later analysis via the $(HF)^2$ computer-controlled data acquisition system. The sensors were hardwired to the patch house (a cable route of approximately 200 ft), from which they were patched into the 160 signal conditioners/amplifiers/filters in the computer room via an additional 150 ft of cable. The signal conditioners, available on 80 of the 160

DAS channels, provided excitation, bridge completion and a DC offset. The amplifier gains were adjusted automatically prior to each data acquisition to achieve the highest possible signal level without exceeding ±5.12 volts. The signals were low-pass filtered at 500 Hz to prevent alliasing problems (when the full complement of 160 channels is used, as it was in this test, 500 Hz is the maximum frequency range which can be recorded). The signals were then digitized, multiplexed and sent out to the magnetic tape in pulse code modulated (PCM) form. All pertinent information related to the data, such as test identification, amplifier gains, filter settings and sensor-amplifier locations, were automatically stored on disk for use in later analysis of the data.

Because the 210 vibration sensors used in this test program exceeded the 160 data channels available, two separate DAS plans were used. The first plan (Table B-1), used in the first phase of the test program, concentrated primarily on Jet Pumps 1 and 2, although key sensors from Jet Pumps 3 and 4 were also included. The second plan (Table B-2), utilized in the second phase of the test program, included all Jet Pumps 3 and 4 sensors, all Jet Pumps 1 and 2 pressure transducers, and key Jet Pumps 1 and 2 accelerometers.

The pertinent hydraulic conditions, which are quasistatic, were recorded on the Housekeeping side of the DAS (250 Hz frequency range), and were also printed out in hard copy at the completion of each test.

2.3.4 Data Analysis

The vibration data were analyzed using the $(HF)^2$ FASST analysis system, which is a minicomputer-controlled signal processing system capable of providing printed and plotted results in a reasonably short time and which can also provide on-line viewing of data analysis in real time. Processing of the input data is done primarily by an array processor, which has the capability of calculating Fourier transforms very quickly. The output from the analysis included time histories, power spectral densities, cross correlations, probability densities and RMS and peak values. The one-sigma error in the RMS calculations is generally not greater than 2%. This represents the square root of the sum of the squares of the one-sigma errors for the sensor, data acquisition system and data analysis system.

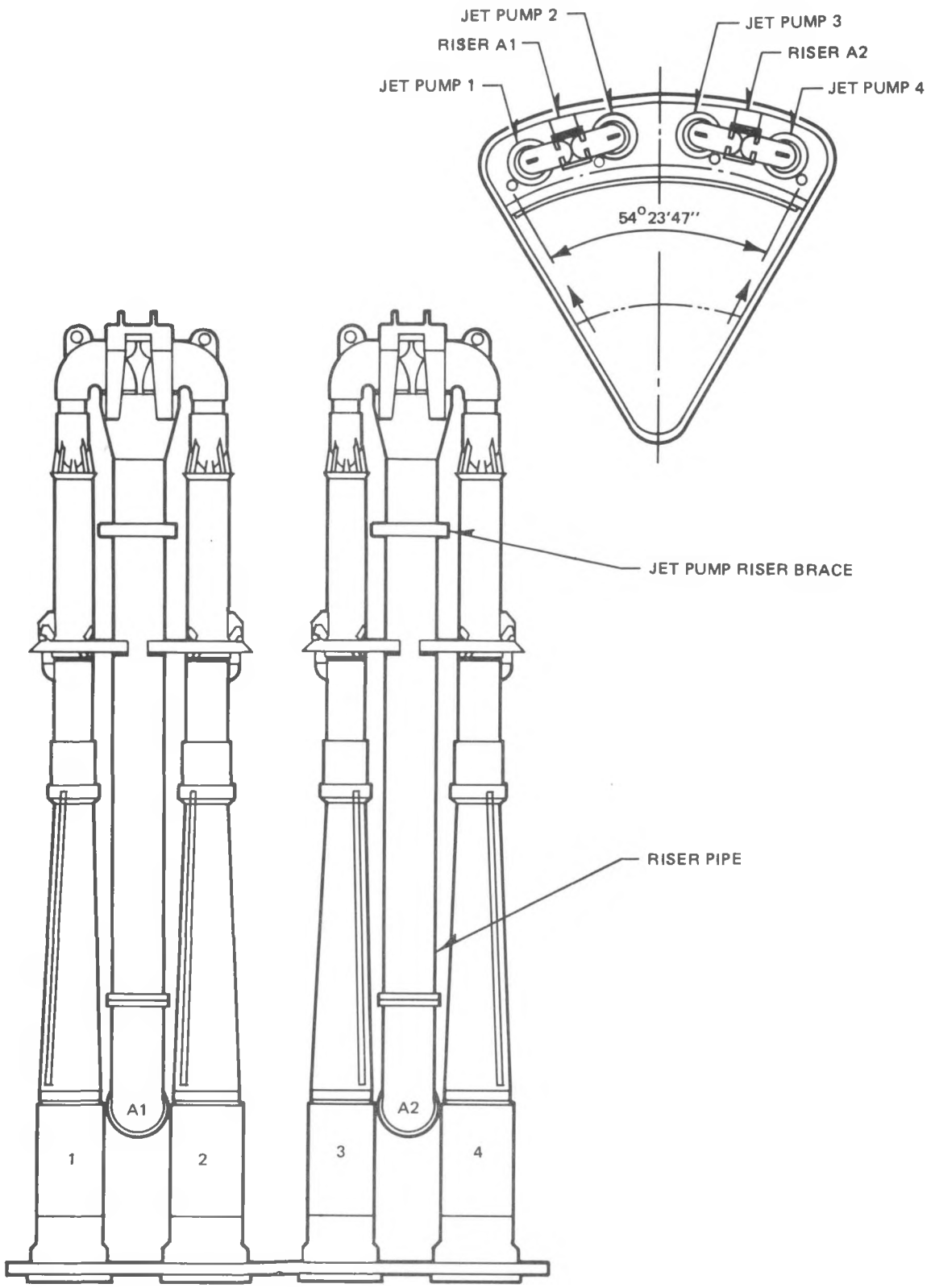

Figure 2-1. Jet Pump Pairs A and B

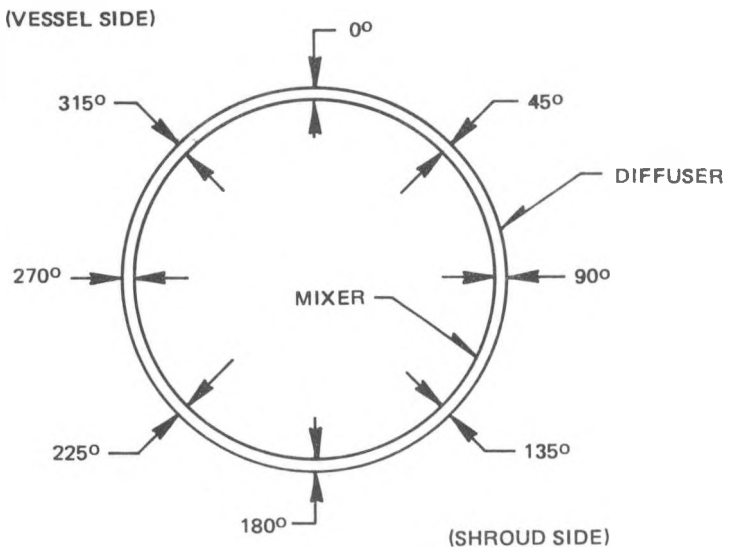

(VIEW FROM ABOVE)

AZIMUTHAL LOCATION (deg)	SLIP JOINT GAP (mils)			
JET PUMP	1	2	3	4
0	8	4	6	5
45	7	3	3	5
90	4	5	4	4
135	5	5	4	5
180	8	3	5	3
225	7	5	5	3
270	5	5	5	5
315	5	5	5	6

Figure 2-2. Jet Pump Slip Joint Gap at Installation

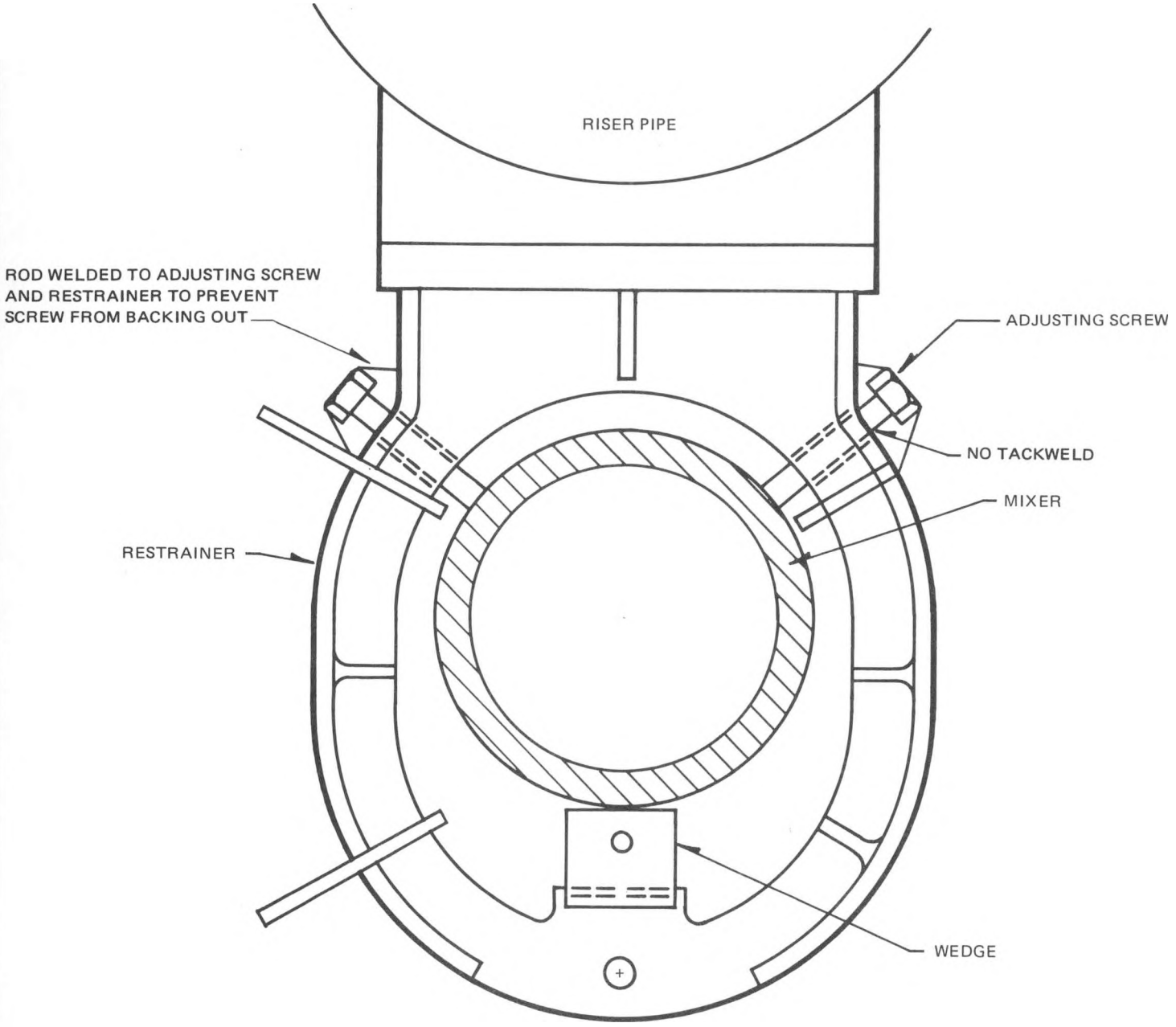

Figure 2-3. Restrainer Bracket Conditions at $(HF)^2$ - Prototypical BWR/6-238 Restrainer Bracket but Modified Adjusting Screw Tackweld Arrangement

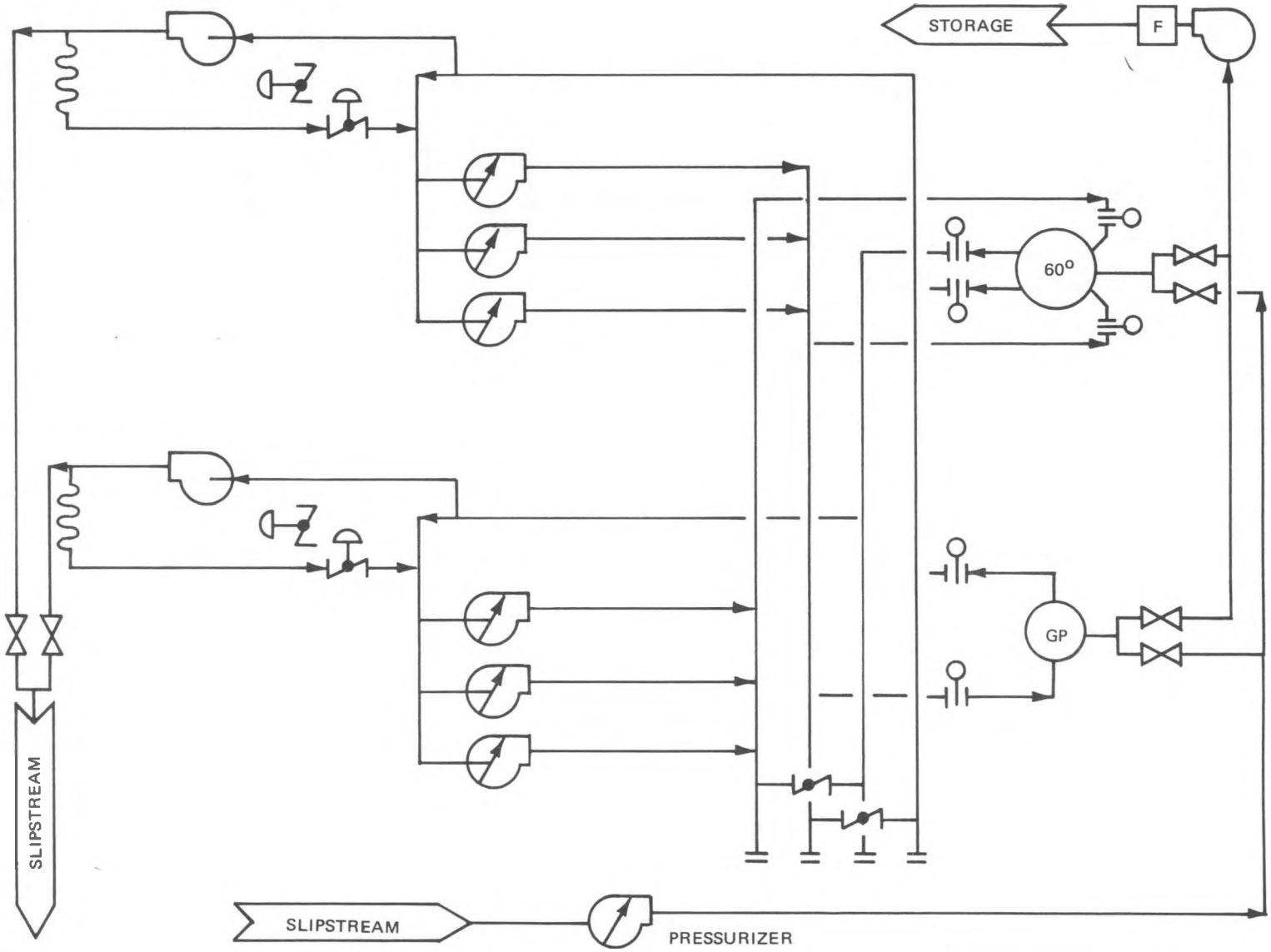

Figure 2-4. $(HF)^2$ Loop Schematic

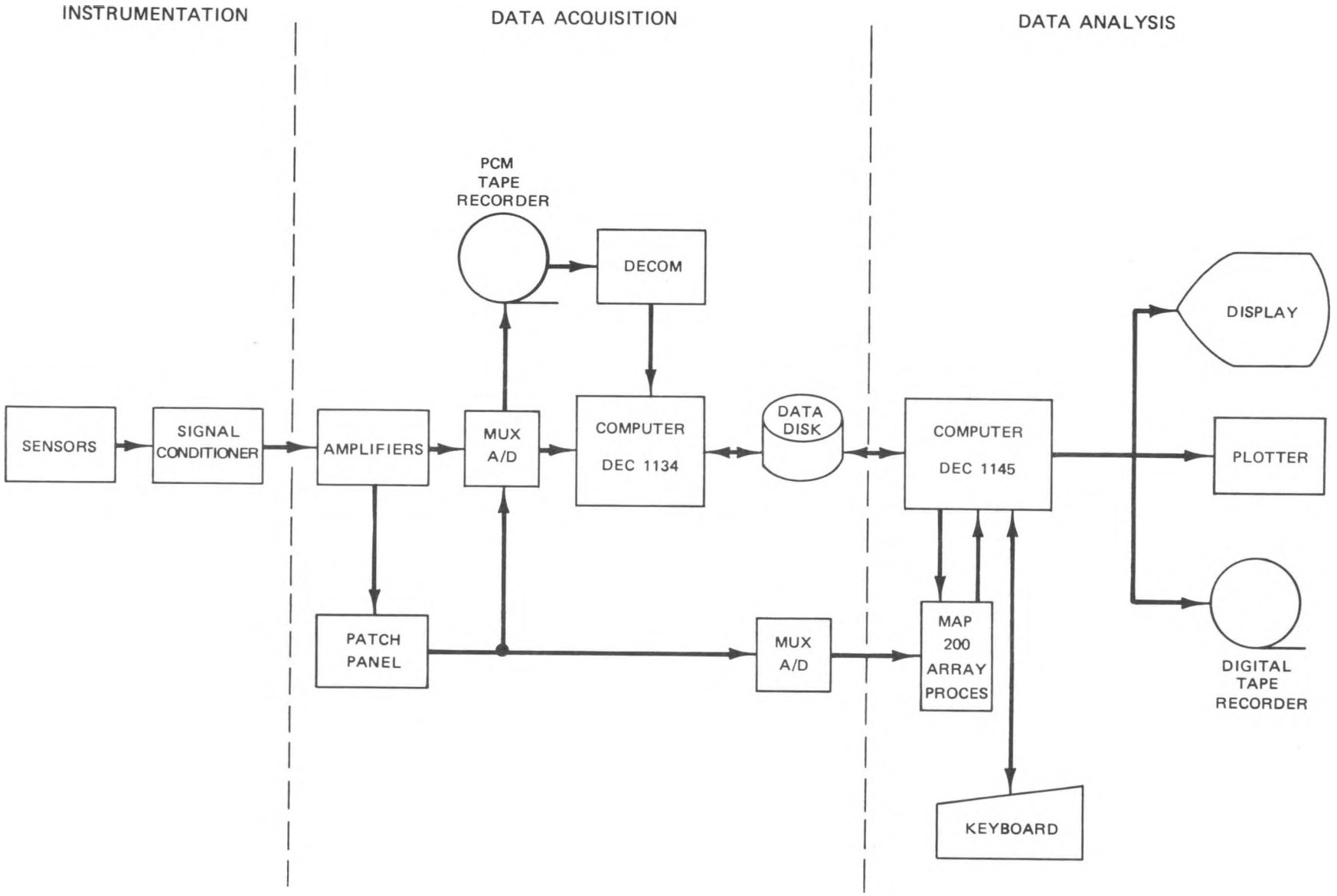

Figure 2-5. $(HF)^2$ Data System Block Diagram

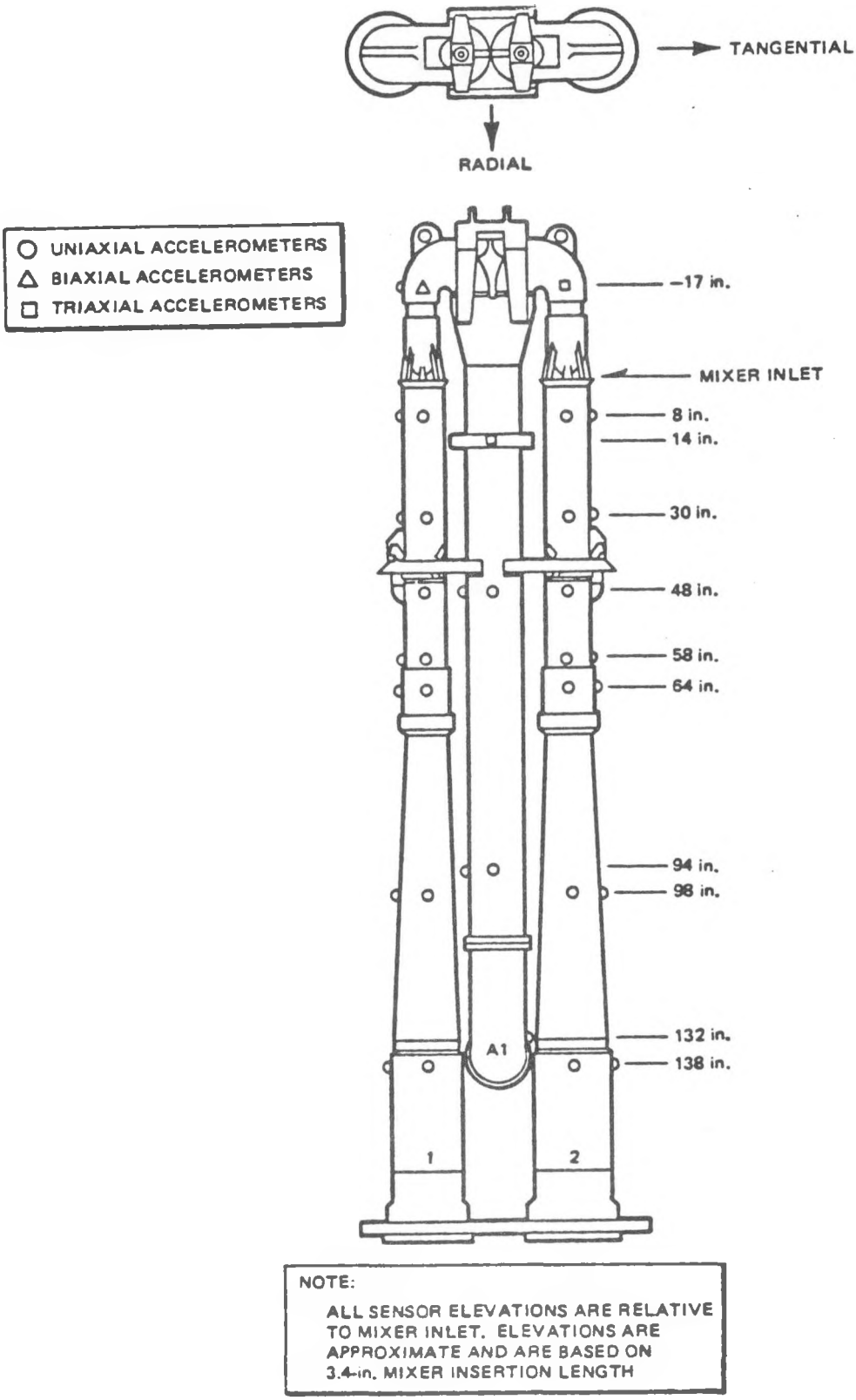

Figure 2-6. Jet Pump Pair A - Accelerometers for Mode Shapes

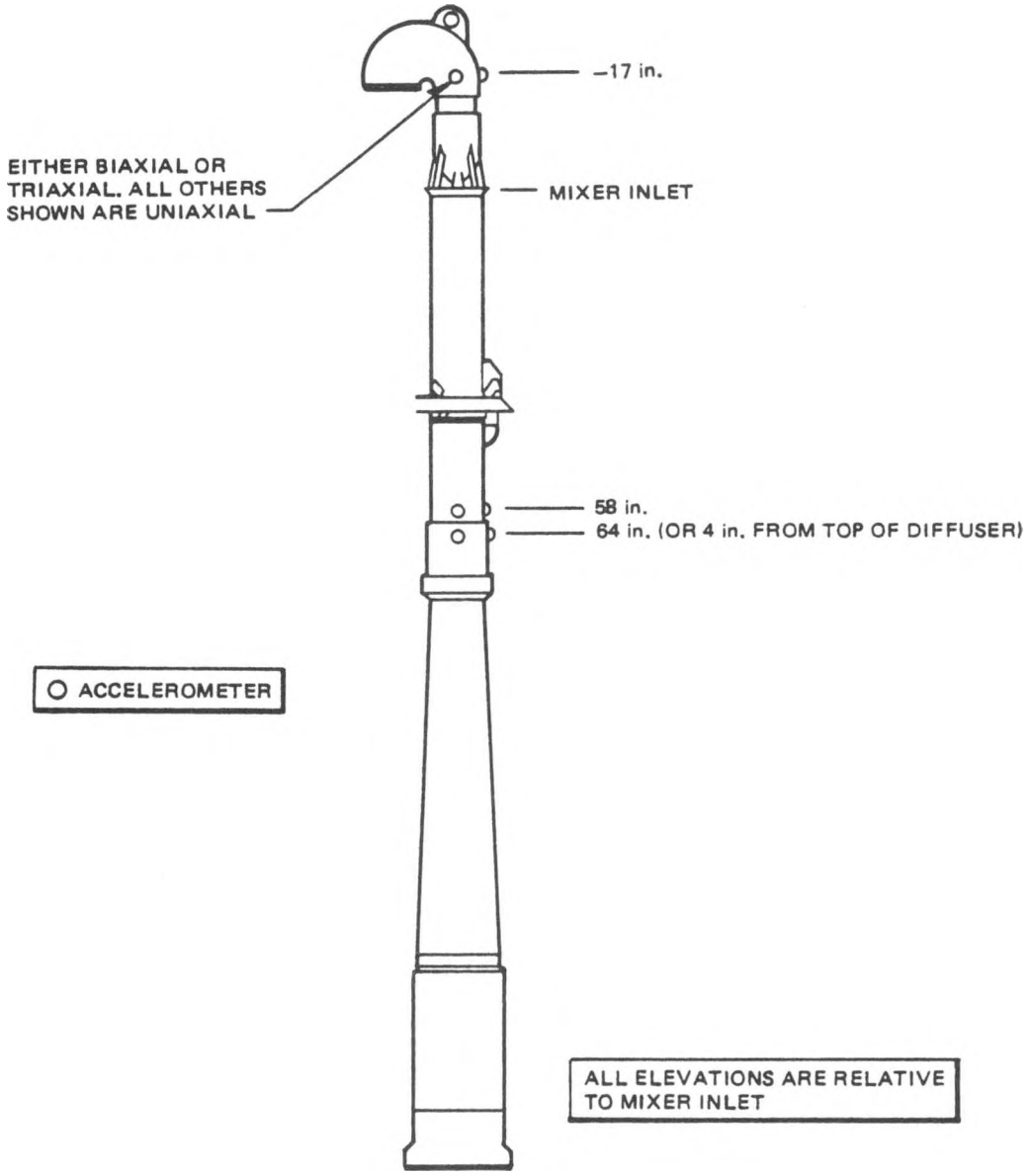

Figure 2-7. Accelerometers to Measure FIV Response (on All Jet Pumps)

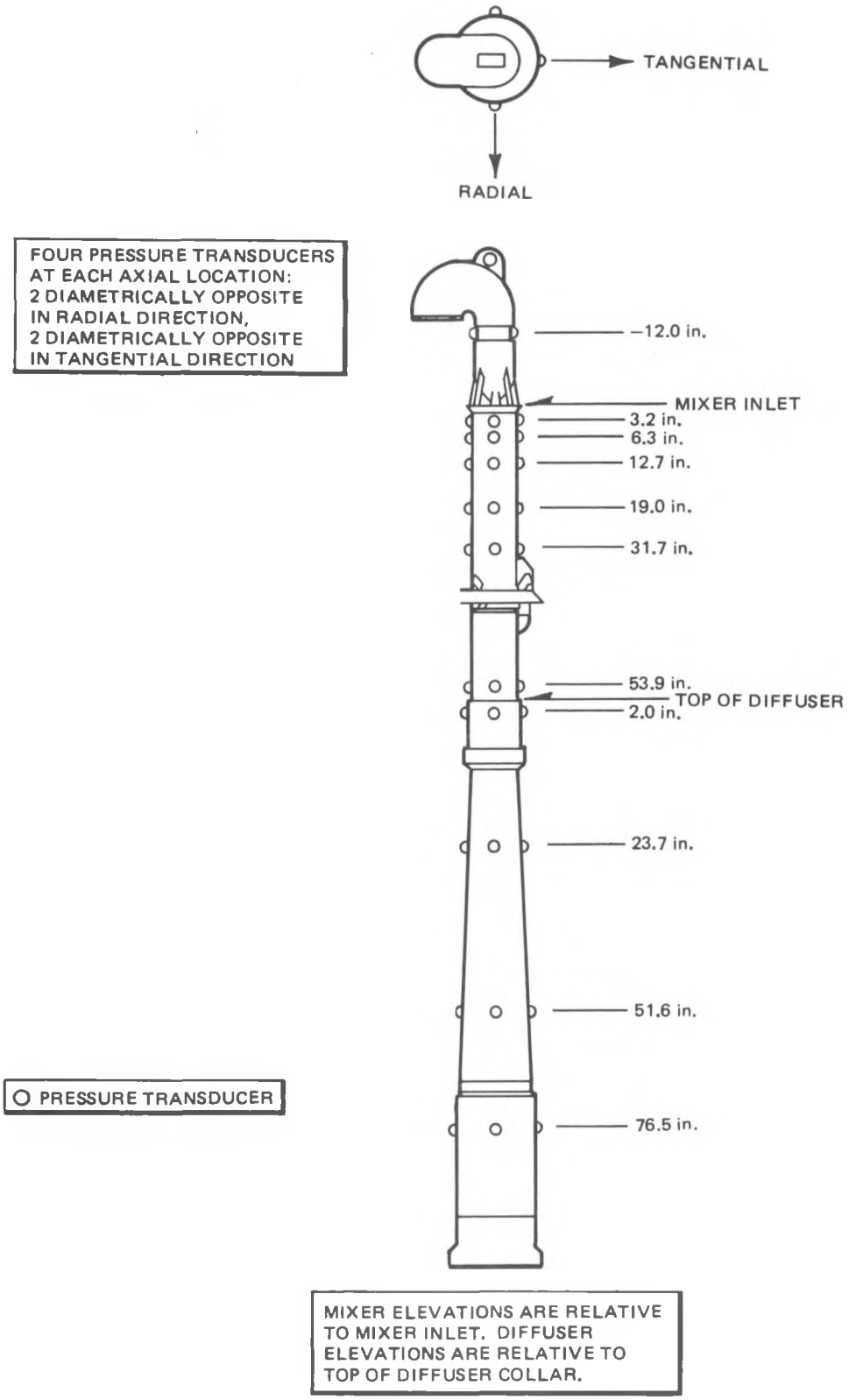

Figure 2-8. Jet Pump 2 Pressure Sensors

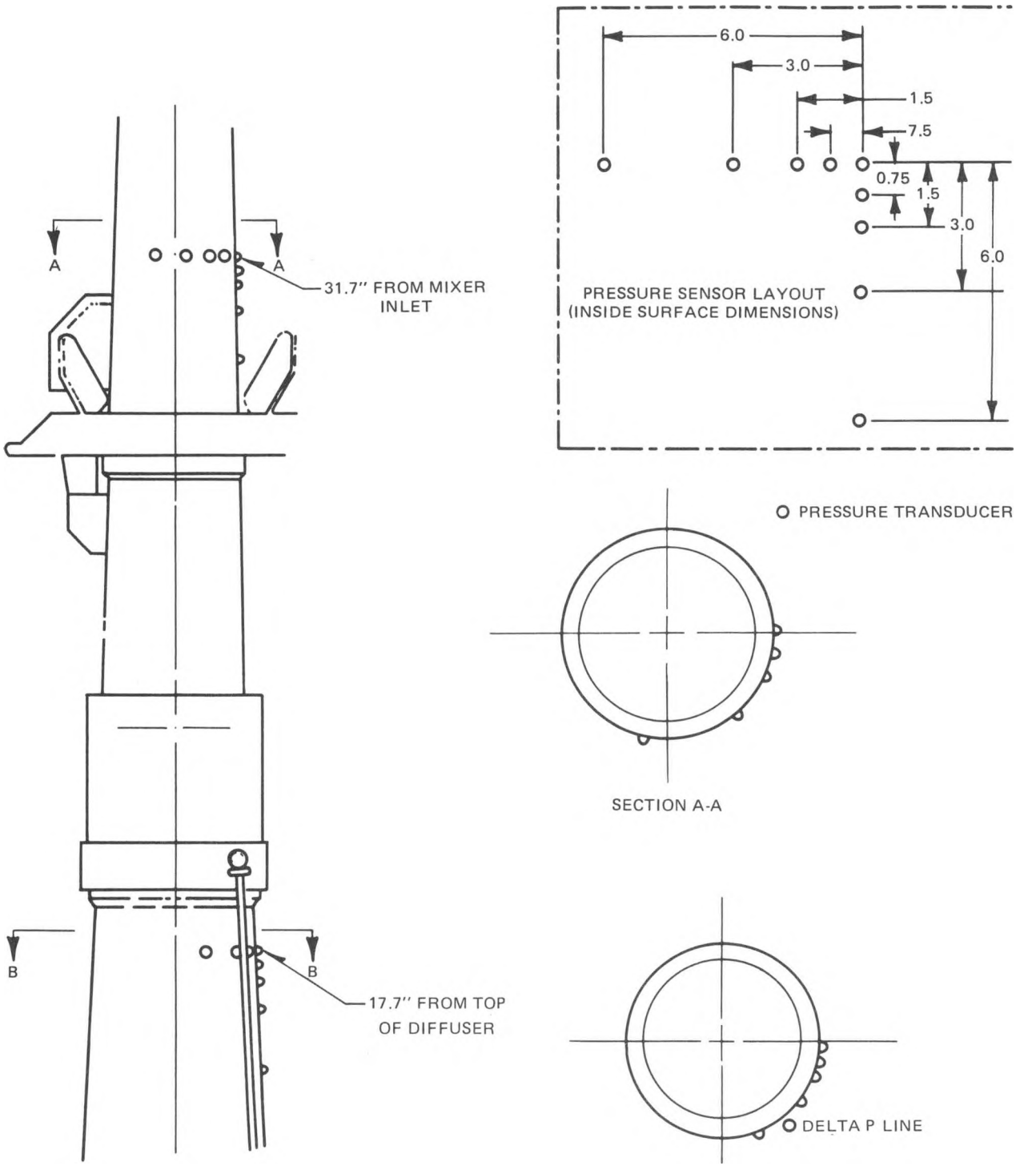

Figure 2-9. Jet Pump 3 Pressure Sensor Array (for Spatial Correlation)

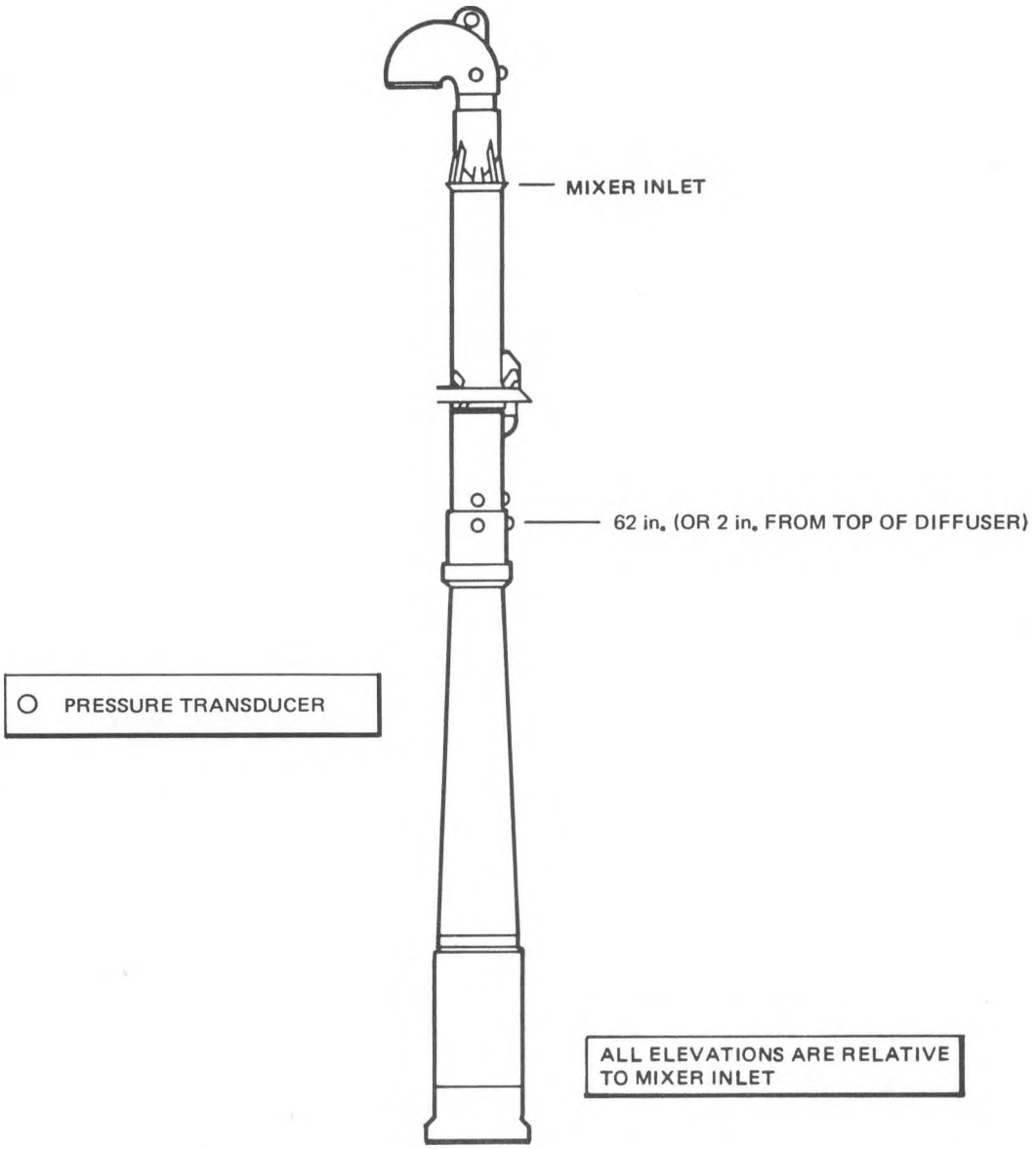

Figure 2-10. Pressure Transducers at Slip Joint to Measure Dynamic Pressures (on All Jet Pumps)

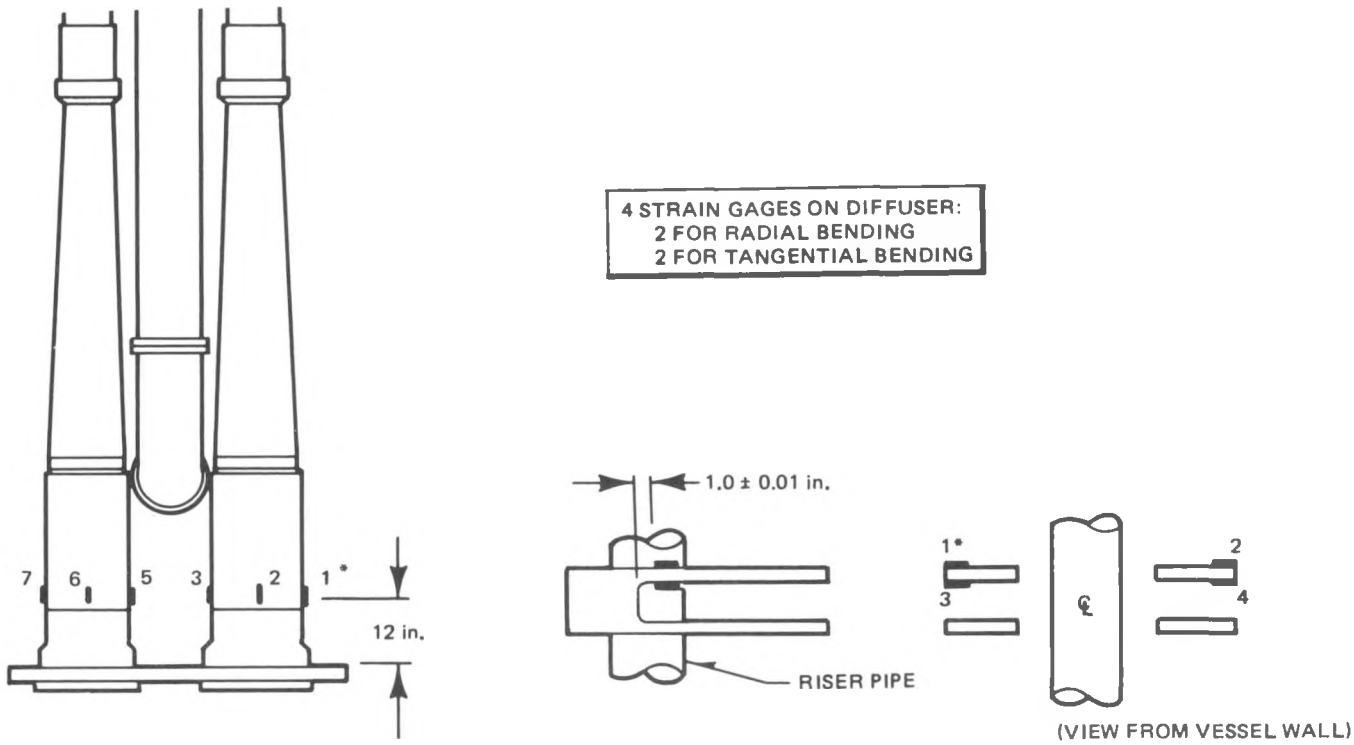

* STRAIN GAGE NUMBERING SYSTEM IS THAT REPORTED IN NEDE-23840, "VIBRATION ANALYSIS FOR THE REACTOR INTERNALS OF BWR/6 238 PLANTS" (NOTE : DIFFUSER STRAIN GAGES 4 and 8 (ON VESSEL SIDE OF TAILPIPES) ARE NOT SHOWN).

Figure 2-11. Strain Gage Locations to Satisfy Plant Preoperational and Startup Test Requirements

3. TEST RESULTS

3.1 HYDRAULIC CHARACTERISTICS

At each steady-state test condition, a complete set of thermal-hydraulic test facility data was obtained. These data, which include the parameters known to affect the vibration response of the jet pumps (e.g., drive flow, M-ratio, slip-joint pressure drop and temperature), are documented in Tables A-1 and A-2.

It was useful for later vibration analysis purposes to identify the relationship between M-ratio, drive flow, slip-joint differential pressure and temperature for the $(HF)^2$ jet pumps. This was accomplished by starting with the hypothesis, developed by L.V. LaCroix and documented in his report entitled "Flow-Induced Vibration Characteristics of BWR/6 Jet Pumps" (NEDE-24190), that the slip-joint pressure drop is related to the kinetic energy of the fluid in the jet pump:

$$SJDP = \frac{\rho V_T^2}{2} \cdot f(M) \qquad (3\text{-}1)$$

where

SJDP = slip-joint differential pressure across slip joint (psi);
ρ = fluid mass density (slugs/ft^3);
V_T = total velocity in mixer (ft/sec);
M = M-ratio (ratio of suction to drive); and
f(M) = some function of M.

Equation 3-1 may be written in terms of the volumetric flow rate, W_T:

$$SJDP = \frac{\rho (W_T)^2}{2A^2} \cdot f(M) \qquad (3\text{-}2)$$

where

W_T = total volumetric flow rate in the mixer (ft^3/sec), and
A = cross-sectional area of mixer throat.

Now noting that the total flow equals the drive plus suction flows:

$$W_T = W_D + W_S$$
$$= W_D(1 + M) \qquad (3\text{-}3)$$

where

W_D = driven flow, and
W_S = suction flow (= W_D · M).

Substituting Equation 3-3 into Equation 3-2,

$$SJDP = \frac{\rho(W_D)^2}{2A^2} (1+M)^2 \cdot f(M) \qquad (3\text{-}4)$$

For this study, it was convenient to make the following modifications to Equation 3-4:

(1) normalize the density about the 180°F water density (1.883 slugs/ft^3);

(2) normalize the drive flow about the design operating condition (564 ft^3/sec; or 4221 gpm); and

(3) bring the mixer throat area, A, into the as yet undefined function term f(M), since A will not be changing in this study.

Equation 3-4 now becomes:

$$SJDP = \rho_n W_{D_n}^2 (1+M)^2 \cdot f(M) \qquad (3\text{-}5)$$

where

$\rho_n = \rho/1.883$ (1.883 slugs/ft^3 = density at 180°F), and

$W_{D_n} = W_D/564$ (564 ft^3/sec = design operating condition volumetric drive flow).

To determine the validity of Equation 3-3 and, if possible, to evaluate the function f(M), a plot of $SJDP/\rho_n W_{D_n}^2 (1+M)^2$ versus M was generated for Jet Pump 1 for the various test points covered by the program. The data plotted in Figure 3-1 clearly show that the hydraulic data have been collapsed into a surprisingly narrow band about an exponentially decaying curve. By curve-fitting these collapsed data over the M-ratio range of interest (approximately 1 to 2.6), the relationship between slip joint pressure drop, M-ratio, density, and drive flow can be expressed as:

$$\frac{SJDP}{\rho_n W_{D_n}^2 (1+M)^2} = e^{-1.55\ (M-2.8)_{-1.55}} \qquad (3\text{-}6)$$

The fit is illustrated in Figure 3-2.

The greatest uncertainty associated with Equation 3-6 was the density term: that is, does SJDP vary linearly with density over the entire temperature range of interest (up to 532°F)? A comparison of the 70°F and 180°F data (Figure 3-1) seemed to indicate this to be correct. However, the change in density over this range is only 3%; whereas, the change from 180°F to 532°F is 30%, making the application of this formula to reactor temperature without further verification risky. To resolve this, a study was made of the jet pump hydraulic data reported in Tables 5-2 and 5-5 of NEDE-24190. These data, which include both 180°F and 532°F conditions, were plotted in the same manner as was done with the $(HF)^2$ jet pump data: $SJDP/\rho_n W_{D_n}^2 (1+M)^2$ versus M. The results, plotted in Figure 3-3, show that the density term collapses the data, thus proving that the slip joint pressure drop is linearly related to the density, as Equation 3-6 indicates.

3.2 FIV CHARACTERISTICS

Most of the FIV tests were performed at 180°F, since this is the maximum capability of $(HF)^2$ and, therefore, comes as close as possible to simulating reactor temperature conditions (532°F). Tests performed at lower temperatures were designed primarily to determine the effects of temperature on the FIV response of the jet pumps. Results presented in this report will be for the 180°F conditions, except when addressing the issue of temperature effects.

3.2.1 FIV Response at Design Operating Drive Flow and M-Ratio

Vibration data were acquired at the design operating conditions volumetric drive flow (4221 gpm) and M-ratio (2.26). The typical vibration response is illustrated by the acceleration time history and power spectral density (PSD) plots shown in Figures 3-4 through 3-7. It can be characterized as low-level random ($<0.25g_{rms}$), with the energy spread over a 20-200 Hz frequency range and spectral peaks situated at the natural frequencies. The vibration amplitudes were normally greatest at the mixer-diffuser slip joint and at the top of the mixer elbow.

Typical strain time history and PSD plots for the strain gages located on the riser brace leaves and diffuser tailpipes in accordance with the BWR/6-238 plant preoperational and startup vibration program's instrumentation plan are shown in Figures 3-8 through 3-11. The maximum peak strains observed were 18 μin./in. for the riser brace and 6 μin./in. for the diffuser, induced primarily by jet pump vibration in the first and second tangential modes. These strain levels are approximately 10% of the BWR/6-238 vibration criteria.

3.2.2 Drive Flow Effects

Tests were performed to determine the relationship between mixer drive flow and the FIV response of the jet pumps. The jet pumps were first set at end-of-life design hydraulic conditions (M-ratio of 2.26 at 4221 gpm) by varying the 24 core plate valves which provide the required resistance (simulate core pressure drop). Now, leaving the core valves unchanged, the drive flow was set at a variety of levels from a minimum of 25% of design operating conditions to a maximum of 125% and vibration data recorded. Results are summarized in Figures 3-15 and 3-16. The vibration responses were found to vary approximately with the square of the drive flow. The magnitudes of the mixer and diffuser responses were similar up to about 80% drive flow, beyond which the mixer response increased at a greater rate. At 125% drive flow, the average RMS acceleration response of the mixers was 35% higher than that of the diffusers.

Jet Pump 2 mixer and diffuser slip-joint acceleration time histories and PSDs are shown in Figures 3-17 through 3-24 for drive flows of 50, 75, 100 and 125%, respectively. These plots, which typify the responses of the four jet pumps, show the vibrations under all drive flow conditions tested to be low-level

random ($0.5g_{rms}$) with spectral peaks in evidence at some of the natural frequencies. The modes most highly excited vary with the level of drive flow.

3.2.3 M-Ratio Effects

Tests were performed to determine the effects of M-ratio on the jet pump vibration response. The tests consisted of setting the drive flow to specified values (25, 50, 75, 100, and 125% of design operating conditions) and varying the M-ratio about the end-of-life design operating condition. M-ratio changes were accomplished by opening or closing the 24 core valves, thus changing the core plate resistance and consequently the back pressure. The typical sequence followed was to begin with the maximum M-ratio condition achievable (all valves open) and slowly shut valves, one at a time, reducing the M-ratio to prescribed values, where vibration data were then recorded. This step-by-step reduction was continued until the vibration response became excessive ($6g_{rms}$), at which time the test was terminated, the core valves reopened and a new drive flow condition established.

The relationship between vibration response and M-ratio was found to be similar to that exhibited in previous jet pump FIV test programs: low-level random at high M-ratios and high-level periodic at low M-ratios. Surprisingly, the transition from low to high-level vibrations was observed to change during the course of the test program, as illustrated in the Jet Pump 2 mixer radial response plot shown in Figure 3-25. In the early stages, the response varied gradually and uniformly with decreasing M-ratio, making a smooth transition into the high-level vibration region. However, test points recorded midway into the program (after approximately 100 hours of operation) revealed a much more rapid transition to high-level vibration (in some cases, almost that of a step change), with the transition inception occurring at significantly lower M-ratios. This same "rapid transition" behavior was also observed late in the test program and therefore is assumed to be characteristic of these jet pumps after initial "shakedown." (Making the assumption that jet pumps operating in a reactor rapidly reach this shakedown condition, the $(HF)^2$ jet pumps were evaluated using the post-shakedown data only, although the major conclusions would have been unchanged if the pre-shakedown data had been used.)

The effect of M-ratio on the vibration response is illustrated by the PSD plots of the Jet Pump 2 mixer radial acceleration at 100% drive flow, recorded midway through the test program (Figure 3-26). At M-ratios above 2.0, the response,

controlled in this region primarily by the mixer velocity, increased with increasing M-ratio (though never exceeding a magnitude of $0.3g_{rms}$). It is typical of the vibration response of complex structures responding to turbulent buffeting of the fluid, being wide-band random (approximately 30 to 300Hz), with spectral peaks at the natural frequencies.

At low M-ratios, the response (now governed primarily by the mixer-diffuser SJDP) increased dramatically with decreasing M-ratio, rapidly reaching levels one to two orders-of-magnitude above those observed in the high M-ratio region. Its energy tended to concentrate in an increasingly narrow frequency band, with major spectral peaks first appearing in the 100-120 Hz range and, at lower M-ratios, in the 50-60 Hz and 200-240 Hz ranges. It can be generally characterized as sinusoidal with random noise superimposed.

The relationship between drive flow and the M-ratio at which transition to high-level vibration occurs is illustrated in Figure 3-27. As drive flow increased, the M-ratio inception to high-level vibration also increased from about 1.5 at 75% to 1.9 at 100% to 2.1 at 125% drive flow. No transition was observed at 25% or 50% drive flow over the M-ratios covered by the test program (as low as M = 0.65).

3.2.4 Slip Joint Differential Pressure Effects

The relationship between Slip Joint Differential Pressure (JDP), which was monitored and recorded for each jet pump throughout the test program, and jet pump vibration response is illustrated by the Jet Pumps 1 and 2 response plots of Figures 3-28 and 3-29. These figures show that, for the 180°F water temperature used during most of the test program, the vibration response was low-level random up to SJDPs of about 25 psi, beyond which it rapidly transformed to high-level sinusoidal motion. While the inception appeared to be independent of drive flow over the range tested (25 to 125% of design operating condition), the rate of transition (i.e., slope of the response-SJDP curve immediately after inception) was inversely related, being highest at 75% drive flow and lowest at 125% drive flow (SJDPs for the 25% and 50% drive flow tests did not reach the 25 psi inception point). At sufficiently high SJDPs, the response seemed to saturate (flatten out), the levels reached being directly related to the drive flow (highest drive flows produced highest acceleration amplitudes at saturation).

Figure 3-30 shows the vibration response versus SJDP curves for Jet Pumps 1 and 2 at 100% drive flow and 70°F water temperature. While the shapes of the curves are similar to those at 180°F (Figures 3-28 and 3-29), the SJDP at which transition to high-level vibration commenced has increased to approximately 35 psi.

3.2.5 Application of Test Results to Reactor Conditions

The curves mentioned in Subsection 3.2.4 clearly demonstrate the significant effect temperature has on the vibration response and, consequently, the need for extrapolating the $(HF)^2$ test results to reactor temperature (532°F) in order to properly evaluate the BWR/6-238 jet pump. This was accomplished through the following procedure:

(1) Using the 70°F and 180°F $(HF)^2$ data, identify a vibration intensity limit (acceleration in gs rms), beyond which the vibration response is considered to be undesirable.

(2) Determine the SJDPs at 70°F and 180°F required to reach this limit.

(3) Extrapolate the SJDPs identified in Step 2 to reactor temperature.

(4) Verify the Step 3 result using BWR/6-251 jet pump vibration data acquired at 532°F during Moss Landing hydraulic performance tests (the BWR/6-251 jet pump is very similar geometrically to the BWR/6-238; therefore, the vibration-hydraulic characteristics should be similar).

(5) Using the extrapolated 532°F SJDP, evaluate the vibration performance of the BWR/6-238 jet pump at reactor conditions (i.e., compare extrapolated SJDP criterion with plant operating SJDP).

The vibration intensity limit was established by first plotting the Jet Pump 1 mixer slip joint total RMS acceleration response at 100% drive flow as a function of SJDP for the 70°F and 180°F $(HF)^2$ conditions (Figure 3-31). The total RMS acceleration response at the mixer slip joint is defined as:

$$A_{rms} = (A^2_{rad_{rms}} + A^2_{tan_{rms}})^{1/2}$$

where

$A_{rad_{rms}}$ = root mean square of the radial acceleration at the mixer slip joint, and

$A_{tan_{rms}}$ = root mean square of the tangential acceleration at the mixer slip joint.

Jet Pump 1 was chosen, since it had accelerometers operational throughout the 70°F and 180°F test series at locations similar to those in the BWR/6-251 test program at Moss Landing, thus making direct comparison with Moss Landing data possible.

The vibration intensity limit was then chosen to be 1g total rms acceleration at the mixer slip joint. The reason for limiting the response to 1g rms is that, while the strains are well within the BWR/6-238 Plant Preoperational and Startup Vibration criteria (approximately 50% of the allowable), the jet pumps are operating beyond the low-level vibration region of the Response-SJDP curve (Figure 3-31) and small increases in slip joint differential pressure (i.e., decreases in M-ratio) can result in large increases in vibration intensity. From Figure 3-31, the SJDPs corresponding to 1g rms for the 100% drive flow were found to be 39.5 psi at 70°F and 30 psi at 180°F. It should be noted that, while these SJDP values are based on Jet Pump 1 data, $(HF)^2$ test results indicate the other jet pumps to behave similarly.

Figure 3-31 includes a plot of the BWR/6-251 mixer slip joint total RMS acceleration response from 532°F data reported in NEDE-24190 ("Flow-Induced Vibration Characteristics of BWR/6 Jet Pumps"). Using the same criteria as for the $(HF)^2$ jet pumps, the SJDP at $1g_{rms}$ is 18.6 psi.

The SJDPs corresponding to the $1g_{rms}$ response at 70°F, 180°F and 532°F were then plotted against kinematic viscosity on semi-log graph paper (Figure 3-32). Kinematic viscosity was an obvious choice since it significantly affects the slip joint leakage flow and, consequently, the vibration level and is sensitive to temperature. The three points plot almost as a straight line. If a straight line is connected between the 70°F and 180°F $(HF)^2$ points and extrapolated to 532°F, the resultant 532°F SJDP prediction is 20.5 psig, compared to 18.6 psi BWR/6-251 value. The fact that the BWR/6-238 prediction is higher is to be expected, since

the drive flow is also higher (4221 gpm compared with 3835 gpm), thus requiring (as Figures 3-28 and 3-29 illustrate) a slightly larger SJDP to achieve the same high-level vibration.

Based on the consistency of these data, as illustrated in Figure 3-32, it was concluded that 20.5 psi is a reasonable estimate of the SJDP at 100% drive flow and 532°F, which will result in the $1g_{rms}$ acceleration response limit at the mixer slip joint for the BWR/6-238 jet pump. The $(HF)^2$ results as reported in Section 3.2.4 indicate that this 1g rms SJDP will decrease by approximately 14% at 75% drive flow and will increase by about 7% at 125% drive flow. Therefore, the SJDP "limit" (i.e., value at $1g_{rms}$) at 532°F as a function of drive flow may be approximated using a linear interpolation over the drive flow ranges of 75% to 100% and 100% to 125%, and an extrapolation outside these ranges, as follows:

$$SJDP_{LIMIT} = 20.5 \left(1 + 0.14 \frac{W_{D_n} - 1}{0.25}\right) \qquad (3\text{-}7a)$$

$$W_{D_n} \quad 1$$

$$SJDP_{LIMIT} = 20.5 \left(1 + 0.07 \frac{W_{D_n} - 1}{0.25}\right) \qquad (3\text{-}7b)$$

$$W_{D_n} \quad 1$$

where W_{D_n} = normalized drive flow (ratio of drive flow to 100% design operating drive flow).

Note that, while Equations 3-7a and 3-7b may not be very accurate outside of the 75% - 125% drive flow range (data are unavailable to base a judgment), the evaluation of the jet pump will be unaffected, since, under reactor operating conditions, the jet pump will not be operated beyond 125% nor at the hydraulic conditions (i.e., very low M-ratios) necessary to achieve high-level vibration at drive flows less than 75%.

Using Equations 3-7a and 3-7b to define the SJDP limits, and Equation 3-6 to define the relationship between SJDP, drive flow, and M-ratio, a map was developed of the high and low vibration operating regions for the BWR/6-238 (Figure 3-33). The BWR/6-238 predicted recirculation system performance curve, when plotted on this map, demonstrates that the BWR/6-238 jet pump is designed to operate well within the $1g_{rms}$ vibration region.

3.3 $(HF)^2$ RISER BRACE LEAVES VIBRATION CHARACTERISTICS

Accelerometers were placed on the riser brace leaves to characterize their vertical response due to FIV. The typical response (Figure 3-34) is almost totally a superposition of a large sinusoidal component at about 300 Hz with a smaller one at about 280 Hz. The 300 Hz component appears to be the first bending mode of the adjacent riser brace leaves as they vibrate in-phase, while the 280 Hz component is the first mode when out-of-phase, the difference in natural frequency caused by the hydrodynamic mass effects in the region between the leaves. Because the frequencies are close together and both are being excited, obvious beating occurs.

3.4 JET PUMP HARDWARE POST-TEST INSPECTION

Inspection of the four BWR/6-238 jet pumps after completion of the shake and FIV tests at $(HF)^2$ revealed hardware damage to be extremely minimal. Slight burnish marks were evident on the wedges and mixer bellybands along their contact surfaces. In addition, burnish rings were observed on the inside surface of the diffuser collars, and minor meridianal scoring on the mating mixer elbow spherical seats and riser transition piece connical seats. The mixer bellybands were slightly gouged at the point of contact with the adjusting screws. Several of the rods which tied the adjusting screws to the restrainer brackets were broken at the tack welds, allowing the screws to back out by as much as one-half turn. This apparently produced a gap between the adjusting screw and bellyband, which was less than 2.5 mils for Jet Pumps 2 and 3, 25 mils for Jet Pump 4, and 44 mils for Jet Pump 1. Note: as indicated in Section 2, using rods to prevent adjusting screw backoff was used in the $(HF)^2$ test program only. Reactor installation practice is to tack-weld the screws directly to the restrainer bracket.

The mixer-diffuser slip-joint gaps were carefully measured upon completion of the FIV test program. Results (Figure 3-35) revealed the jet pumps to be in contact, the direction being predominantly radial (within $\pm 30^{\circ}$). The mixer-diffuser

contact force varied from a minimum of 200 lb for Jet Pump 4 to a maximum of 850 lb for Jet Pump 1 (Jet Pump 2 was not measured).

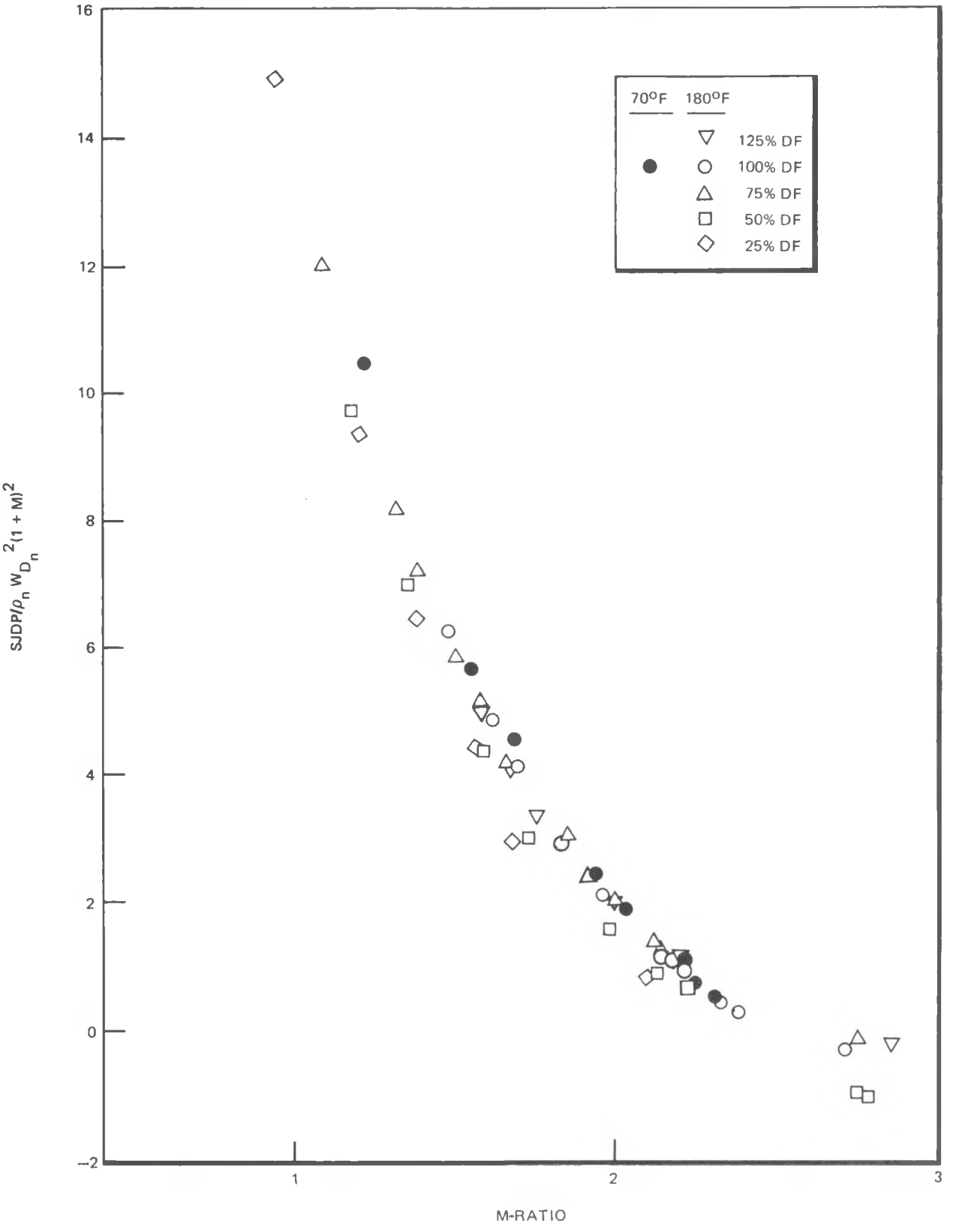

Figure 3-1. $(HF)^2$ Jet Pump 1 Hydraulic Parameters (SJDP, Drive Flow, M-Ratio)

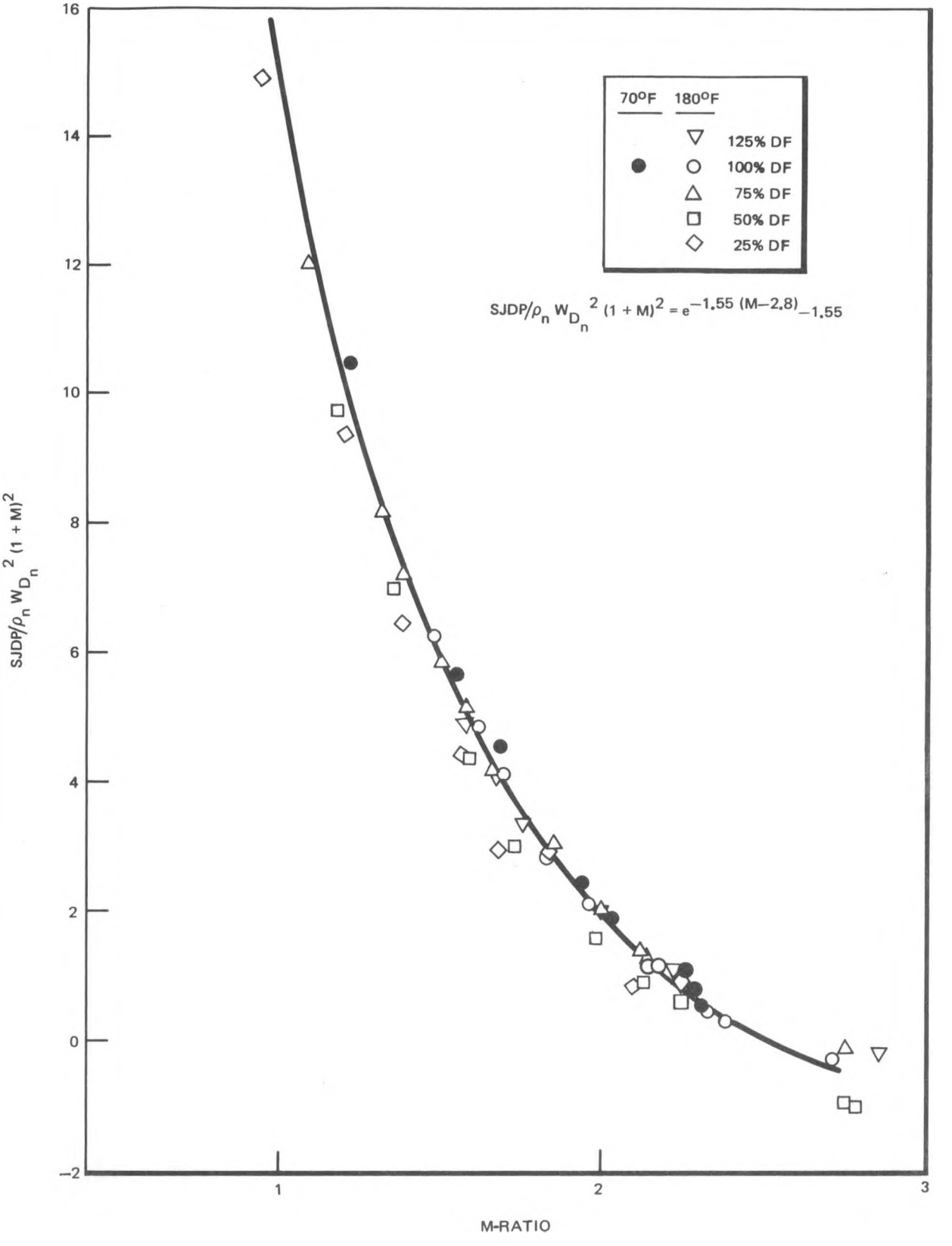

Figure 3-2. Exponential Curve Fit to $(HF)^2$ Jet Pump 1 Hydraulic Parameters (SJDP, Drive Flow, M-Ratio)

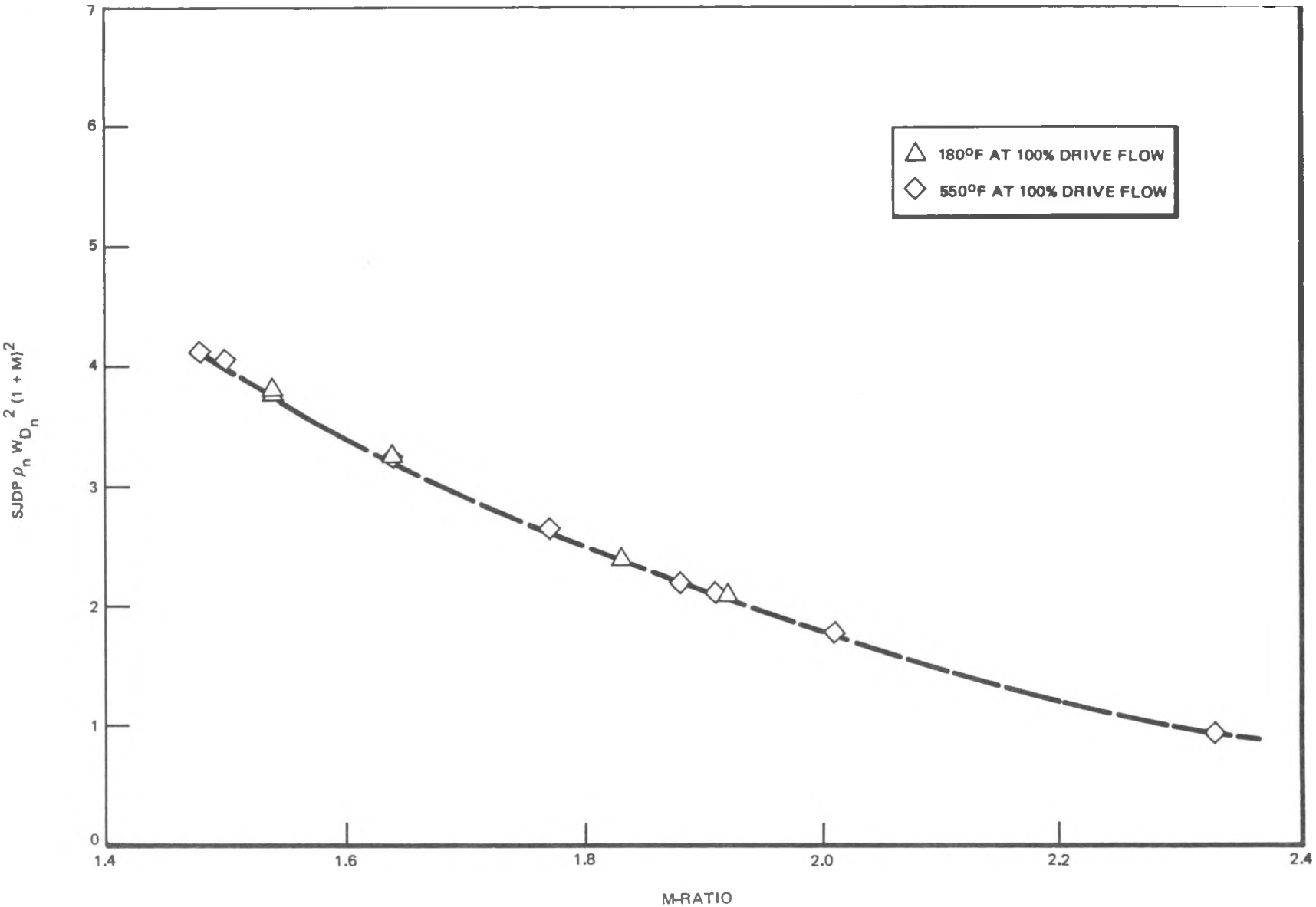

Figure 3-3. Jet Pump Hydraulic Data: 180°F and 532°F (from Moss Landing Test Program)

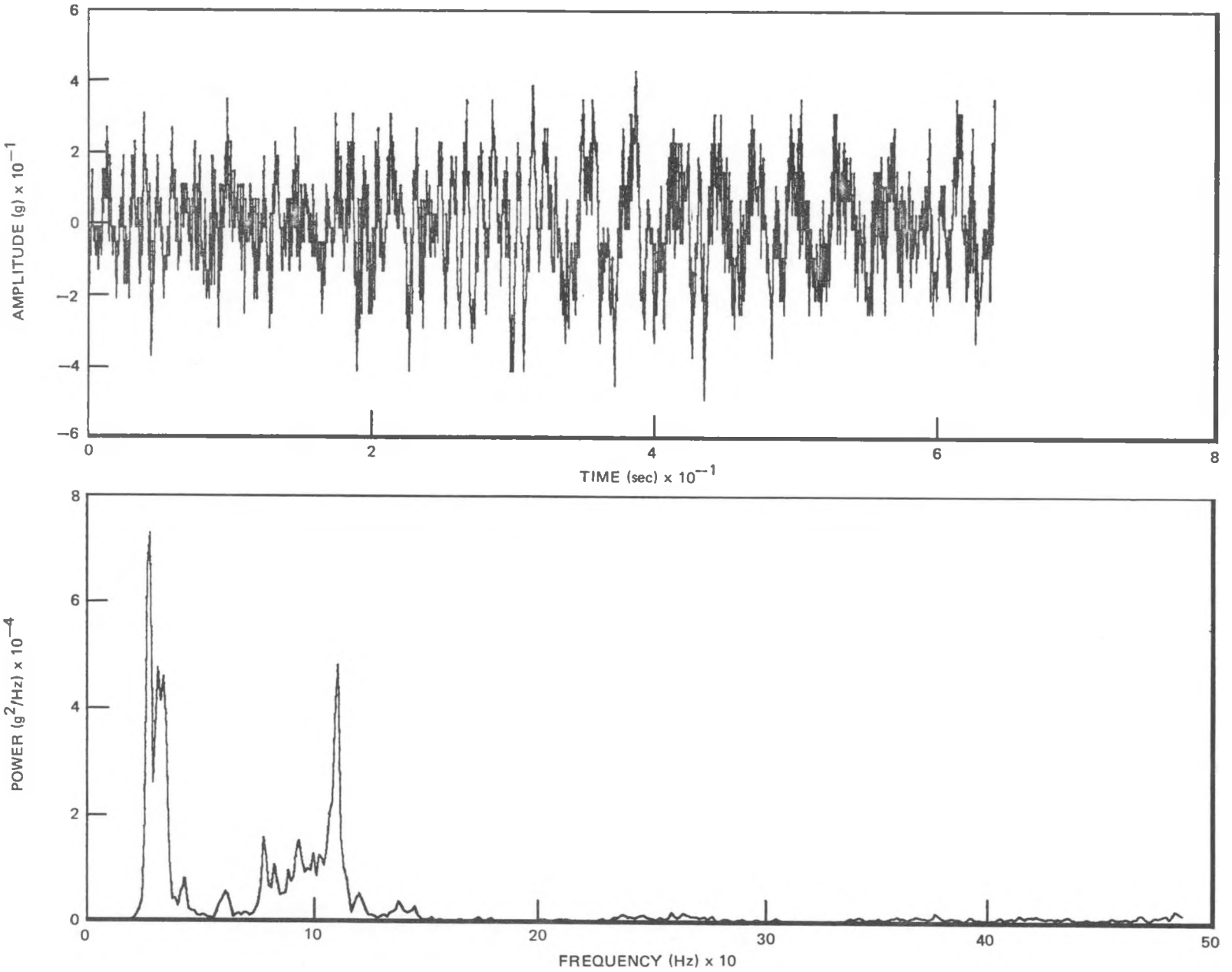

Figure 3-4. Jet Pump 1 Radial Response at Design Operating M-Ratio and Drive Flow - Mixer at Slip Joint (Response = $0.14 g_{rms}$); Midway into Test Program

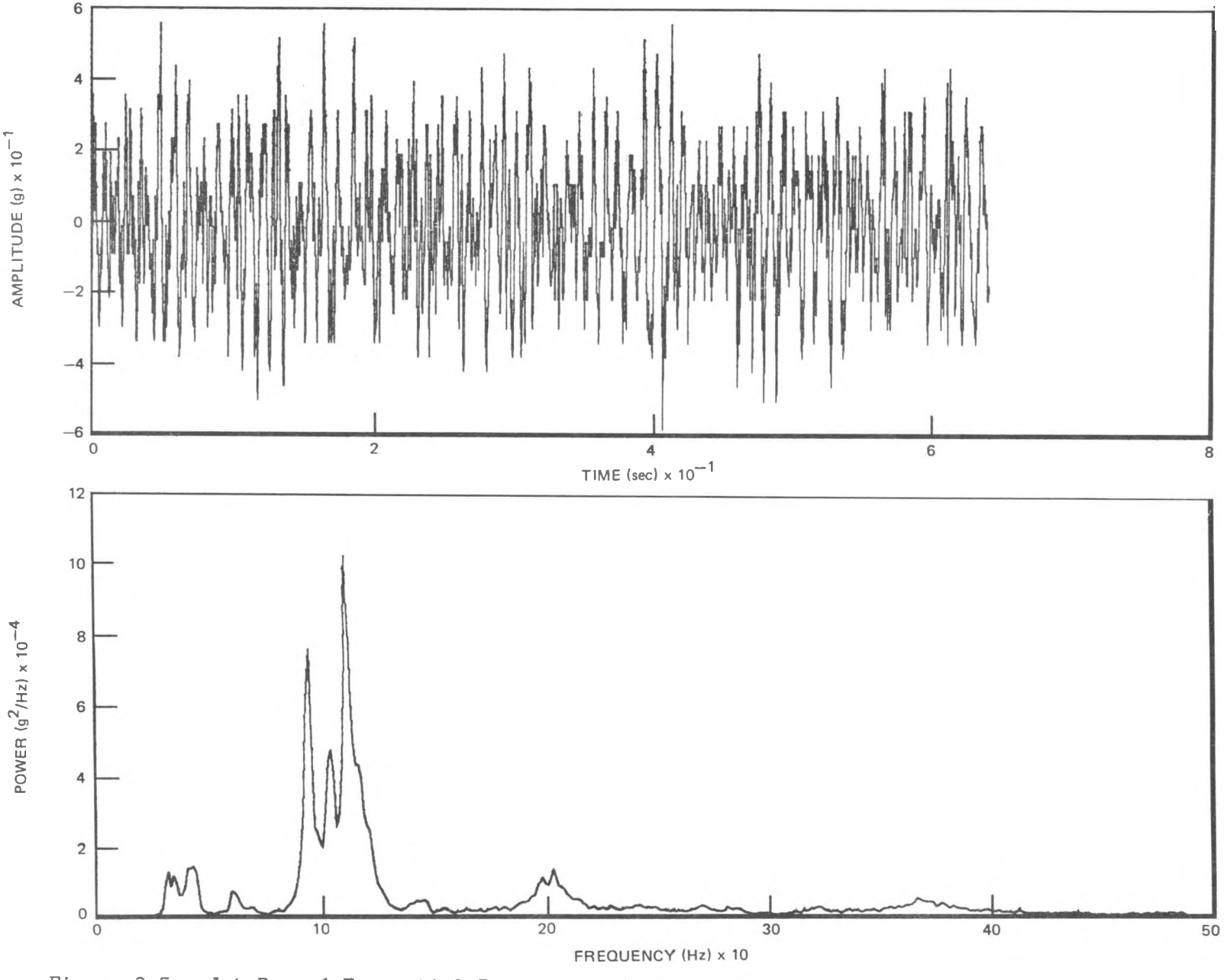

Figure 3-5. Jet Pump 1 Tangential Response at Design Operating M-Ratio and Drive Flow - Mixer at Slip Joint (Response = $0.18g_{rms}$); Midway into Test Program

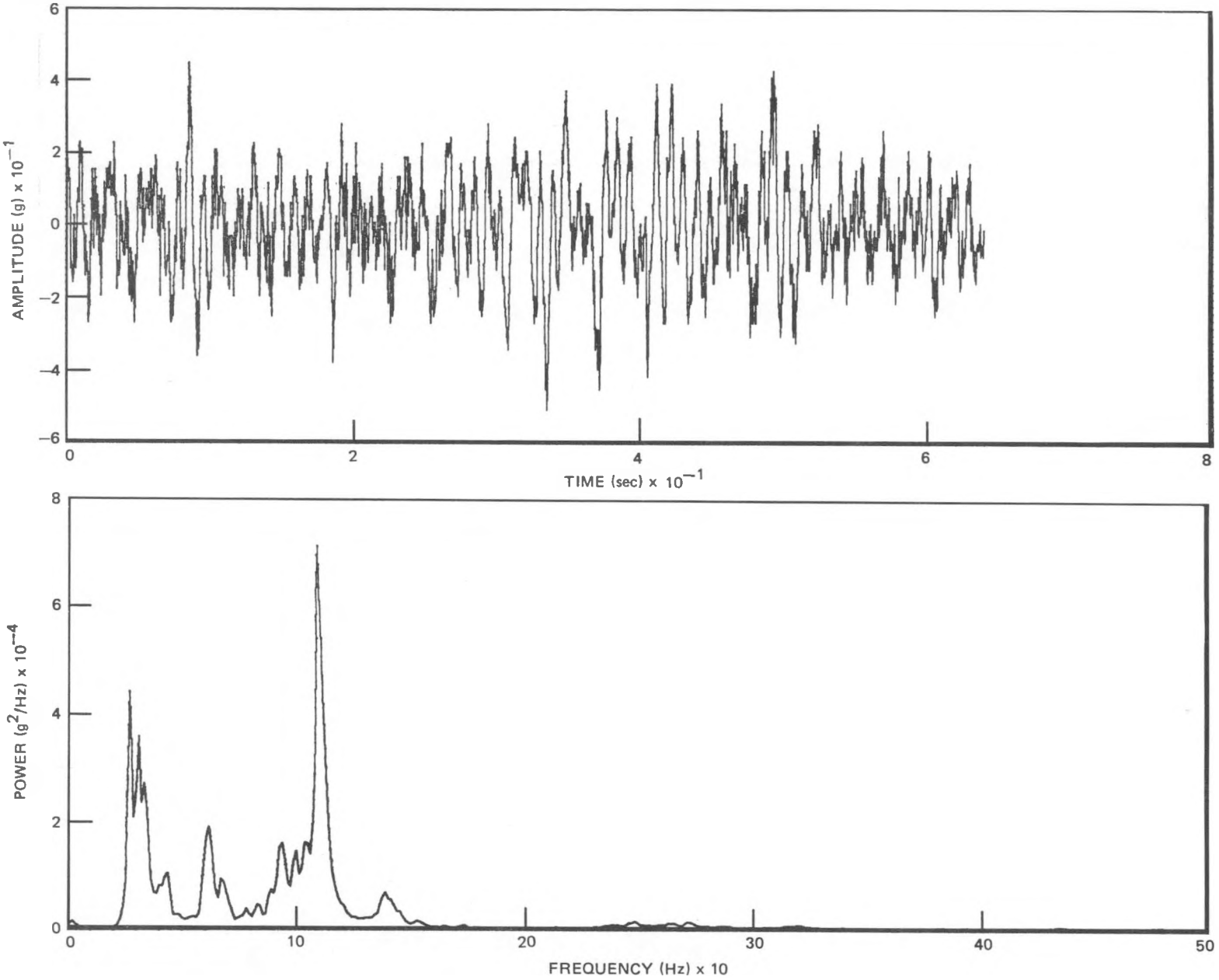

Figure 3-6. Jet Pump 1 Radial Response at Design Operating M-Ratio and Drive Flow - Diffuser at Slip Joint (Response = $0.17g_{rms}$); Midway into Test Program

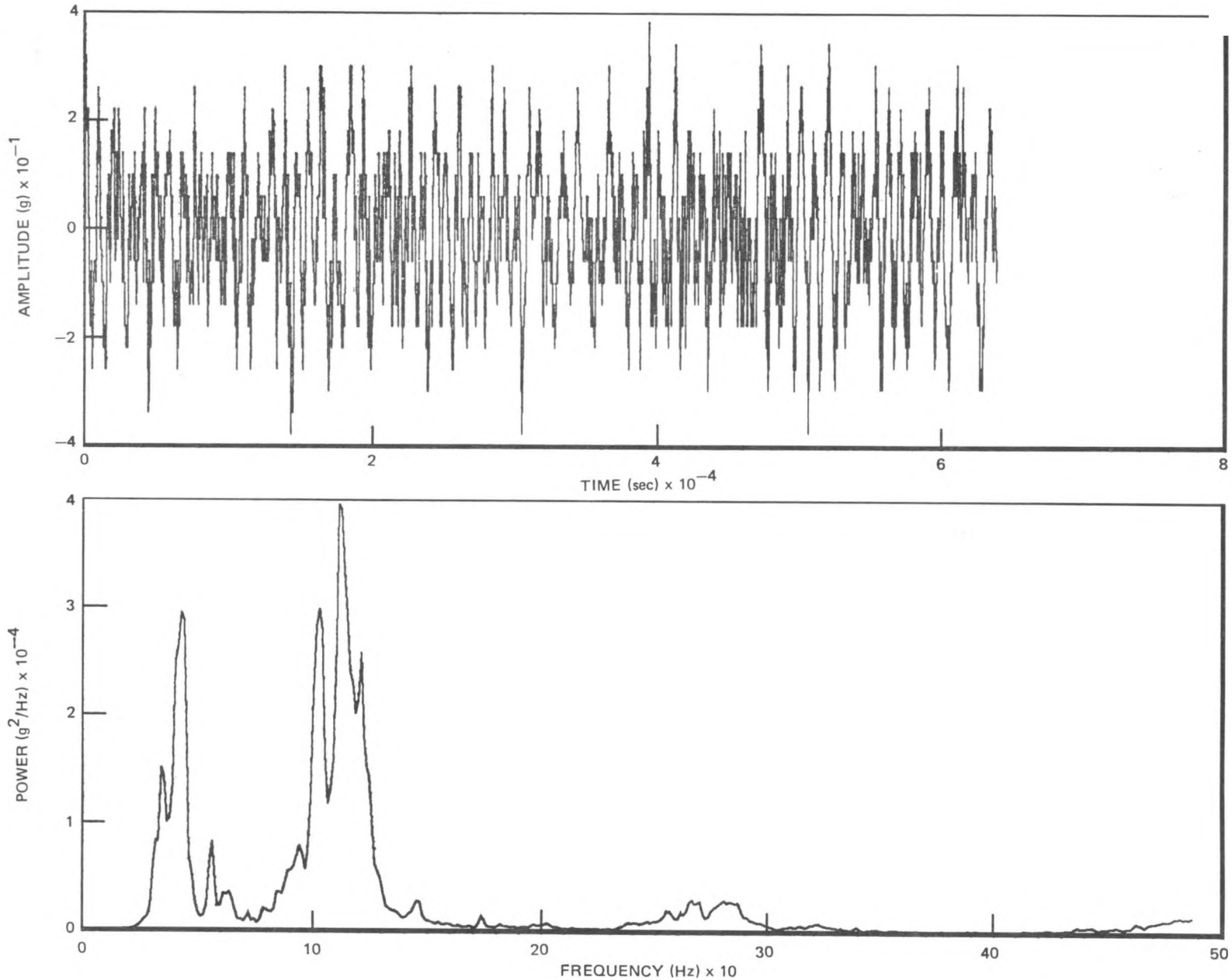

Figure 3-7. Jet Pump 1 Tangential Response at Design Operating M-Ratio and Drive Flow - Diffuser at Slip Joint (Response = $0.10g_{rms}$); Midway into Test Program

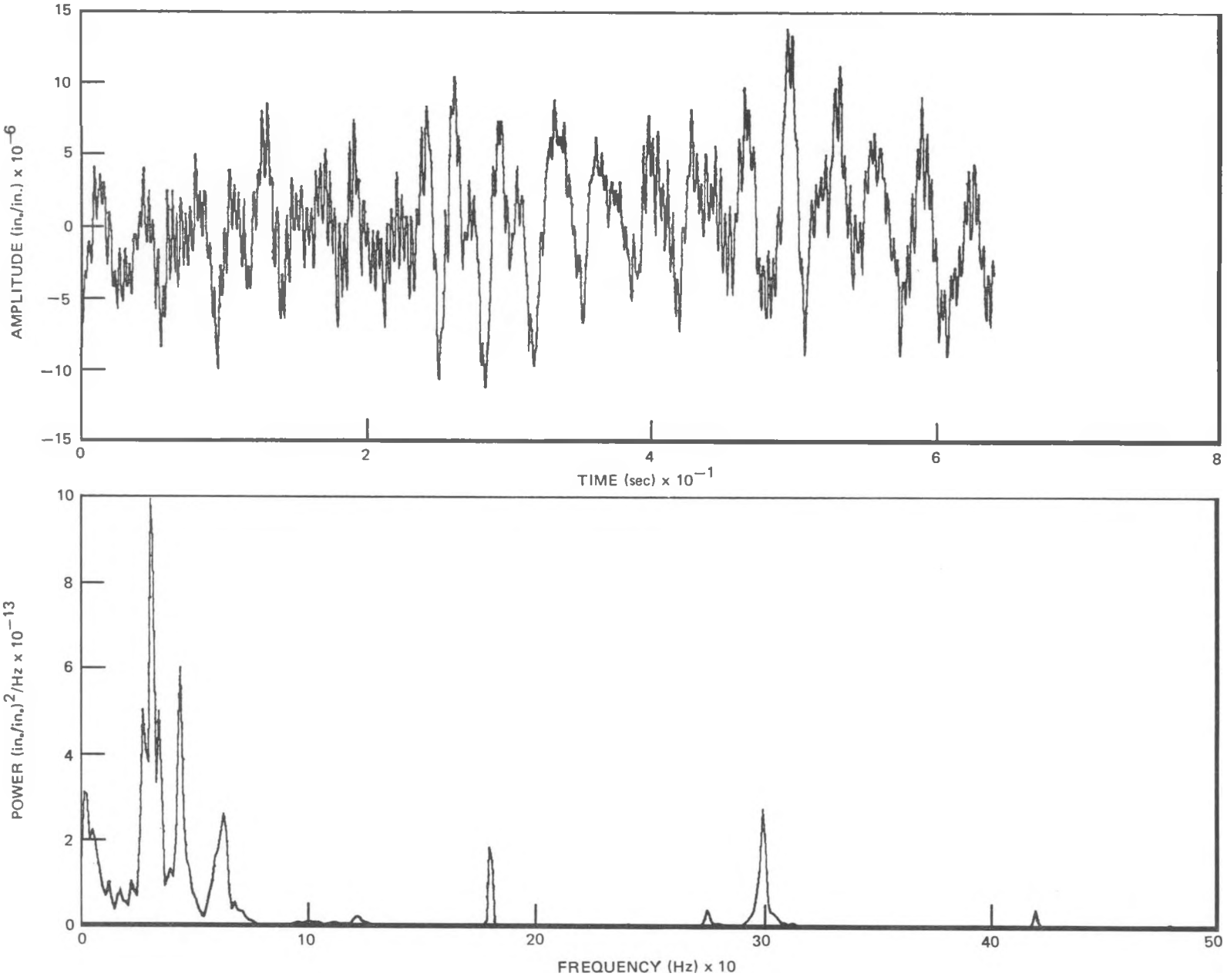

Figure 3-8. Riser Brace A1 Strain at Design Operating M-Ratio and Drive Flow (Strain Gage 1 of Figure 2-11). Peak Strain = 14 μin./in; Midway into Test Program

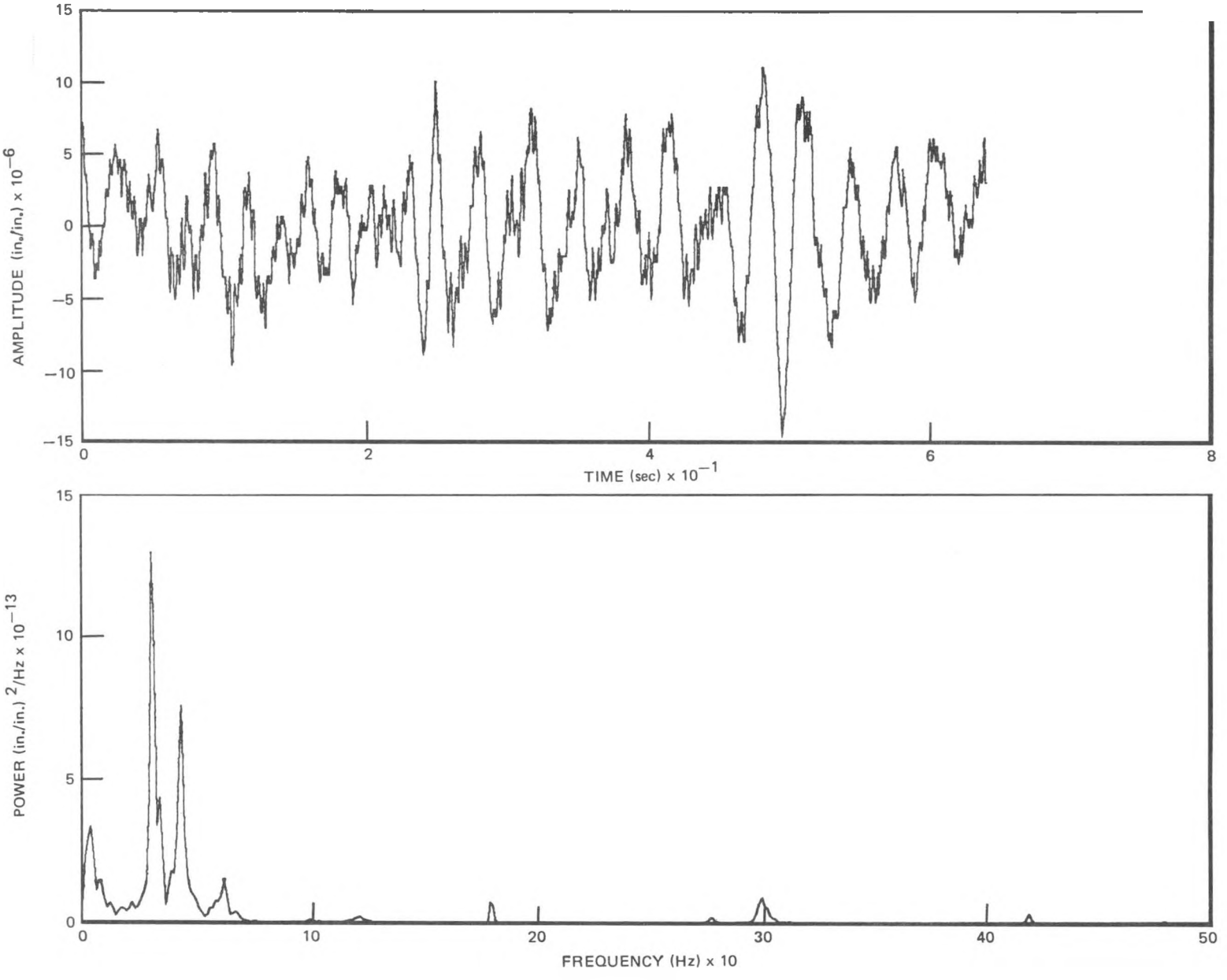

Figure 3-9. Riser Brace A1 Strain at Design Operating M-Ratio and Drive Flow (Strain Gage 2 of Figure 2-11). Peak Strain = 15 μin./in.; Midway into Test Program

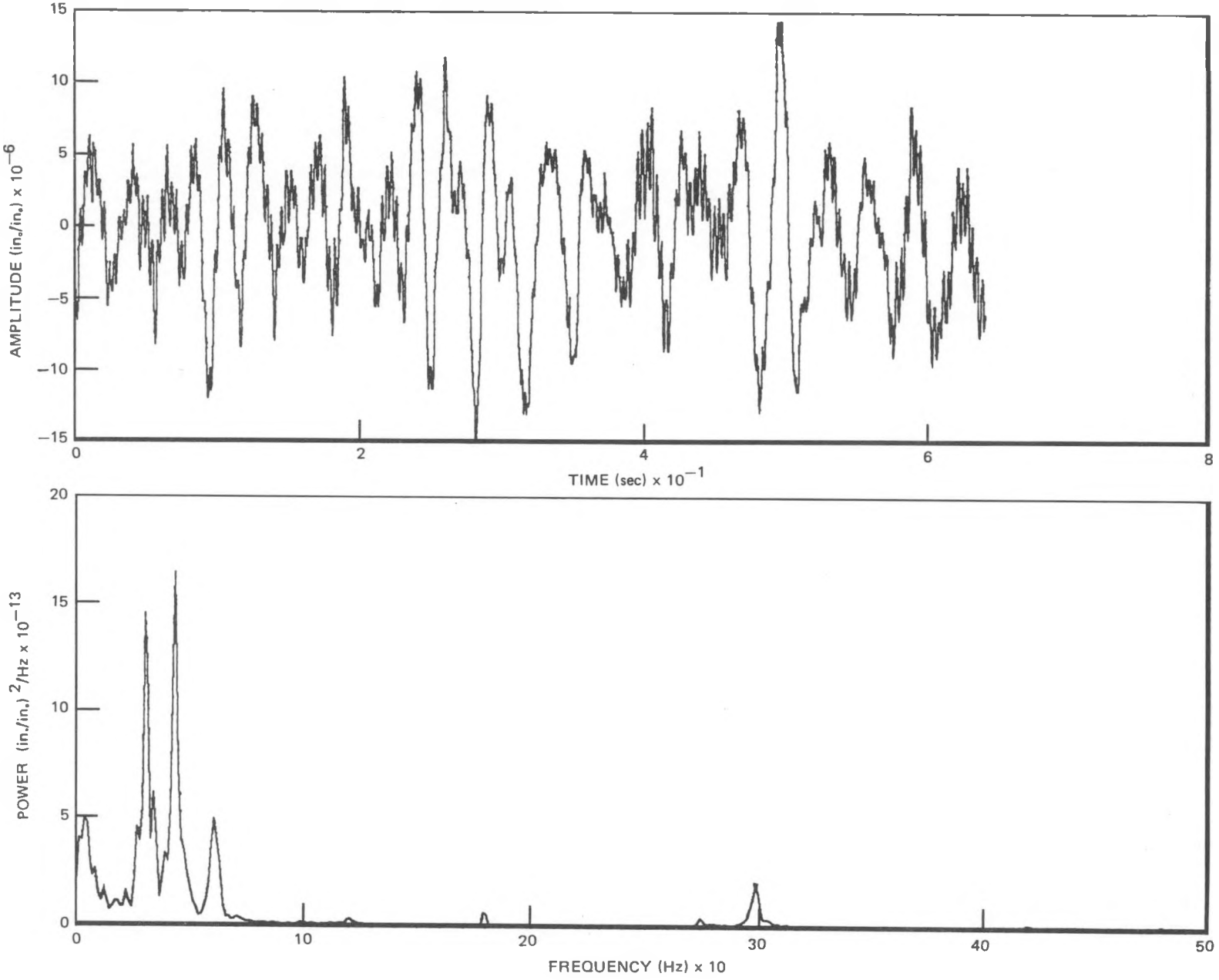

Figure 3-10. Riser Brace A1 Strain at Design Operating M-Ratio and Drive Flow (Strain Gage 3 of Figure 2-11). Peak Strain = 15 μin./in.; Midway into Test Program

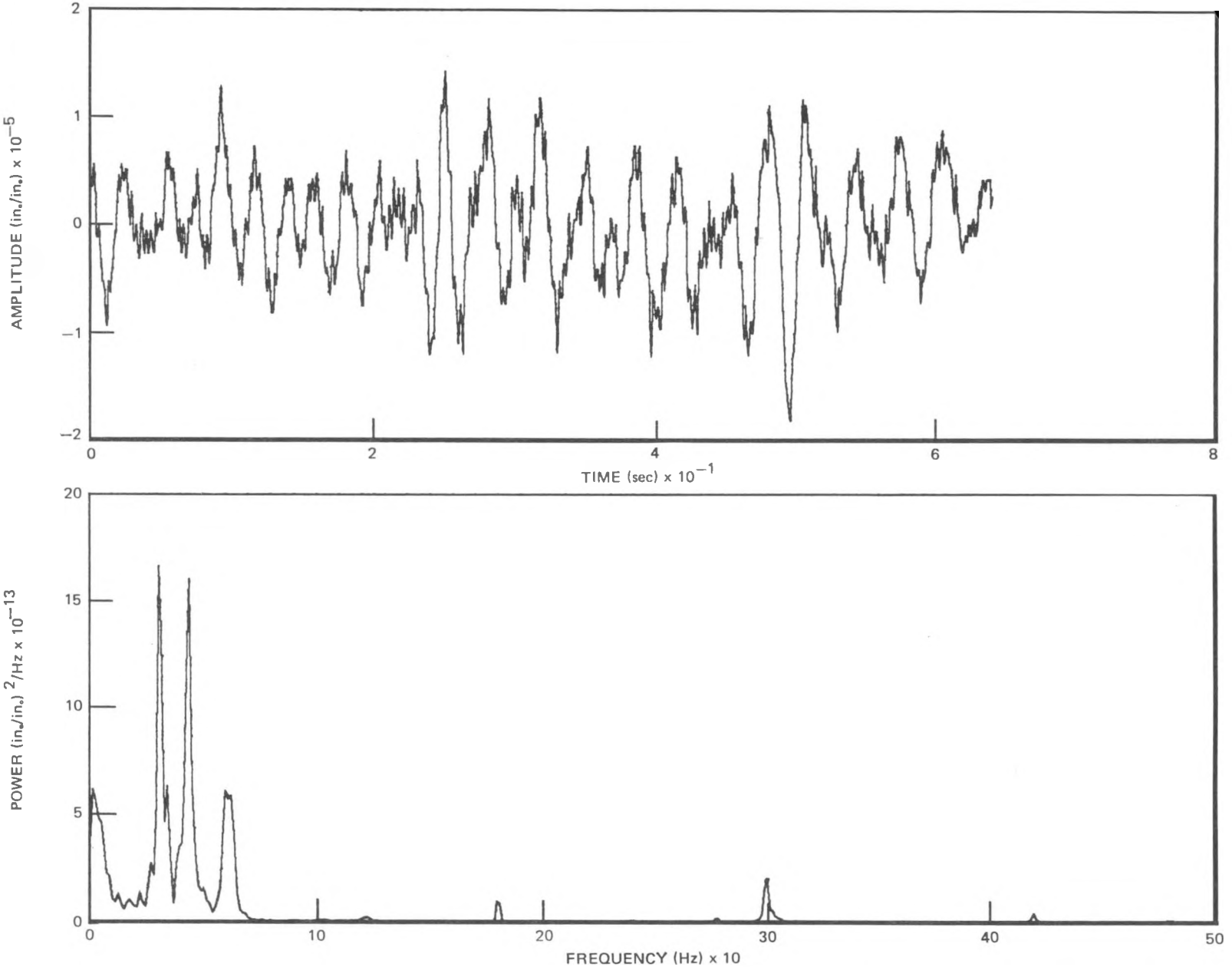

Figure 3-11. Riser Brace A1 Strain at Design Operating M-Ratio and Drive Flow (Strain Gage 4 of Figure 2-11). Peak Strain = 18 μin./in.; Midway into Test Program

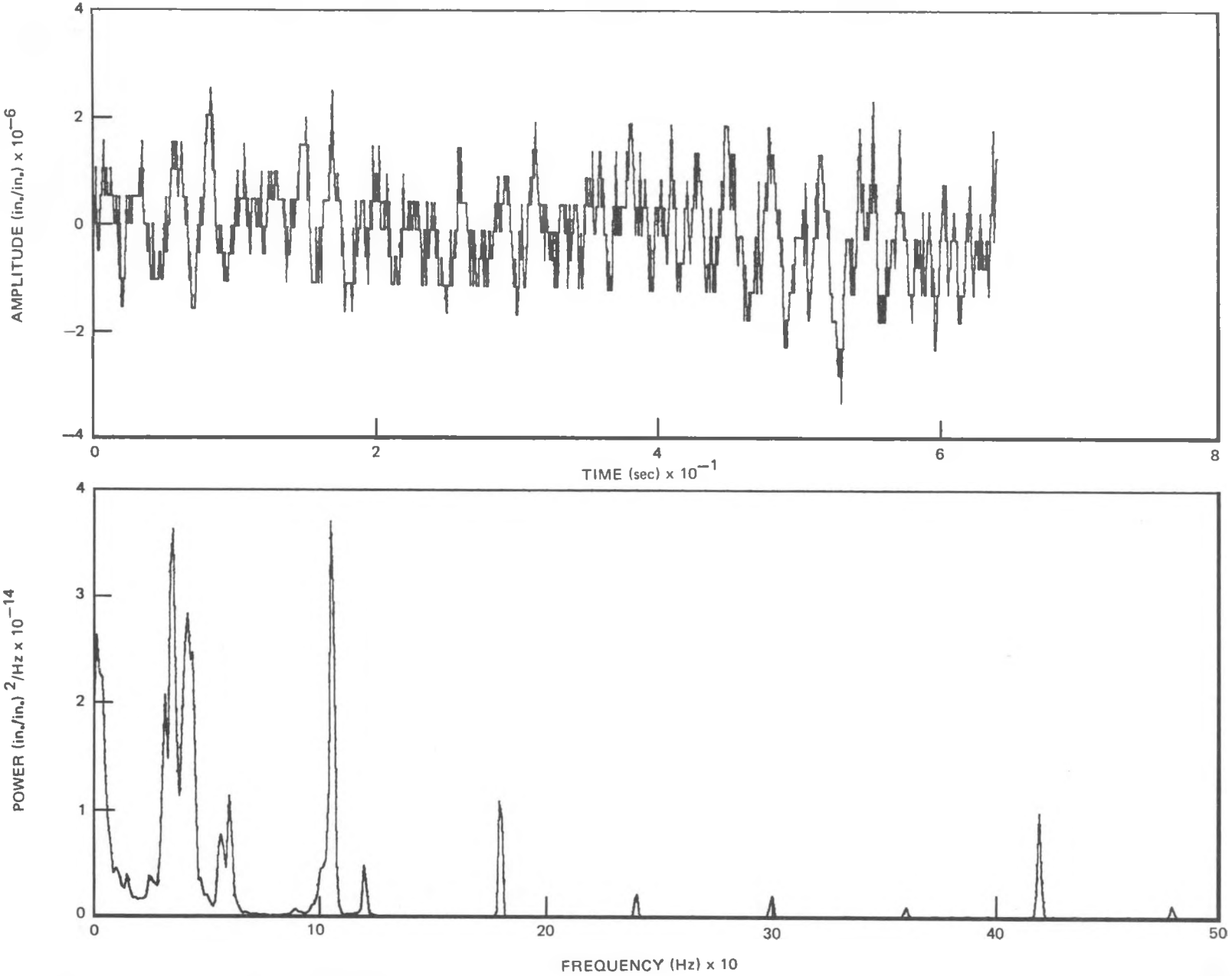

Figure 3-12. Jet Pump 1 Diffuser Strain at Design Operating M-Ratio and Drive Flow (Strain Gage of Figure 2-11). Peak Strain = 3 μin./in.; Midway into Test Program

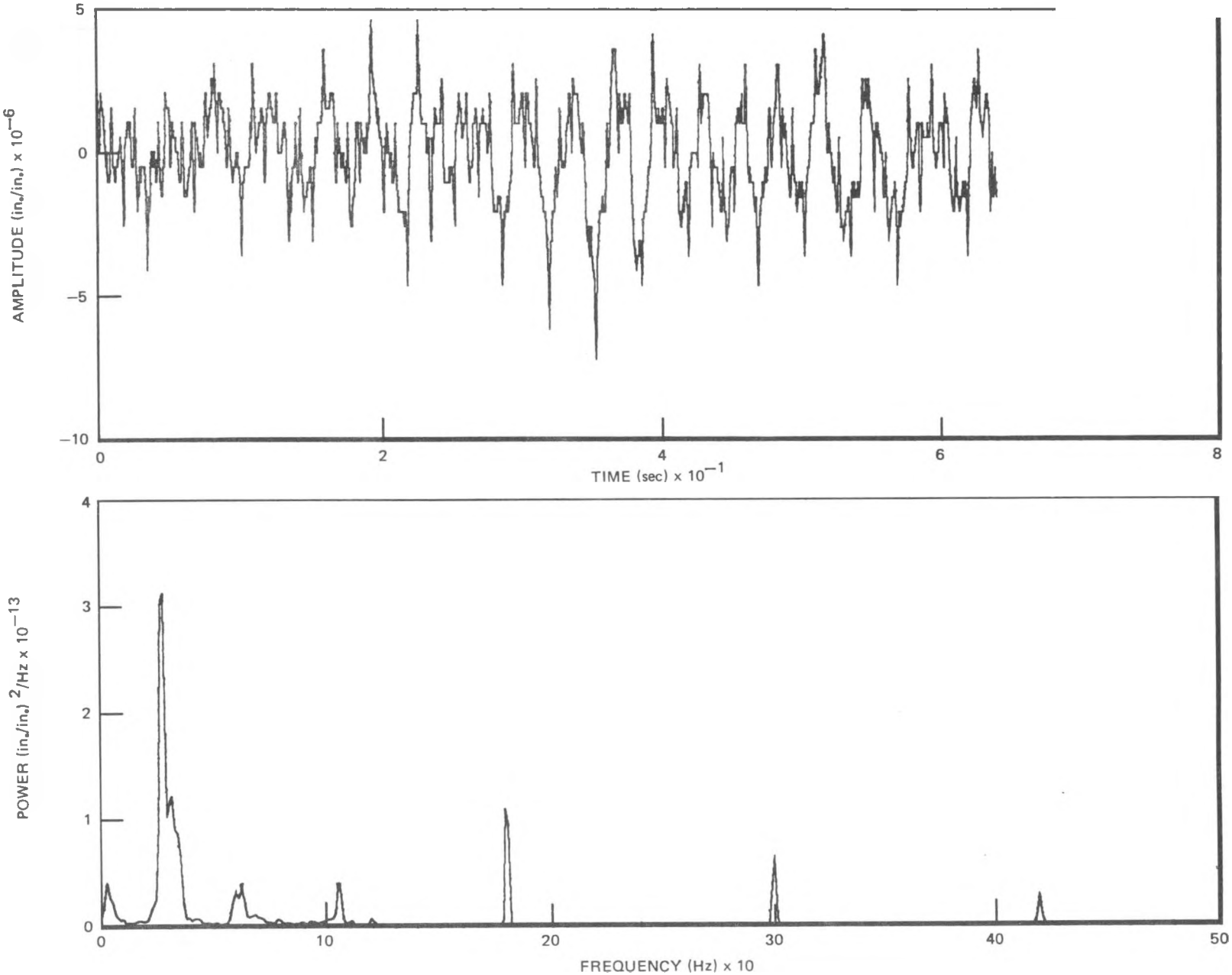

Figure 3-13. Jet Pump 1 Diffuser Strain at Design Operating M-Ratio and Drive Flow (Strain Gage 6 of Figure 2-11). Peak Strain = 7 μin./in.; Midway into Test Program

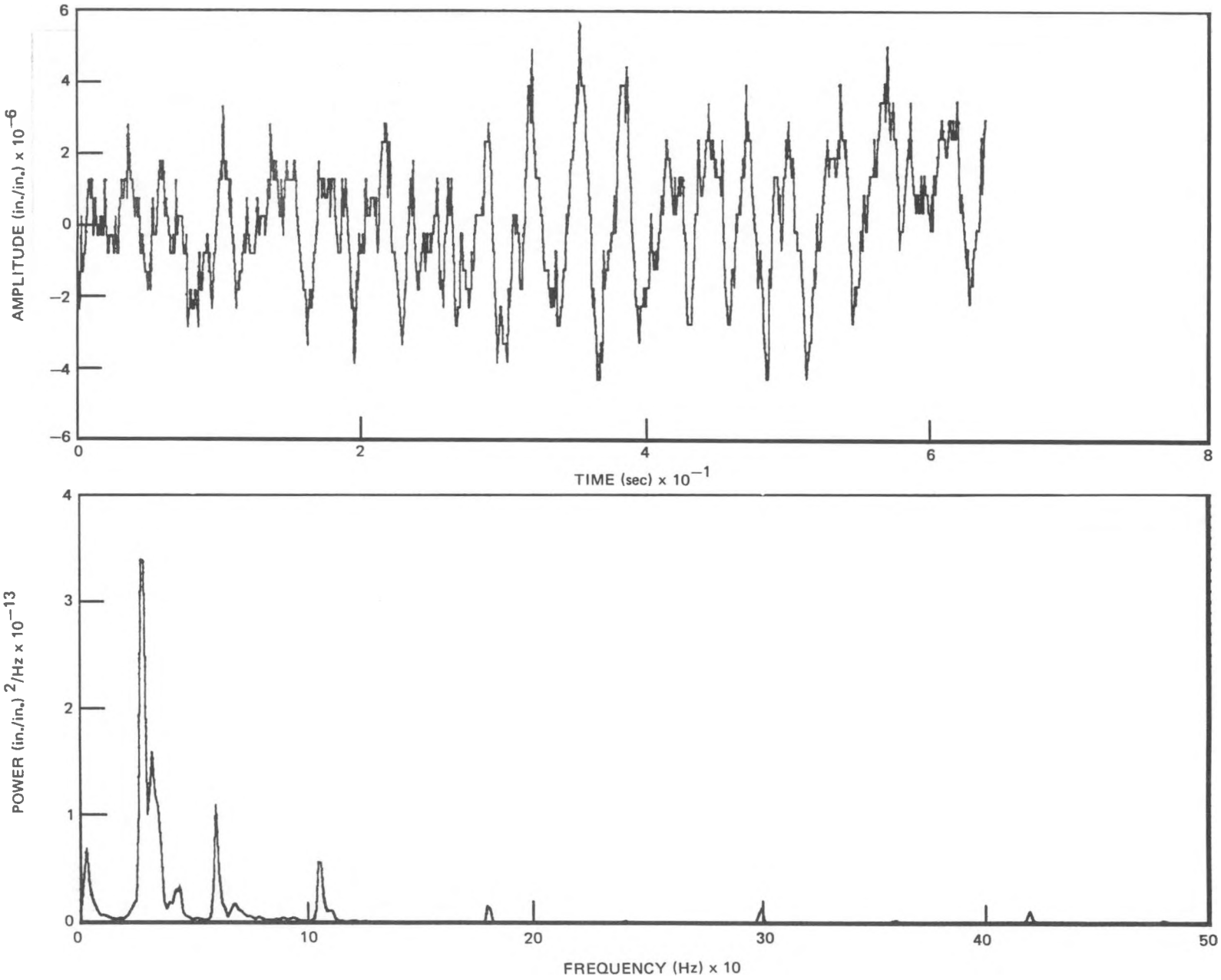

Figure 3-14. Jet Pump 1 Diffuser Strain at Design Operating M-Ratio and Drive Flow (Strain Gage 8 of Figure 2-11). Peak Strain = 6 μin./in.; Midway into Test Program

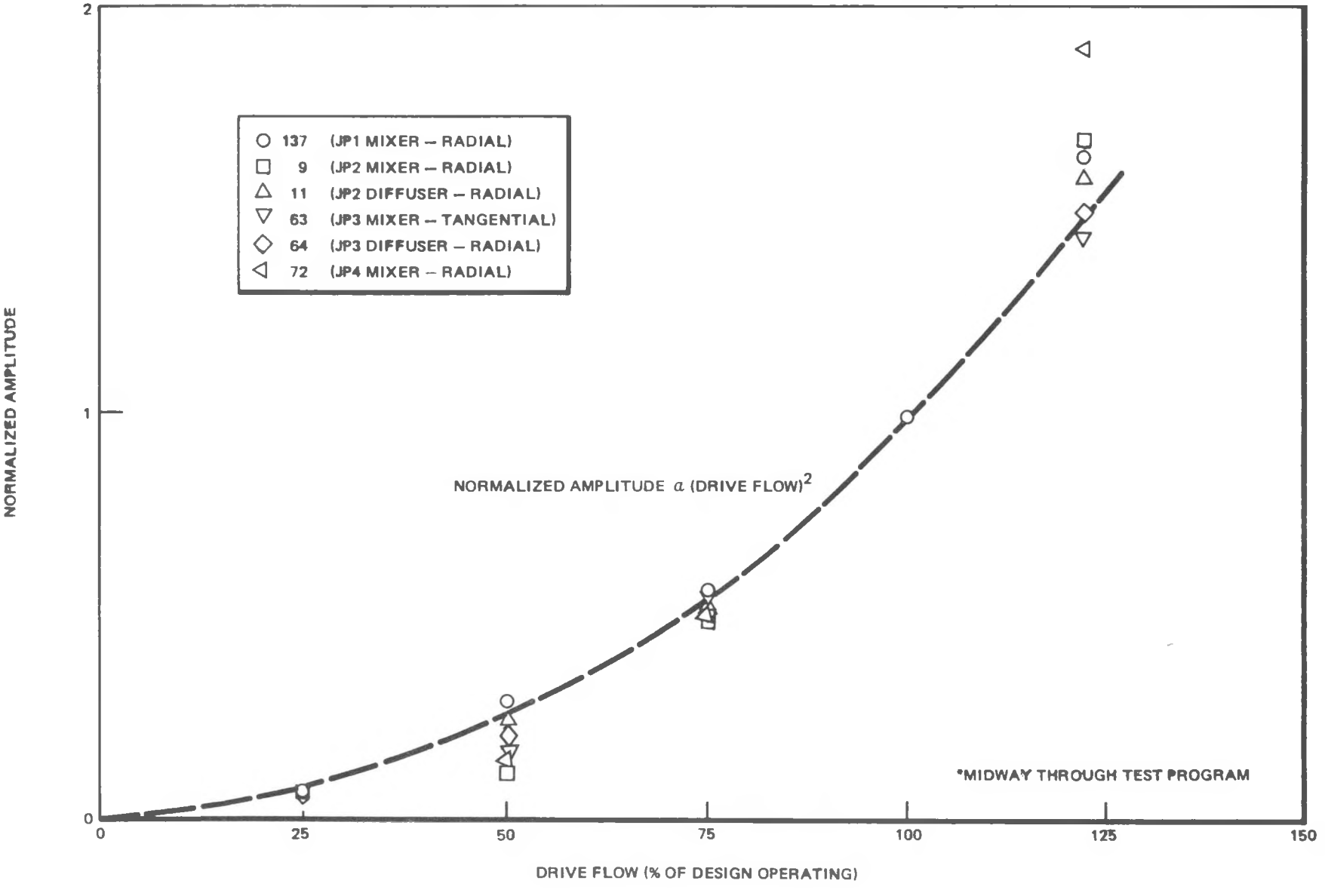

Figure 3-15. $(HF)^2$ Jet Pump Acceleration Response at Slip Joint (Normalized about 100% Drive Flow Response) Versus Drive Flow

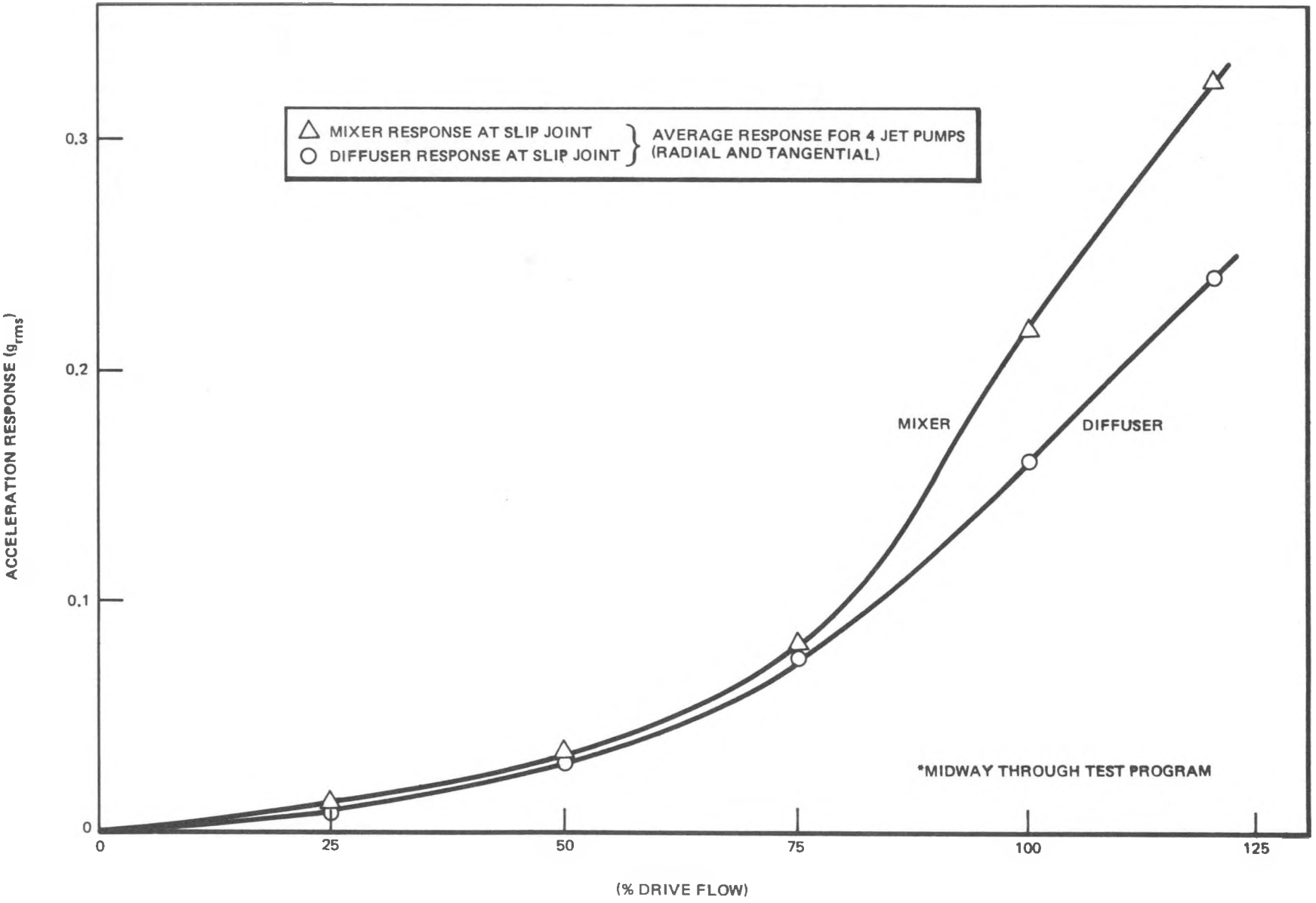

Figure 3-16. Averaged Mixer and Diffuser Response at Slip Joint Versus Drive Flow at Design Operating M-Ratio

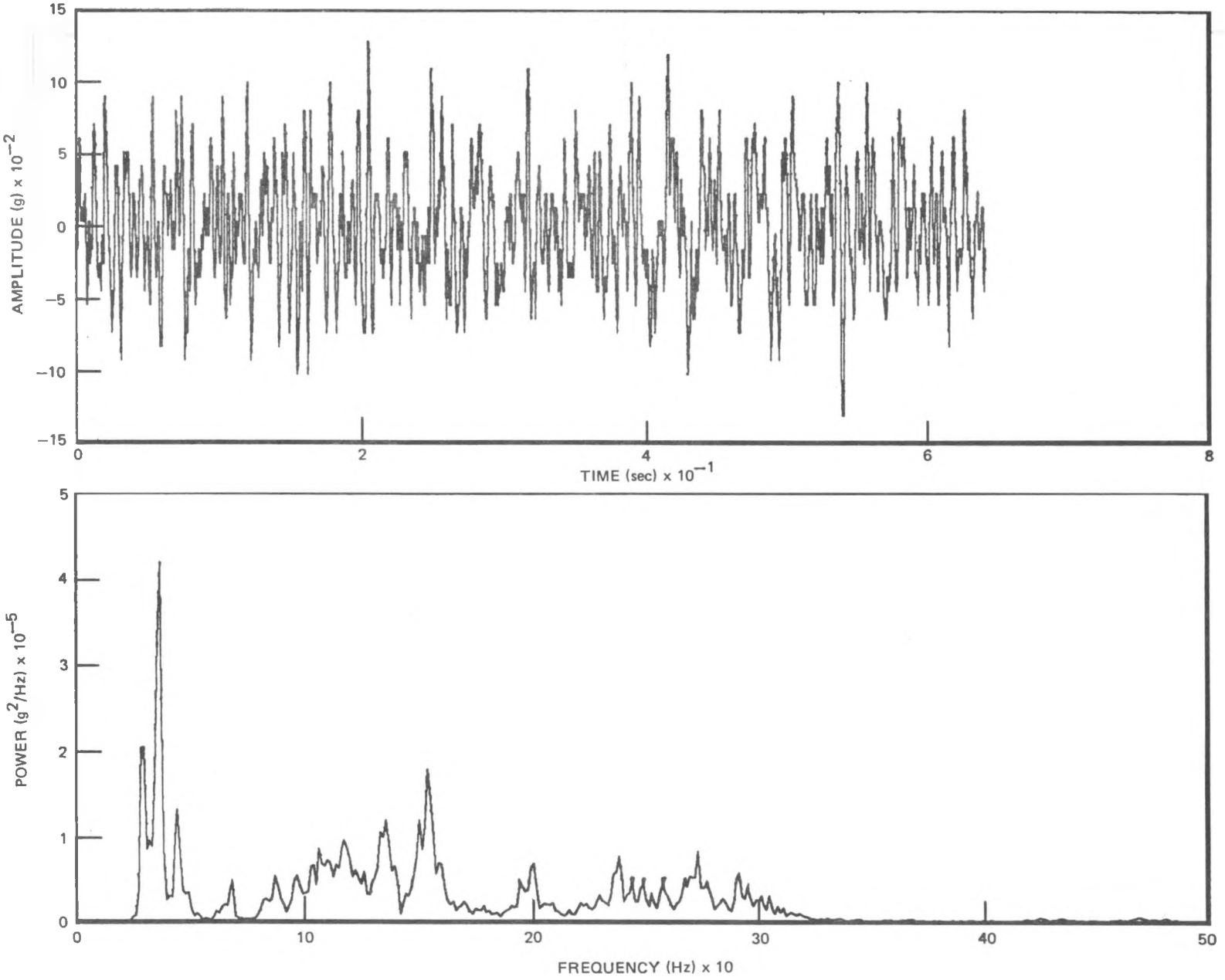

Figure 3-17. Jet Pump 2 Mixer (Slip Joint) Radial Response at 50% Drive Flow, Operating M-Ratio (Response = 0.037g_{rms}); Midway into Test Program

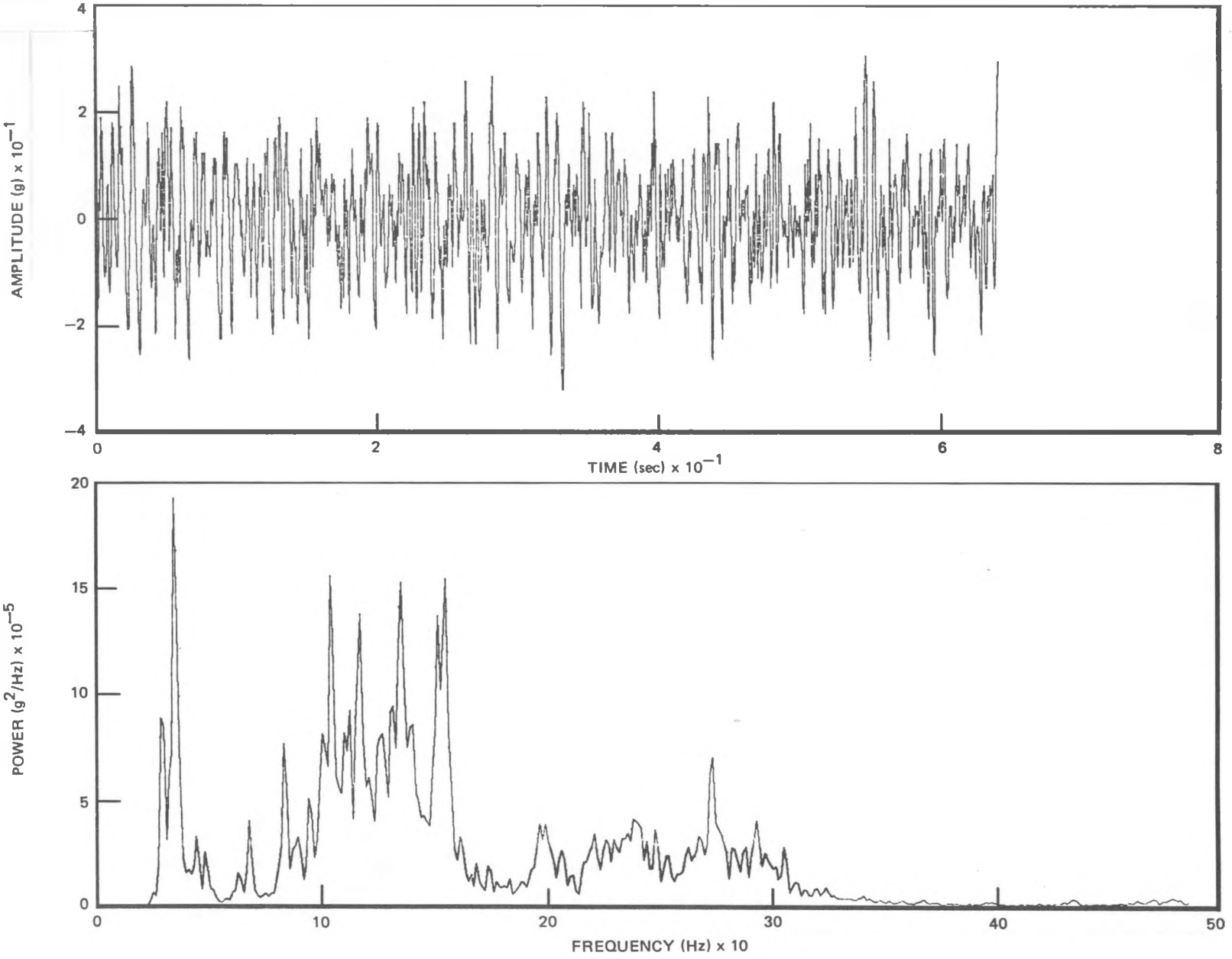

Figure 3-18. Jet Pump 2 Mixer (Slip Joint) Radial Response at 75% Drive Flow, Operating M-Ratio (Response = 0.10g_{rms}); Midway into Test Program

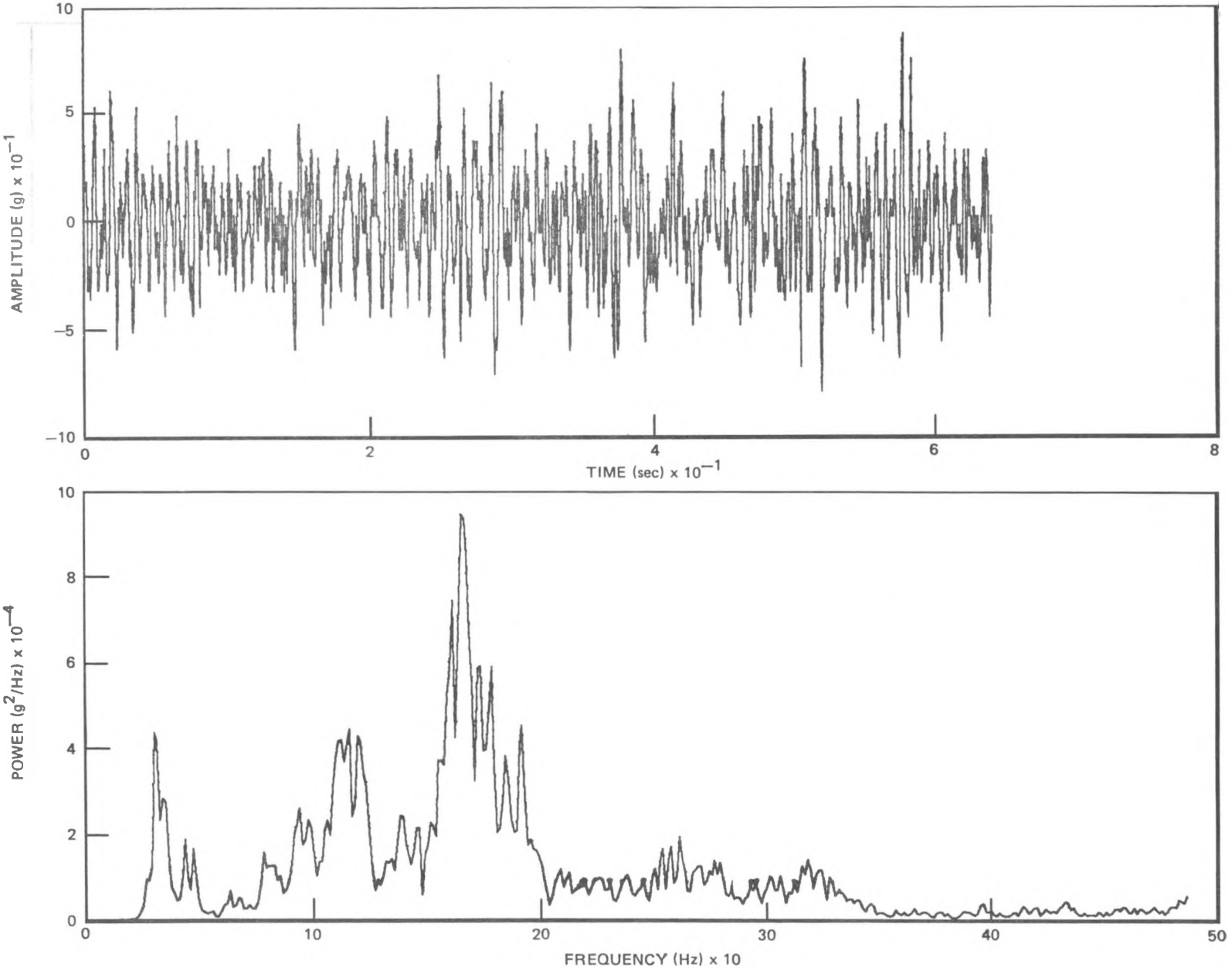

Figure 3-19. Jet Pump 2 Mixer (Slip Joint) Radial Response at 100% Drive Flow, Operating M-Ratio (Response = $0.25g_{rms}$); Midway into Test Program

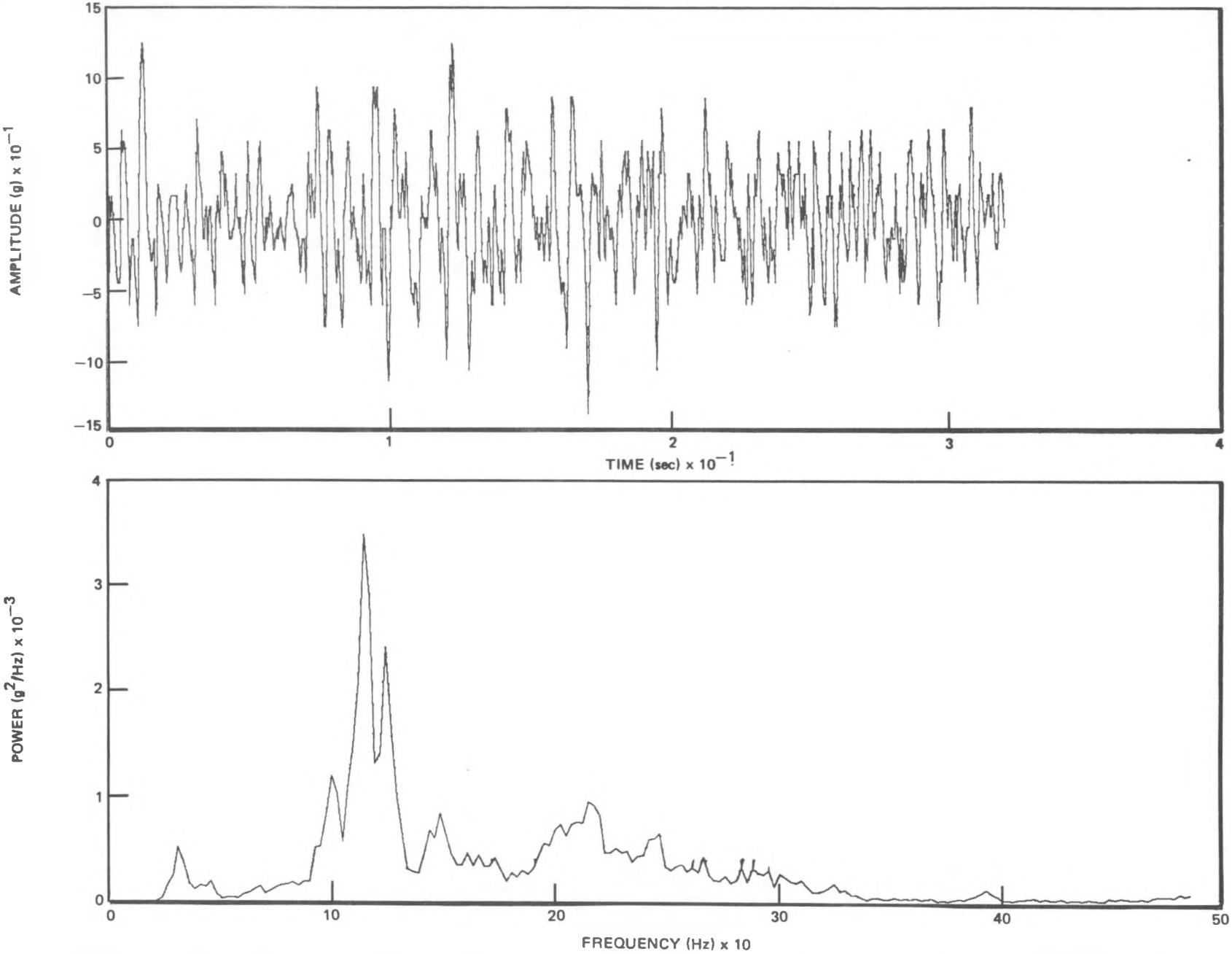

Figure 3-20. Jet Pump 2 Mixer (Slip Joint) Radial Response at 125% Drive Flow, Operating M-Ratio (Response = $0.42g_{rms}$); Midway into Test Program

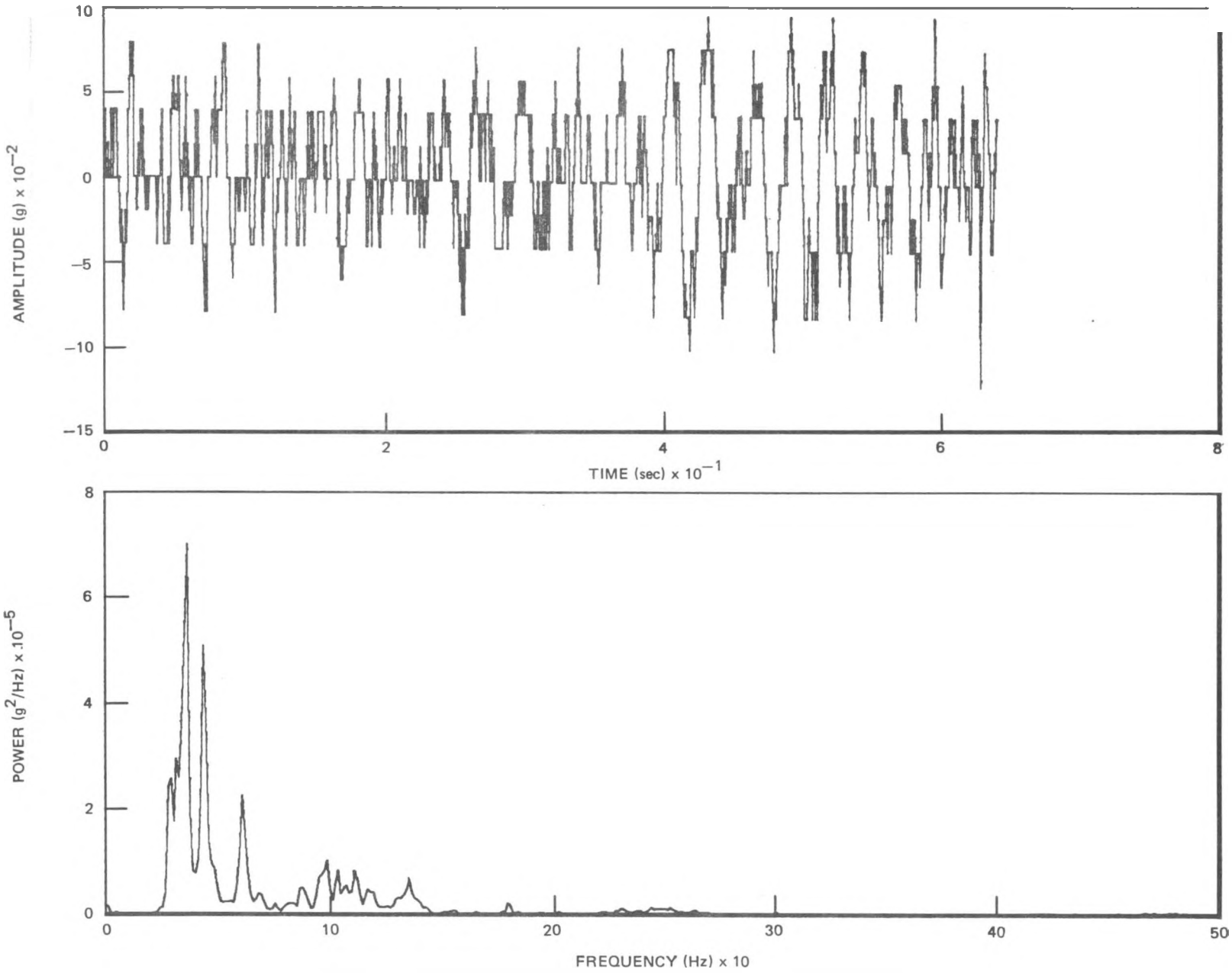

Figure 3-21. Jet Pump 2 Diffuser (Slip Joint) Radial Response at 50% Drive Flow, Operating M-Ratio (Response = $0.034 g_{rms}$); Midway into Test Program

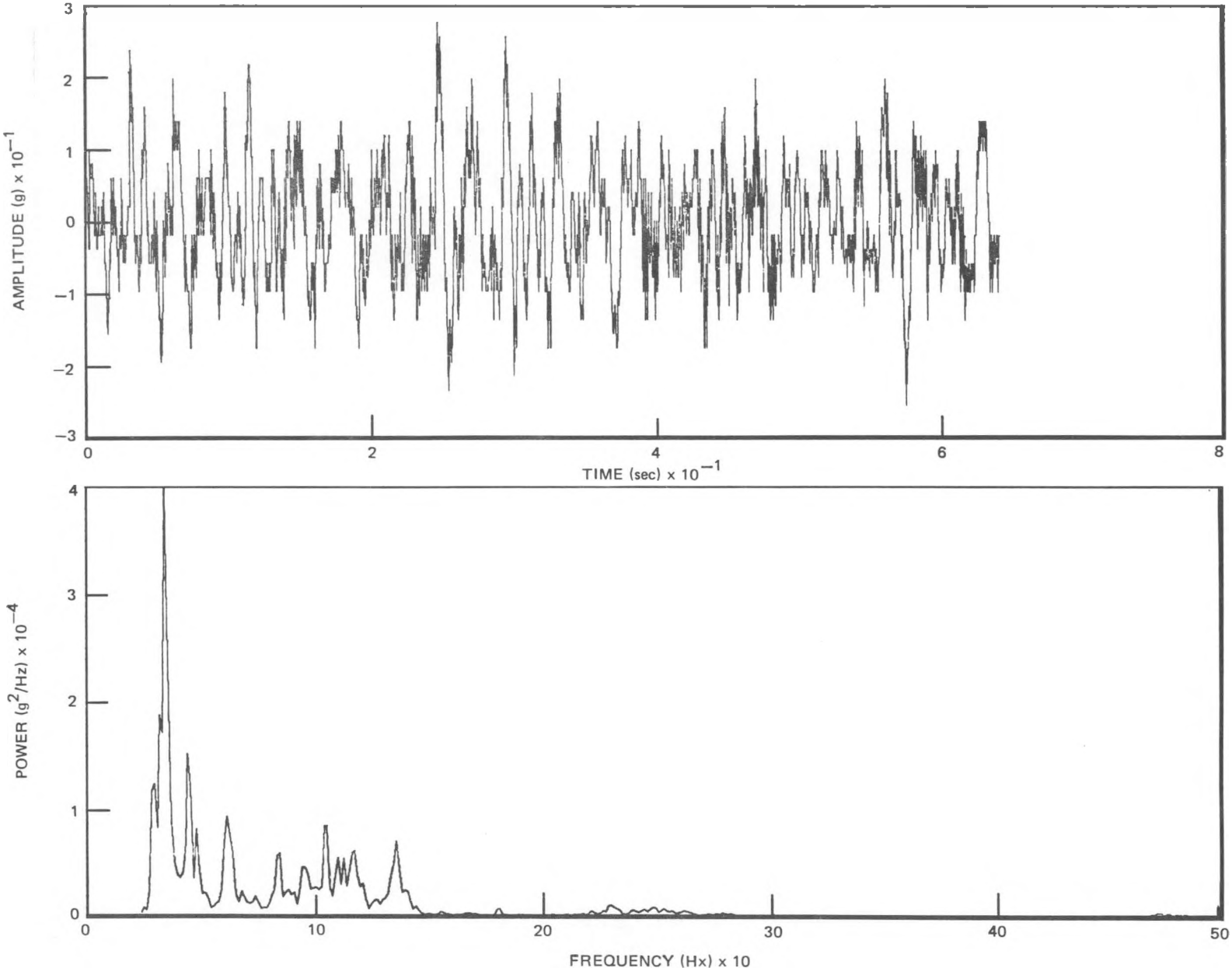

Figure 3-22. Jet Pump 2 Diffuser (Slip Joint) Radial Response at 75% Drive Flow, Operating M-Ratio (Response = $0.083 g_{rms}$); Midway into Test Program

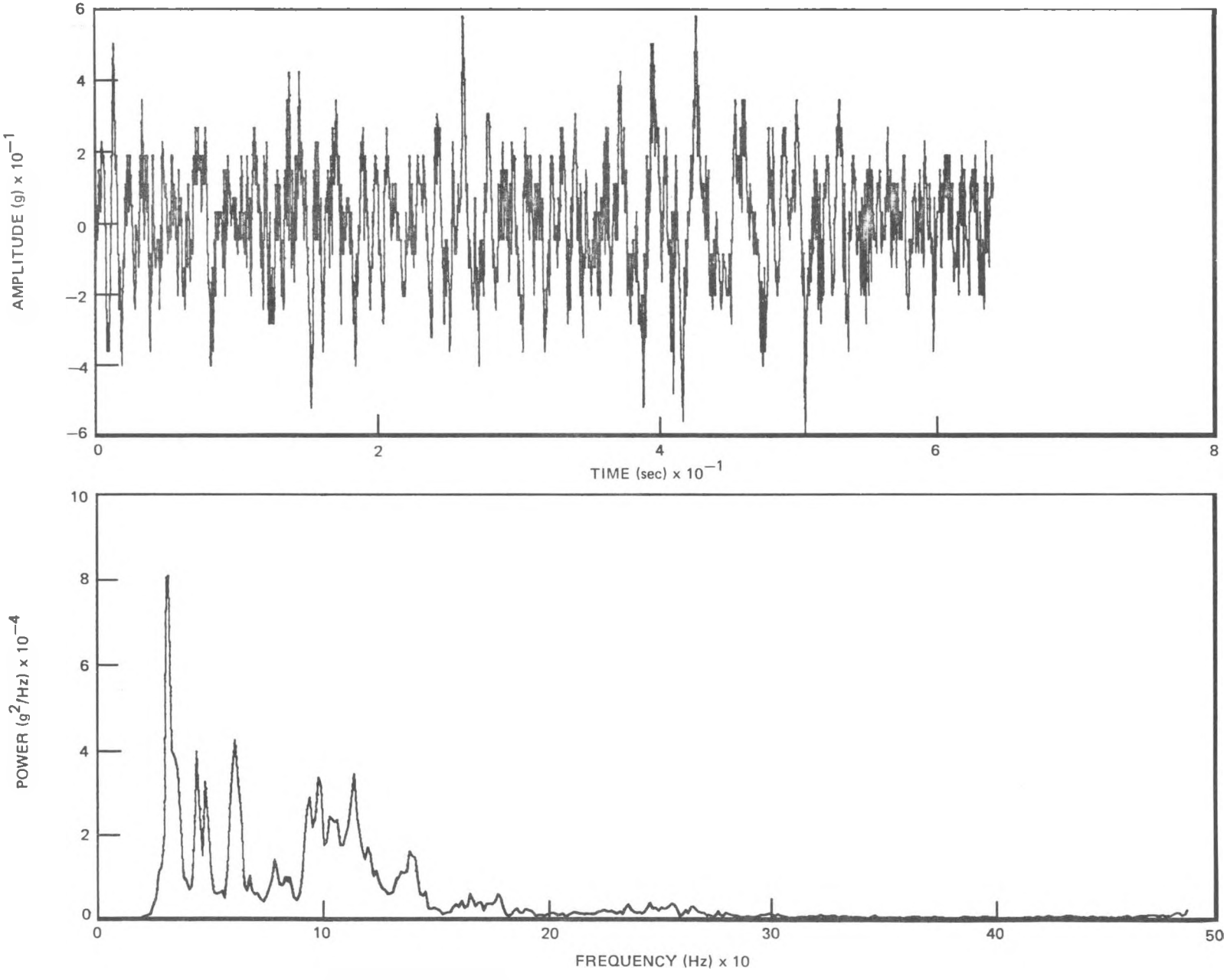

Figure 3-23. Jet Pump 2 Diffuser (Slip Joint) Radial Response at 100% Drive Flow, Operating M-Ratio (Response = $0.16 g_{rms}$); Midway into Test Program

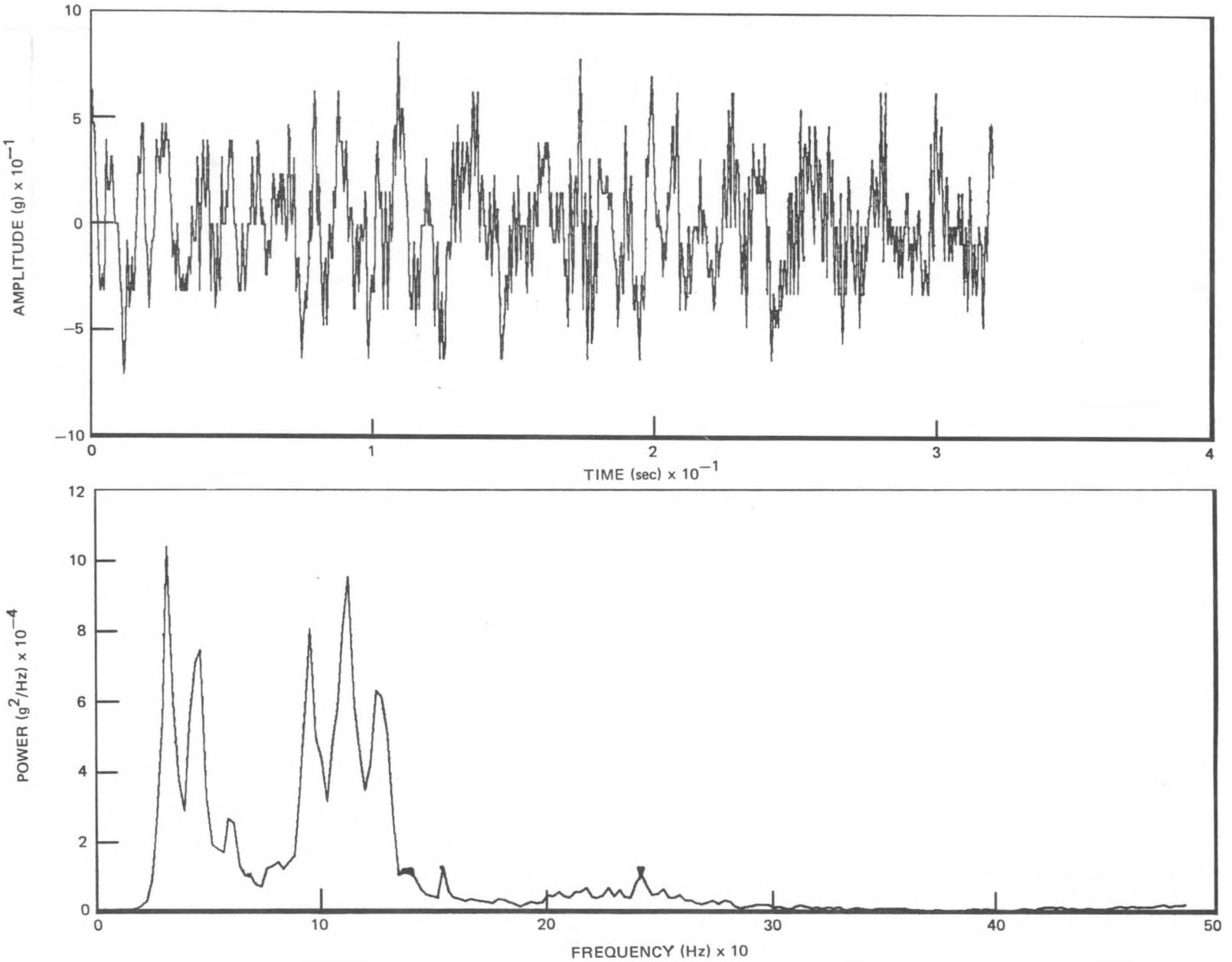

Figure 3-24. Jet Pump 2 Diffuser (Slip Joint) Radial Response at 125% Drive Flow, Operating M-Ratio (Response = 0.27g_{rms}); Midway into Test Program

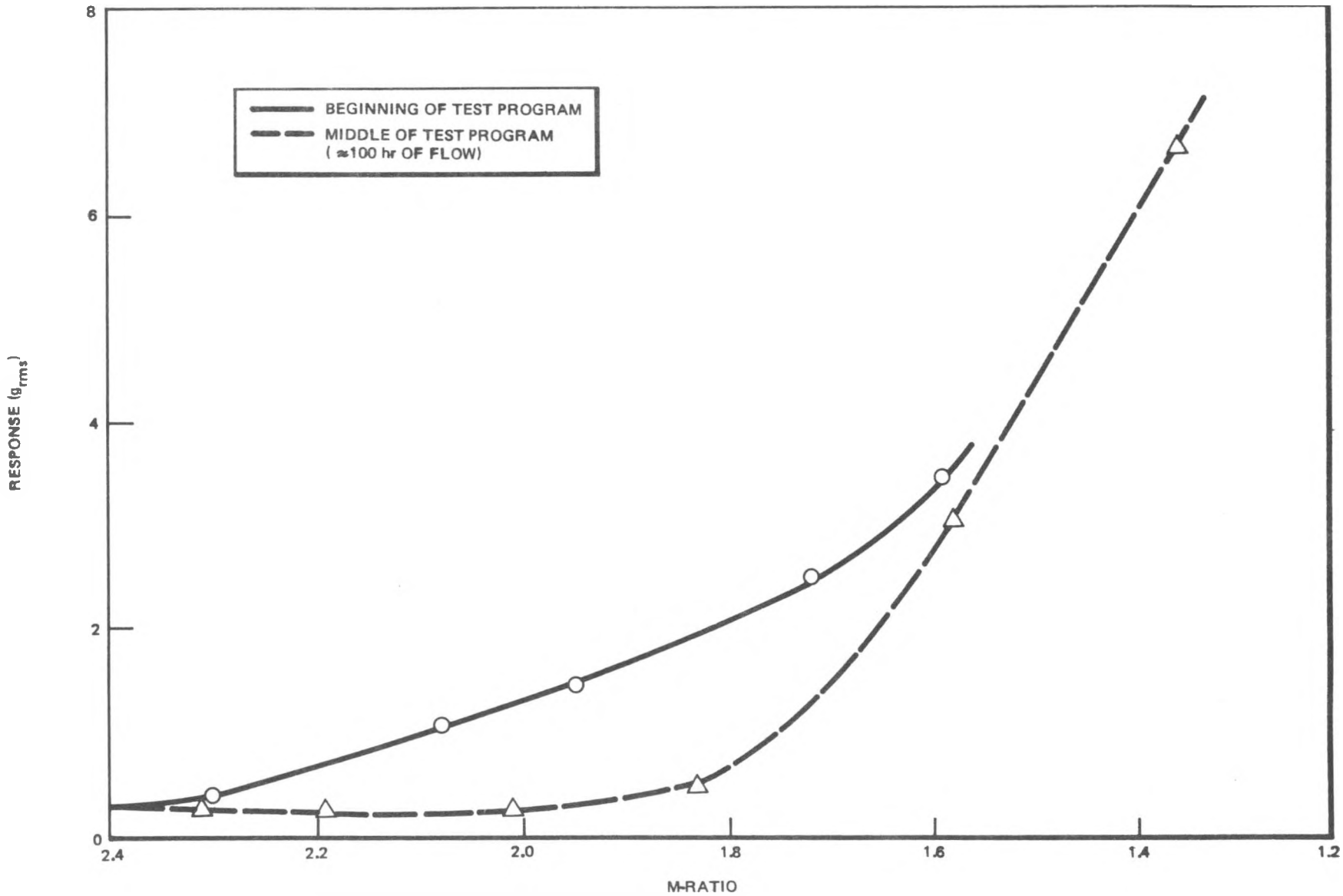

Figure 3-25. Jet Pump 2 Diffuser (Slip Joint) Radial Response at 100% Drive Flow versus M-Ratio; Beginning and Middle of Test Program

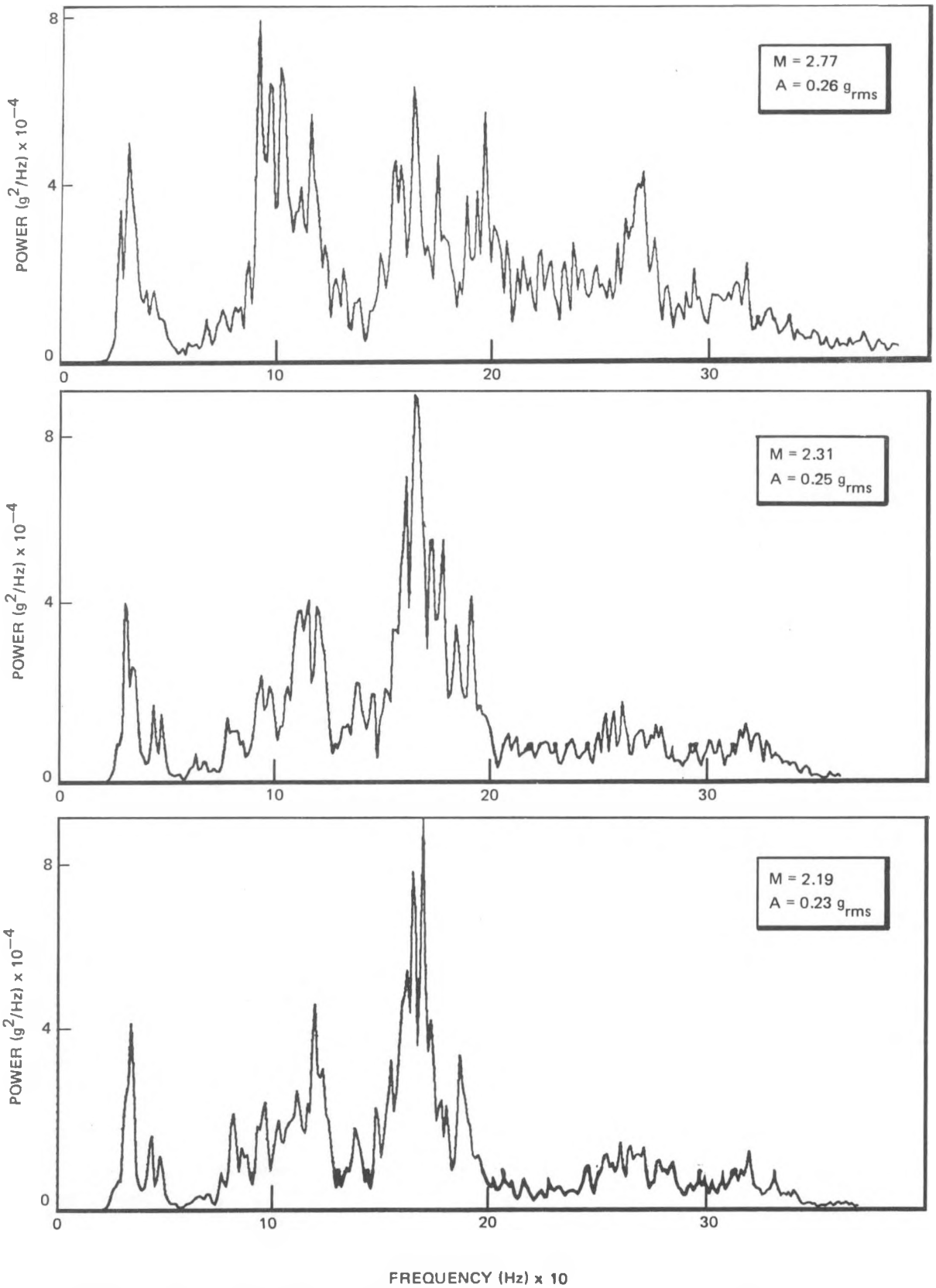

Figure 3-26. PSDs for Jet Pump 2 Mixer Radial Acceleration at Slip Joint for Several M-Ratios

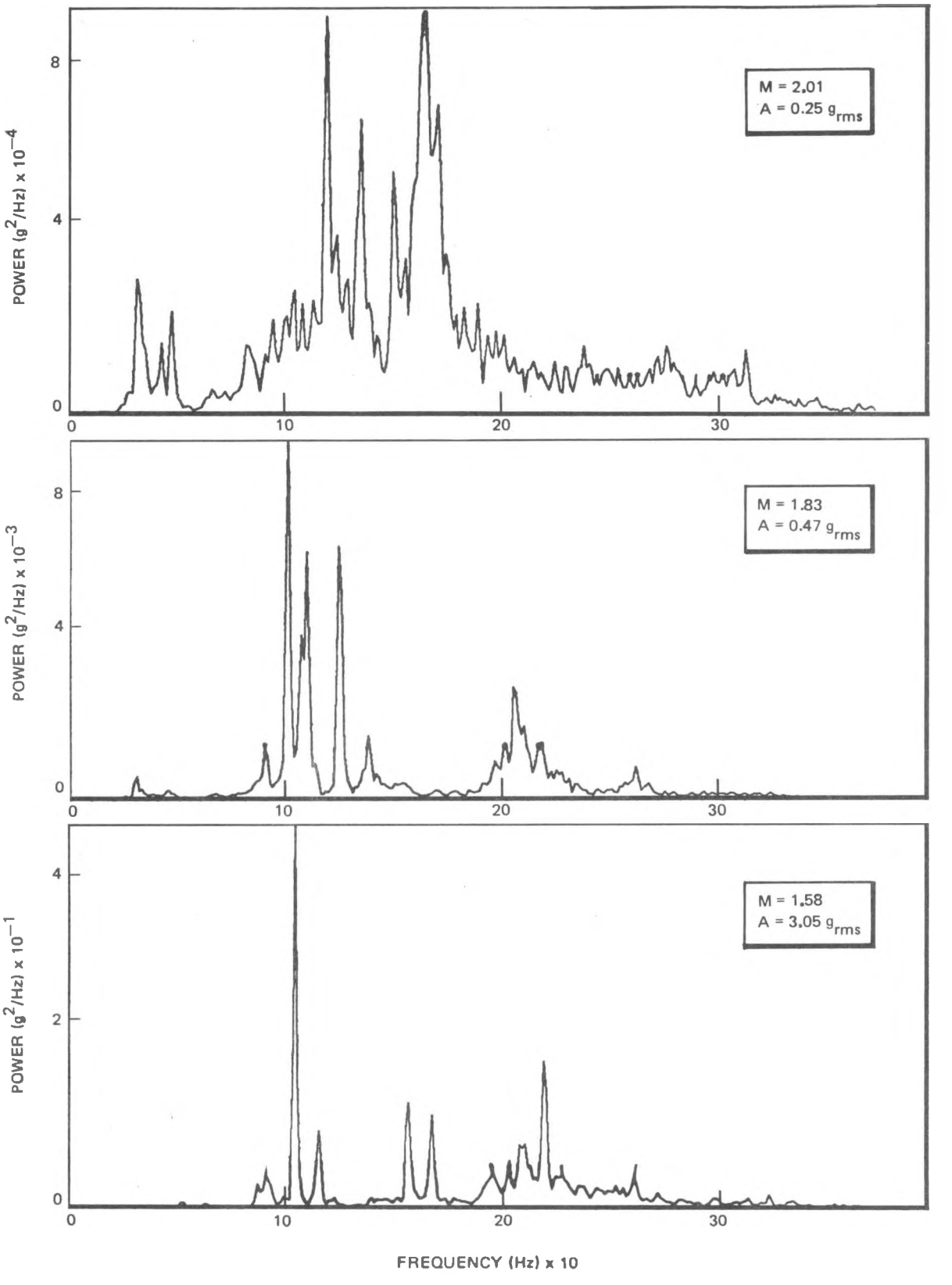

Figure 3-26. (Continued) PSDs for Jet Pump 2 Mixer Radial Acceleration at Slip Joint for Several M-Ratios

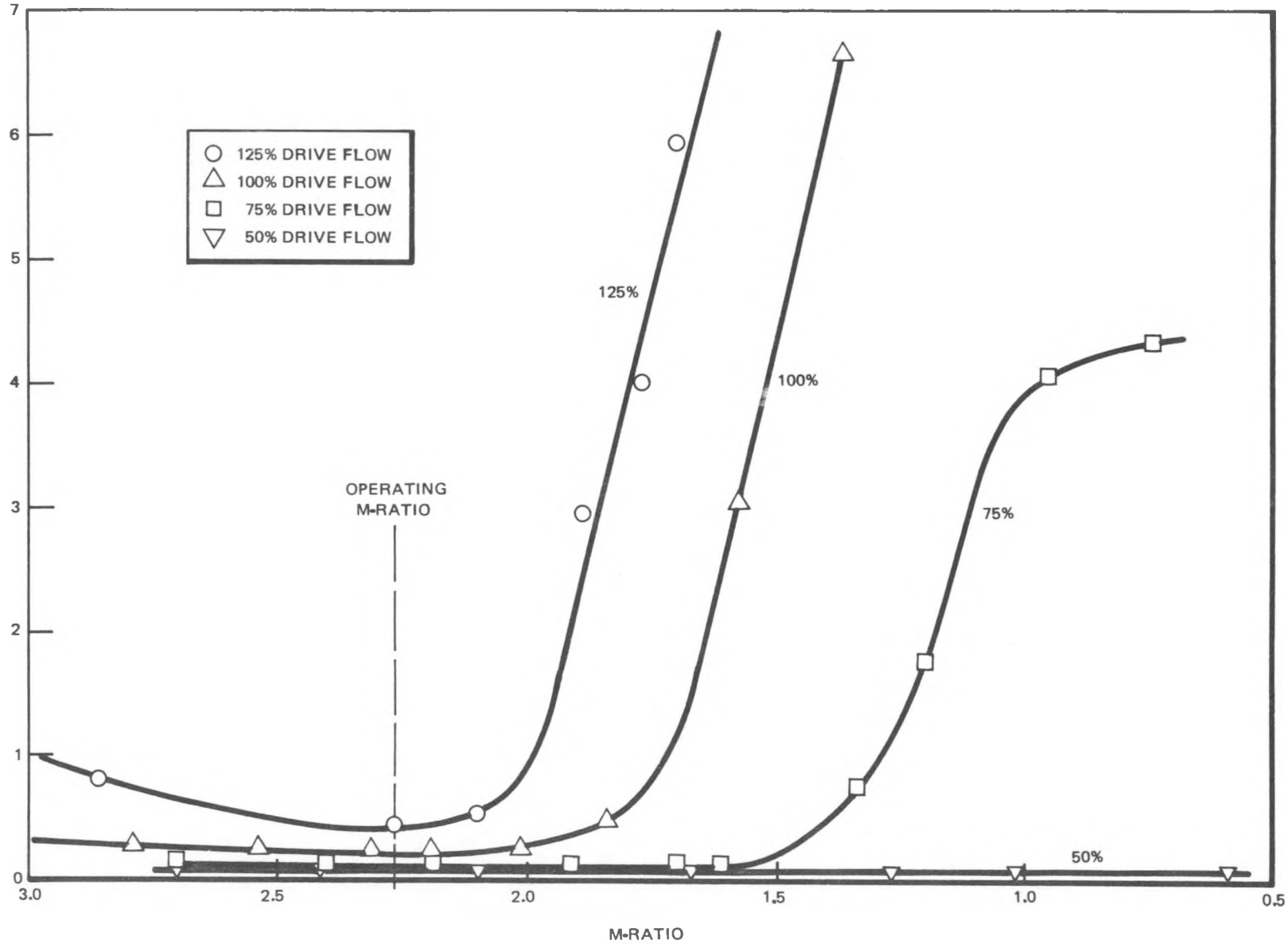

Figure 3-27. Jet Pump 2 Mixer Radial Response versus M-Ratio (Water Temperature = 180°F)

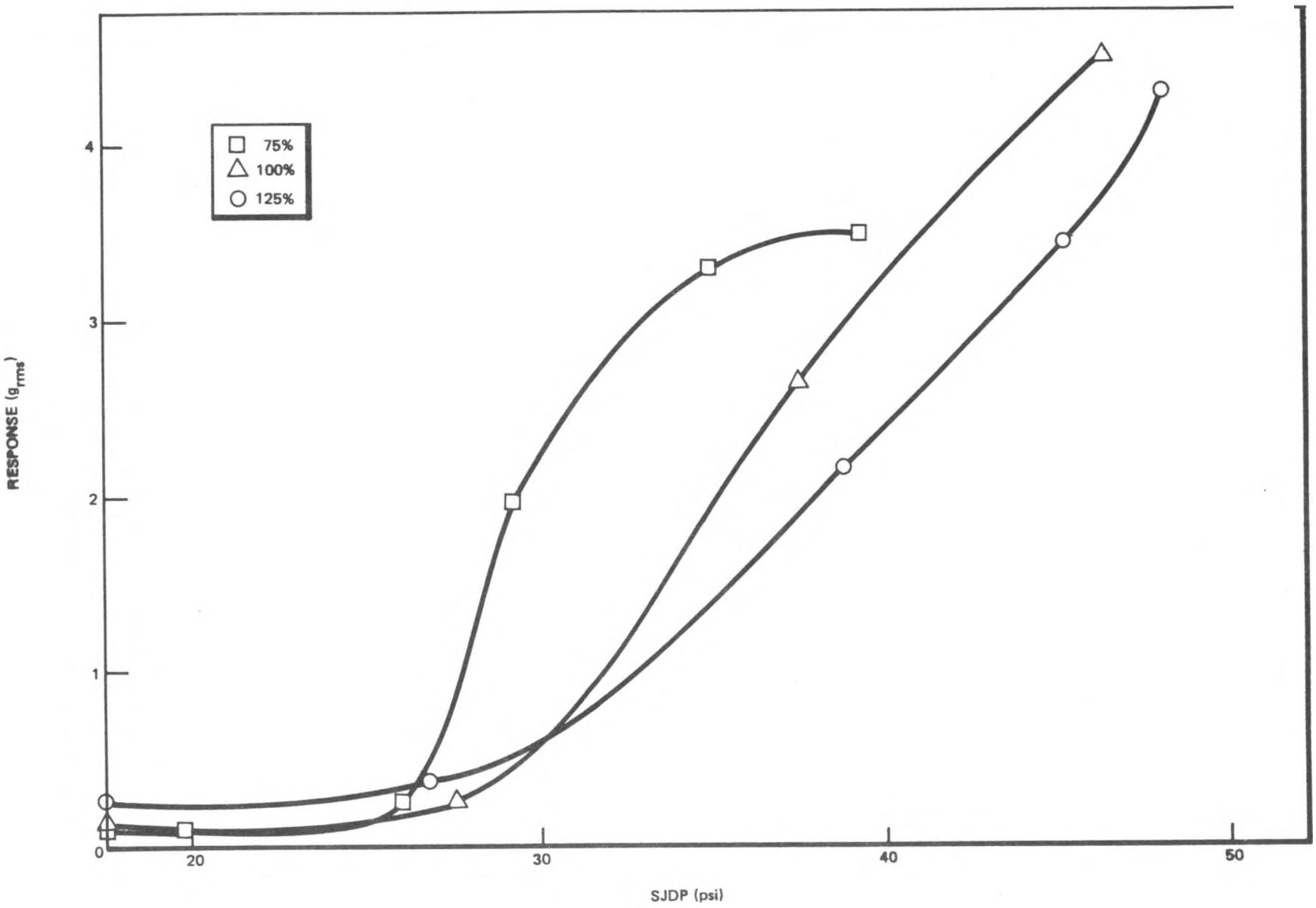

Figure 3-28. Jet Pump 1 Mixer Radial Acceleration as a Function of Slip Joint Pressure Differential (Water Temperature = 180°F)

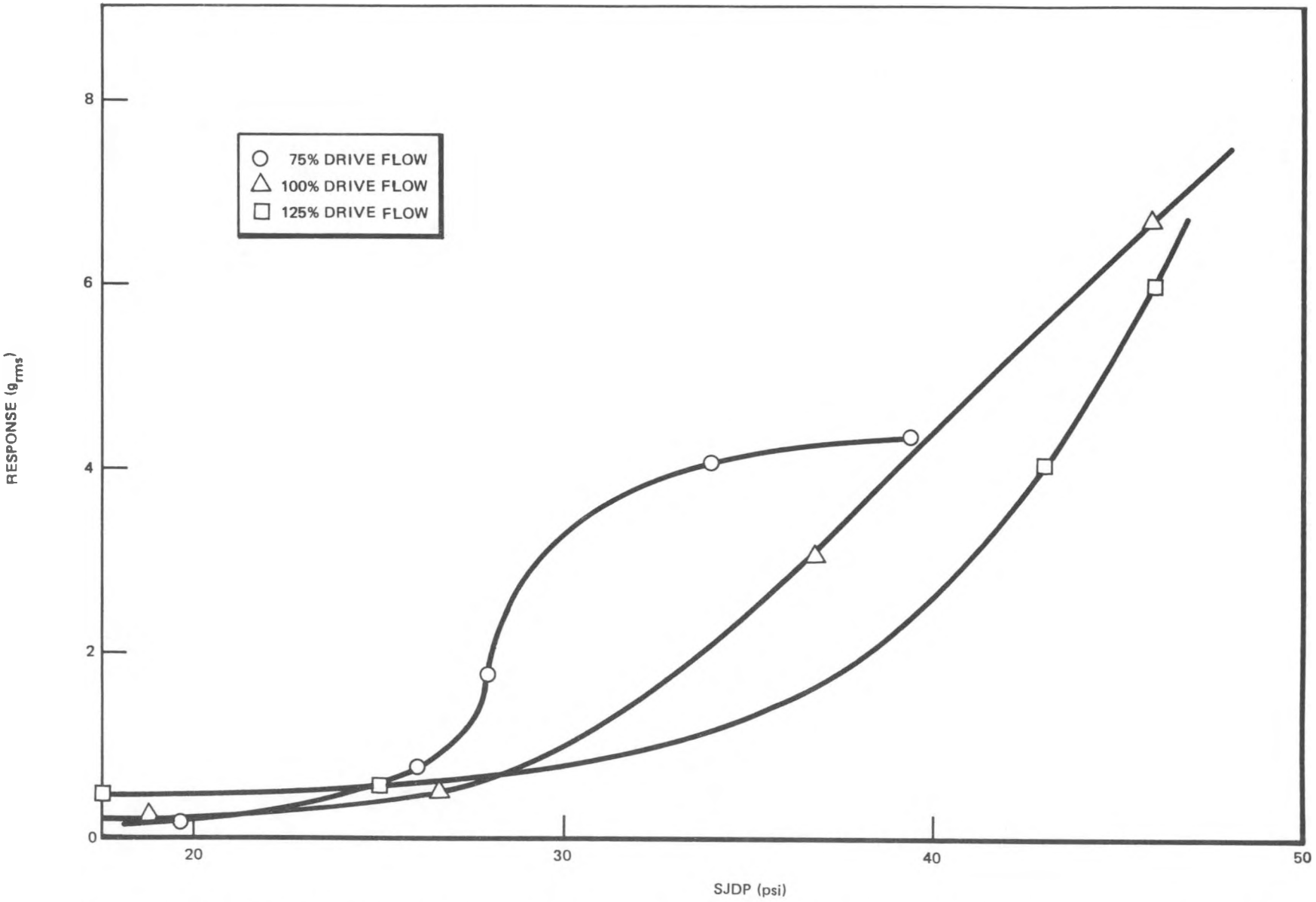

Figure 3-29. Jet Pump 2 Mixer Radial Acceleration as a Function of Slip Joint Pressure Differential (Water Temperature = 180°F)

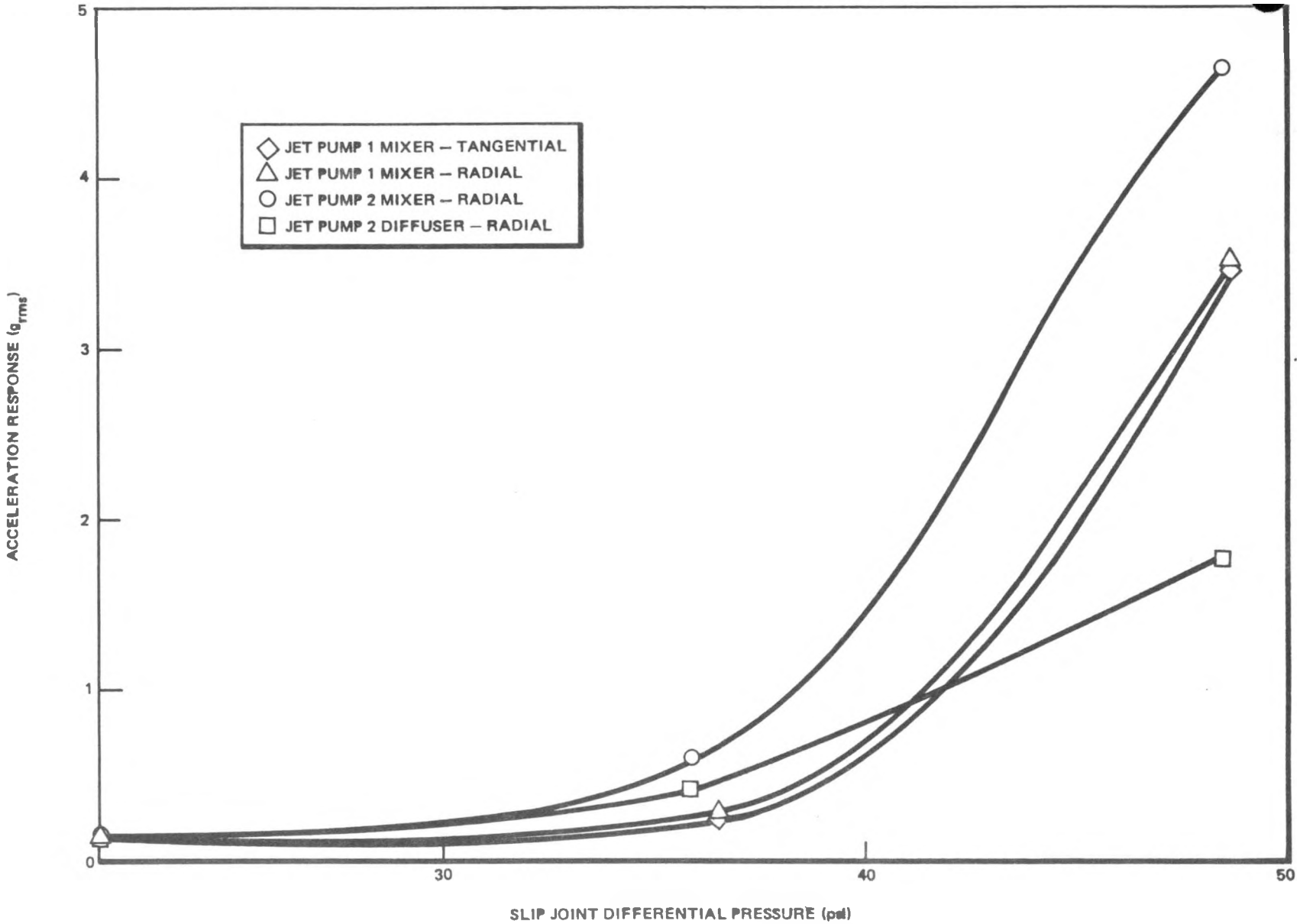

Figure 3-30. Jet Pumps 1 and 2 Acceleration Response at 100% Drive Flow as a Function of Slip Joint Pressure Differential (Water Temperature = 70°F)

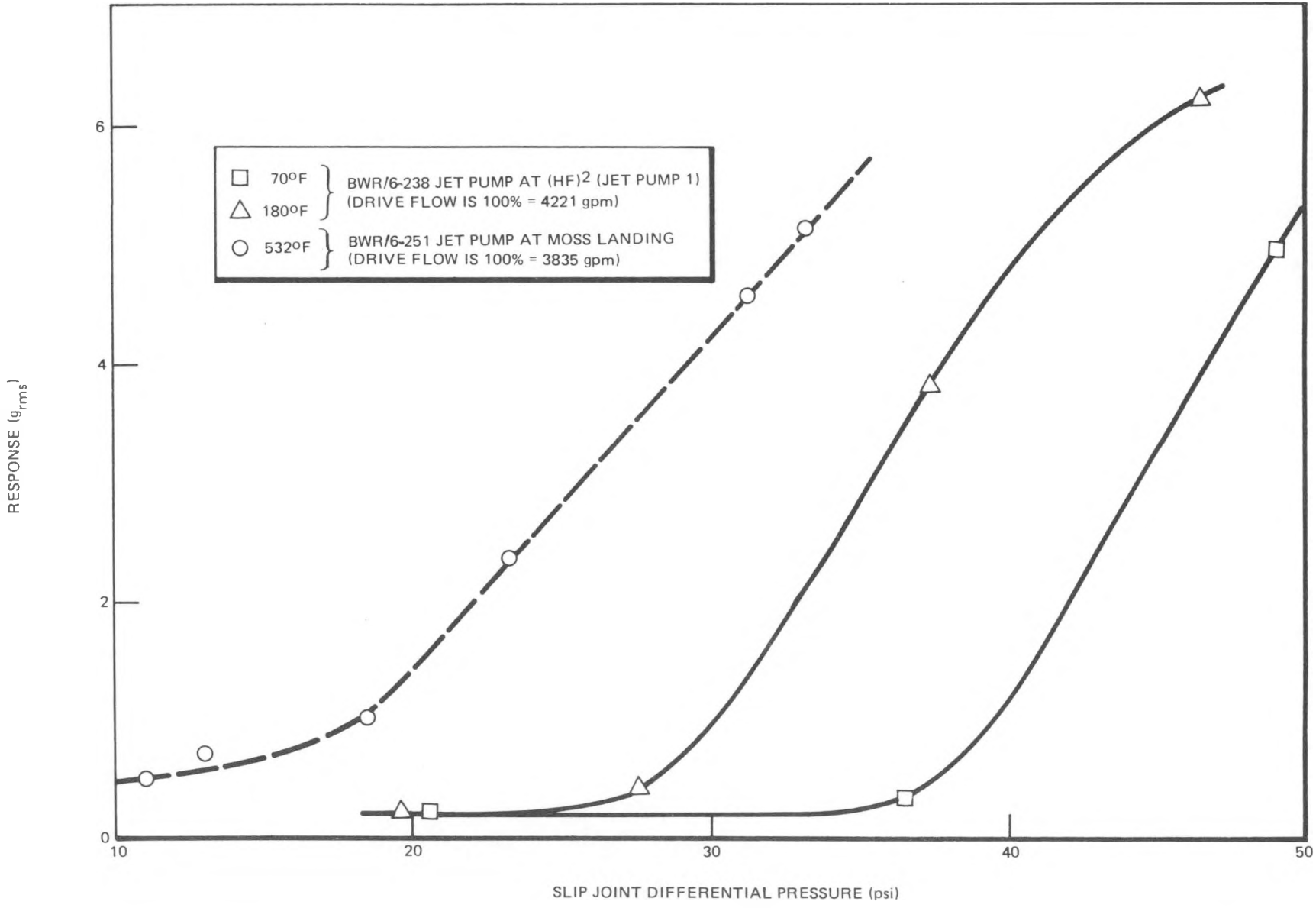

Figure 3-31. Jet Pump Mixer Slip Joint Response at Operating Drive Flow as a Function of Temperature

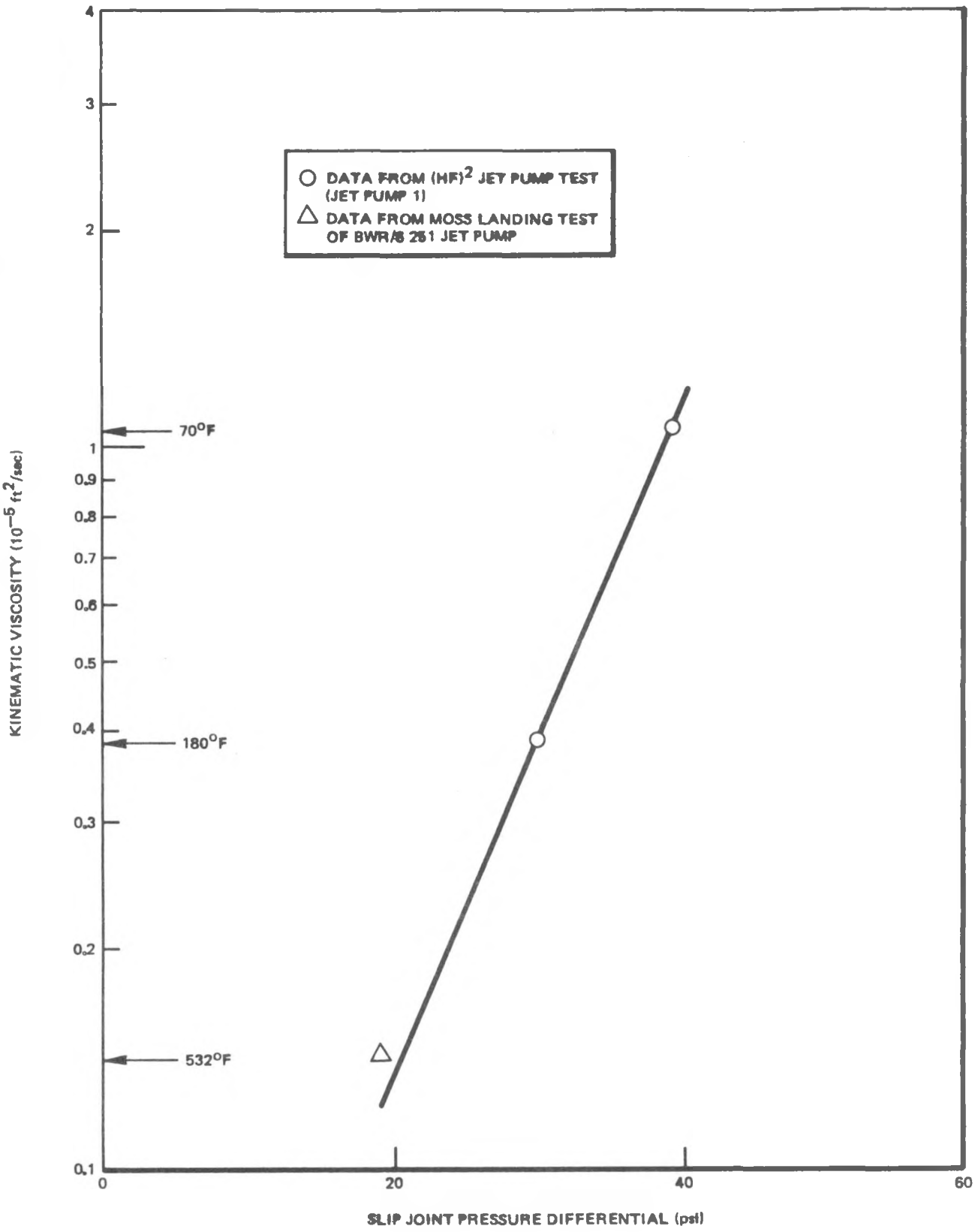

Figure 3-32. Kinematic Viscosity versus Slip Joint Differential Pressure at Onset of High Level Vibration ($1g_{rms}$)

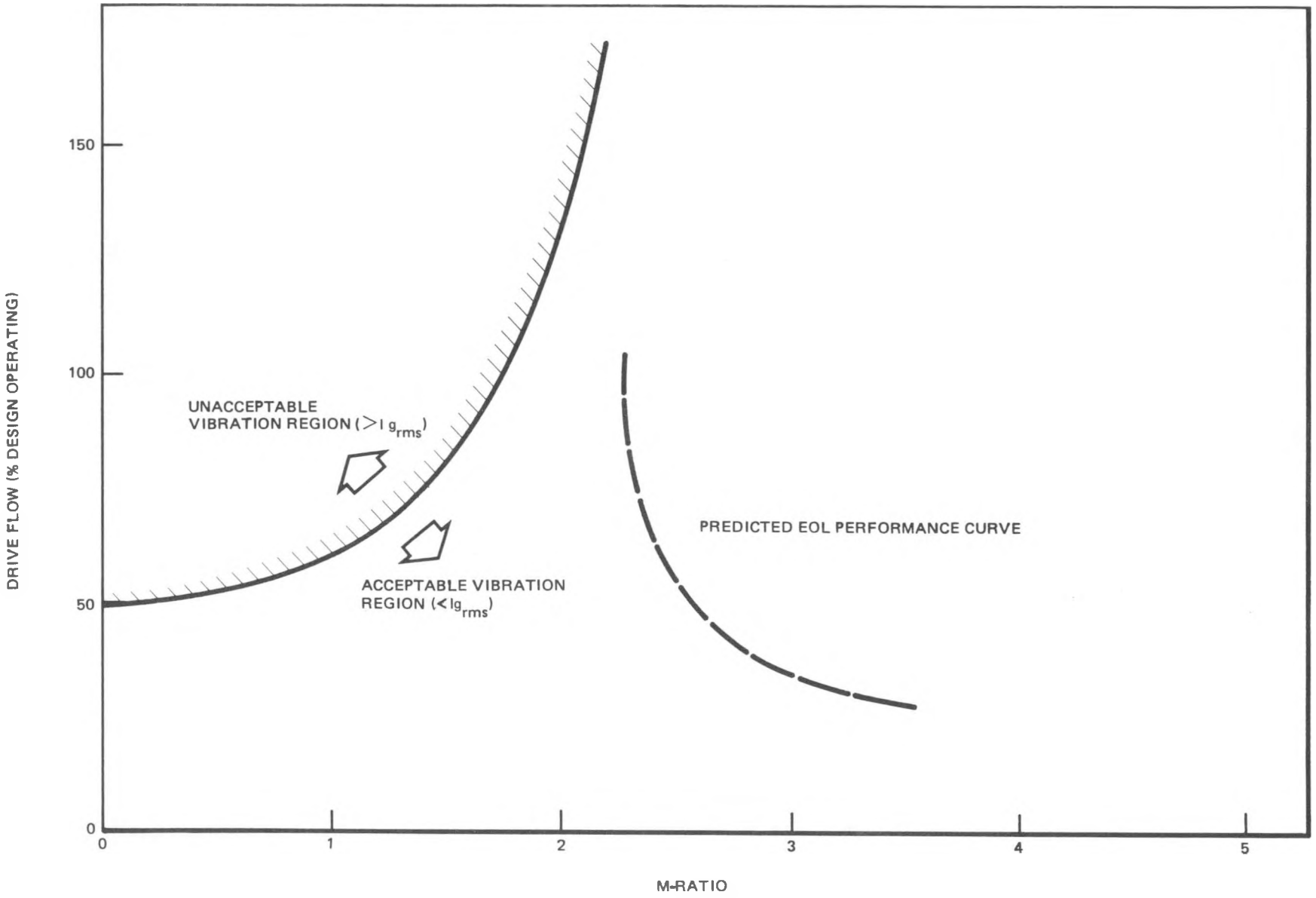

Figure 3-33. BWR/6-238 Jet Pump Operating Map

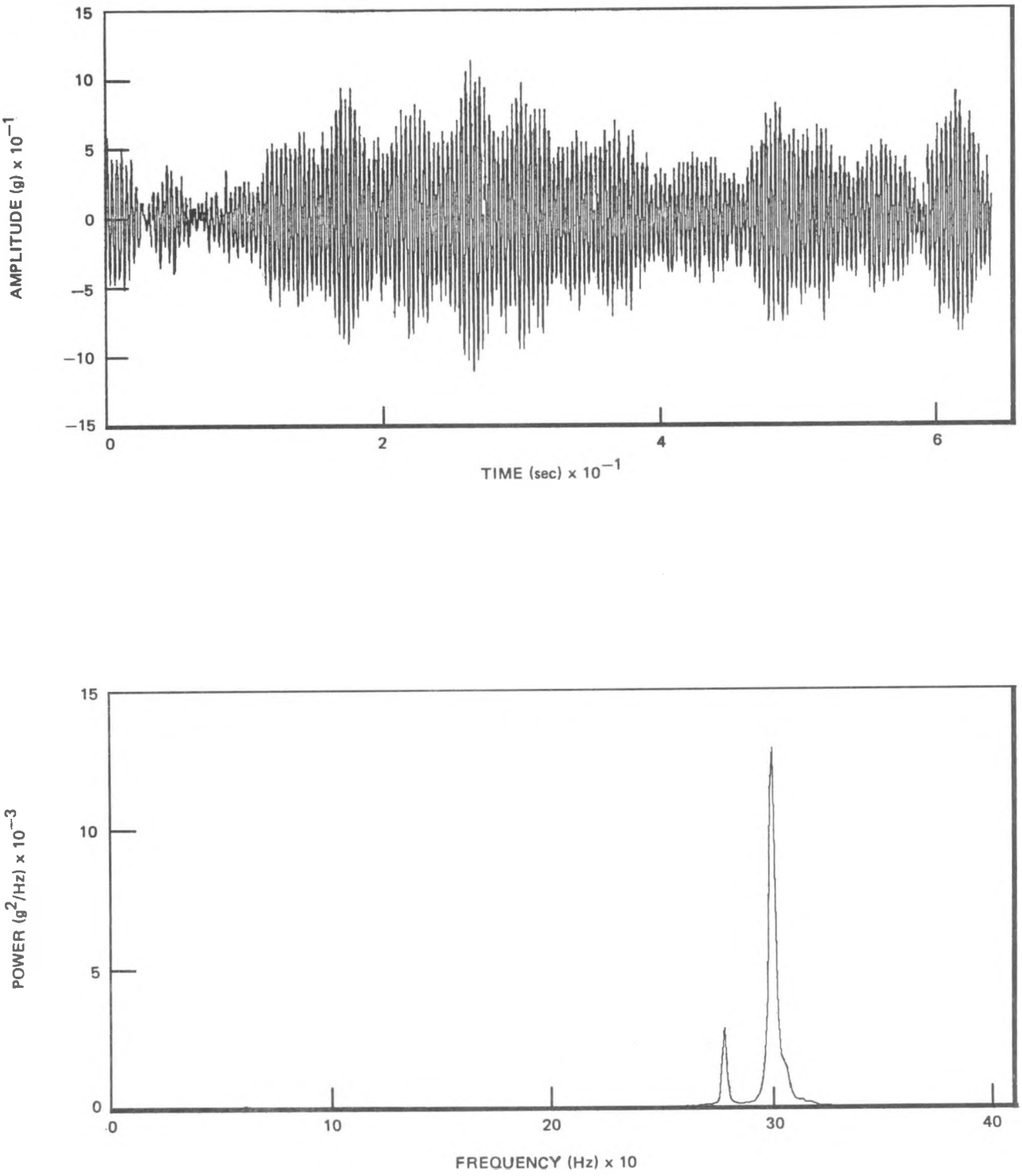

Figure 3-34. Upper Riser Brace Leaf Vertical Acceleration Response at Operating Drive Flow and M-Ratio (Water Temperature = 180°F)

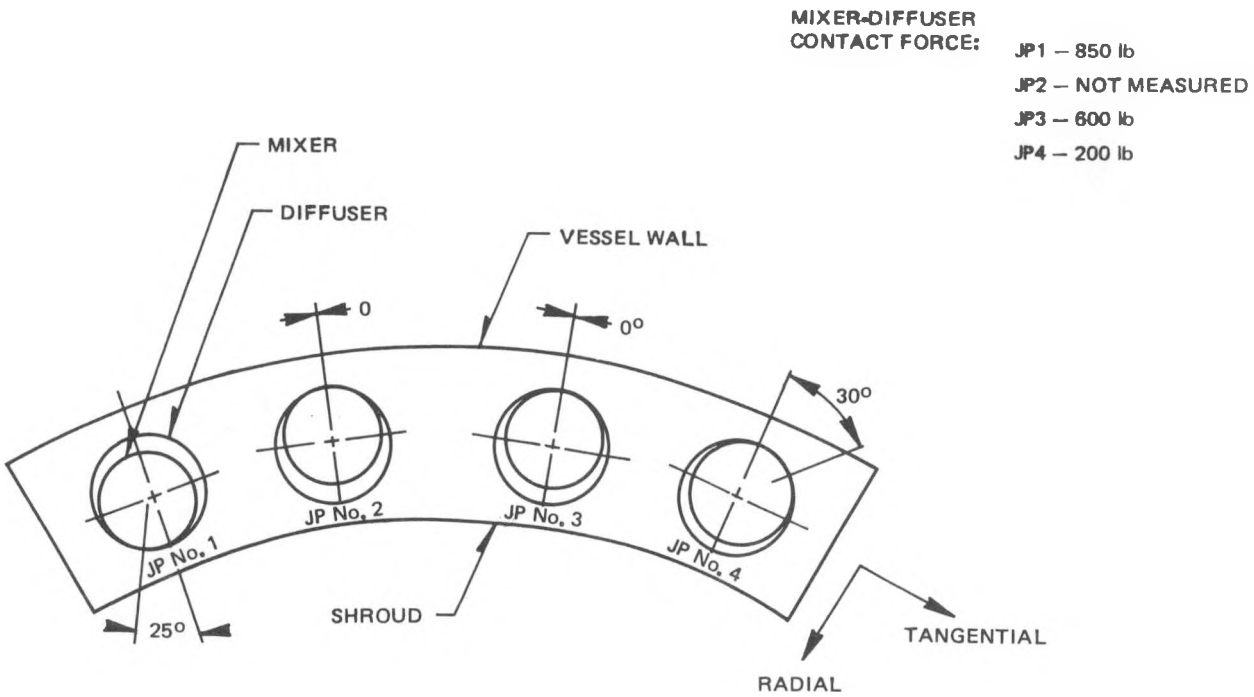

Figure 3-35. Mixer-Diffuser Slip-Joint Contact after Completion of FIV Test

4. DISCUSSION

In general, the $(HF)^2$ jet pump FIV program, using full-size prototypical test components, was successful. The $(HF)^2$ hydraulic system operated sufficiently well to cover the range of flow conditions desired. The vibration sensors utilized, including accelerometers, pressure tranducers and strain gages, were adequately placed to characterize the vibration response of the jet pumps and, with the exception of a slightly greater than expected failure rate, performed well throughout the test program. Finally, the $(HF)^2$ data acquisition and analysis systems (DAS and FASST) successfully processed the data so that it could be analyzed.

The two $(HF)^2$ jet pump pairs exhibited vibration characteristics similar to those observed for the BWR/6-218 and 251 (reported in NEDE-24190), as well as others that have been FIV tested in recent years at the PG&E Moss Landing Large Steam-Water Test Facility. Probably the most significant similarity was the existence of three separate, somewhat distinct vibration regimes. For the BWR/6-238, these may be characterized as:

(1) Low-Level Vibration Regime ($0.5g_{rms}$): the response is fairly random and the energy is spread over a 30-200 Hz frequency band. The vibrations are caused by the turbulent buffeting of the internal flow. The strains are a small fraction of the reactor design startup criteria.

(2) Transition Regime: the response is mid-level (approximately $0.5g_{rms}$ to $1.5g_{rms}$), and the energy is concentrated over smaller frequency bands, particularly in the 100-120 Hz region. The strains typically are still within the reactor design startup criteria.

(3) High-Level Regime: the response is greater than $1.5g_{rms}$ and the energy is concentrated primarily at specific frequencies, seemingly preferring the 100-120 Hz region, followed at increased intensities by the 50-60 Hz and 200-240 Hz regions. The response is caused by leakage flow through the mixer-diffuser slip joint which apparently leads to fluid-elastic coupling. Strains probably exceed the reactor design startup criteria, and continued operation in this regime will almost assuredly result in damage, such as broken tack welds and excessive wear.

The jet pump vibration response was found to be governed primarily by three interrelated parameters: (1) slip joint differential pressure; (2) water temperature; and (3) drive flow. If the water temperature and drive flow were maintained at constant levels, the three vibration regimes could be induced by simply sweeping the SJDP over a sufficiently wide range. At low pressure differentials, the vibrations would be low-level and relatively insensitive to change in SJDP. As the pressure differential was swept upward, the intensity would finally begin to rise, first gradually, as the jet pump entered the second regime, and, shortly thereafter, rapidly, as it entered the third regime. It appears that, at sufficiently high SJDPs, this third regime would tend to flatten, becoming somewhat insensitive to further pressure differential changes.

The effects of drive flow on the vibration response are somewhat more erratic. Increased drive flow will increase the vibration intensity in the low-level regime and the saturation level (level of flattening out) in the high-level regime. However, it has little effect on the transition from the first to second regime and appears to actually delay transition to the third.

Finally, water temperature does not seem to significantly affect the vibration intensity within each regime, but greatly affects the transition from one regime to another. As the temperature increases, the transition SJDPs decrease, being approximately linearly related to the log of the kinematic viscosity. For example, the relationship between kinematic viscosity and the SJDP required to induce $1g_{rms}$ at the slip joint was found to be:

$$SJDP = 40(1 + 0.25\ \ell n(\nu \cdot 10^5))$$

The obvious conclusion from this is that it is much easier to induce high-level (third regime) vibrations in jet pumps at reactor temperature ($532^{\circ}F$) than at the $(HF)^2$ temperatures (70° - $180^{\circ}F$).

The $(HF)^2$ jet pumps exhibited a fairly significant change in behavior during the early stages of the test program. For example, initially the transition from low to high-level vibration under operating drive flow and $180^{\circ}F$ water temperature commenced at an M-ratio of about 2.4 and was very gradual. However, after about 100 hours of operation, the transition was observed to commence at about 1.9 and to be much more rapid (more like a step change). This

modification in behavior, which persisted through the remainder of the FIV test program, is apparently due to geometric changes in the mixer-diffuser slip-joint region. At the beginning of the program, Jet Pumps 3 and 4 had a 3-mil minimum slip-joint gap. Jet Pumps 1 and 2 had no gap (the gaps were lost during shake tests) but, based on shake tests data evaluation, the slip joint preloads were low. However, post-FIV test inspections revealed all four jet pumps to have mixer-diffuser radial contact at the slip joint, with preloads ranging from 200 lb for Jet Pump 4 to 850 lb for Jet Pump 1, thus producing the change in the vibration characteristics. It is concluded from these results that:

(1) The jet pump slip-joint gap established during installation will very likely disappear shortly after the plant commences operation. Contact will probably occur in the radial direction, shortly after commencing operation.

(2) The loss of the slip-joint gap will tend to significantly shift the transition to high-level vibration to a lower M-ratio. However, the actual transition will be much more dramatic (i.e., the slope of the Response-SJDP curve in the second and third regimes will be much higher). For the BWR/6-238 jet pump, the net effect will be a significant increase in safety margin.

It should be noted that, since the responses of the jet pumps at the end of the test program were not significantly different from those at the middle, it was assumed they had now reached somewhat of a "shakedown" condition, similar to that which would exist in a reactor after the first few days of operation. Therefore, the post-shakedown data (that acquired midway into the test program and beyond) were used to evaluate the performance of the $(HF)^2$ jet pumps, although using the data acquired at the beginning of the program would not have altered the conclusions.

FIV test results revealed the $(HF)^2$ jet pump response under design operating drive flow and M-ratio to be low-level random, at approximately 10% of the BWR/6-238 startup vibration criteria. However, since they also revealed the transition to high-level vibration to be related to temperature, it was necessary to extrapolate the results to 532°F in order to properly evaluate the vibration response. This was accomplished through the following process:

(1) An empirically based equation was developed to relate the key hydraulic parameters: SJDP, drive flow, M-ratio, and water density. The method was confirmed by testing it on 180°F and 532°F data from the BWR/5-201 jet pump FIV test at Moss Landing (as reported in NEDE-24153, "Flow-Induced Vibration Characteristics of the BWR/5-201 Jet Pump").

(2) The jet pump FIV response was completely characterized at 180°F, the end result being vibration response curves as a function of drive flow and SJDP.

(3) A vibration intensity limit was established ($1g_{rms}$ at the slip joint), based on the vibration response curves as well as the BWR/6-238 startup vibration criteria, beyond which the response was considered unacceptible ($1g_{rms}$ corresponded to about 50% of the BWR/6 startup criteria, but was at a point on the response plot where small SJDP increases resulted in large increases in vibration intensity).

(4) A relationship between the $1g_{rms}$ vibration intensity and the drive flow and SJDP was developed for the 70°F and 180°F $(HF)^2$ conditions and extrapolated to 532°F, using as a basis the kinematic viscosity (as discussed previously). The 532°F extrapolation was verified using results from the BWR/6-251 jet pump FIV test at the Moss Landing Large Steam-Water Test Facility (as reported in NEDE-24190, "Flow-Induced Vibration Characteristics of BWR/6 Jet Pumps"), since the BWR/6-251 is very similar geometrically.

(5) The equation relating SJDP to drive flow, M-ratio, and water density was coupled with the extrapolated $1g_{rms}$ vibration intensity-SJDP-drive flow relationship to produce an operating map (Figure 3-33), which defines the acceptable and unacceptable drive flow/M-ratio combinations at 532°F (acceptable being those combinations which result in vibration intensities below $1g_{rms}$ at the slip joint).

When the predicted end-of-life (EOL) performance curve for the BWR/6-238 jet pump was plotted on the operating map (Figure 3-33), it was found to lie well within the acceptable vibration level boundary, clearly indicating that the vibration response should be satisfactory at reactor conditions.

The FIV acceleration response of the riser brace leaves was measured, using accelerometers and strain gages, and found to be dominated under most flow conditions by a 300 Hz component and, to a lesser extent, a 280 Hz component. The 300 Hz component apparently is the first bending mode of the adjacent (top and bottom) leaves as they vibrate in-phase. The 280 Hz component is the first bending mode response of the adjacent leaves when out-of-phase. Because the two frequencies are close together, their combined effect is to cause the leaves to beat.

5. CONCLUSIONS

The key conclusions from the $(HF)^2$ jet pump test program may be summarized as follows:

(1) The vibration response of the BWR/6-238 jet pumps in the $(HF)^2$ environment ($70^{\circ}F$ to $180^{\circ}F$) and at reactor volumetric drive flow and M-ratio is low-level random, well within the BWR/6 design vibration criteria. The projected response at $532^{\circ}F$ (reactor conditions), though higher than at $(HF)^2$ conditions, is also well within the criteria.

(2) As has been observed with other jet pumps tested in the past, an increase in drive flow or decrease in M-ratio from the design operating conditions will cause the vibration response to increase. Under certain drive flow/M-ratio combinations, which for the BWR/6-238 are far removed from the predicted operating curve, high-level periodic vibrations can be induced which, if left unchecked, will result in jet pump damage.

(3) The low-level random vibration response, which typically occurs at low drive flows or medium and high M-ratios, is due to the turbulent buffeting of the fluid in the jet pump, and is governed by the fluids' velocity. The high-level periodic response, which occurs at low M-ratios and medium and high drive flows, is primarily related to the leakage flow out of the slip joint and, consequently, to the slip joint differential pressure.

(4) The slip-joint gap, which is set at a minimum of 2 mils during installation to comply with BWR/6-238 installation procedures, probably will not endure very long into reactor operation, with mixer-diffuser contact occurring in the radial direction. The effect will be to require greater slip joint differential pressures to induce high-level vibration, thus providing the BWR/6-238 jet pumps with an additional margin of safety.

(5) In extrapolating the $(HF)^2$ test results to reactor conditions, the following key hydraulic and hydroelastic relationships were demonstrated:

(a) For a given jet pump design, the slip joint differential pressure scales with the fluid kinetic energy. That is, SJDP α ρ $(1+M)^2$ W_D^2, where ρ = water density, M = M-ratio, and W_D = drive flow.

(b) The SJDP at the transition from low level vibration scales with the natural log of the kinematic viscosity. It is relatively insensitive to drive flow.

(6) The fundamental frequency of the riser brace leaves is approximately 300 Hz when adjacent leaves are in-phase and 280 Hz when out-of-phase.

6. REFERENCES

1. L. V. LaCroix, **Flow-Induced Vibration Characteristics of the BWR/5-201 Jet Pump**, NEDE-24153, January 1979.

2. L. C. LaCroix, **Flow-Induced Vibration Characteristics of BWR/6 Jet Pumps**, NEDE-24190, May 1979.

3. J. F. Schardt, **Modal Characteristics of BWR/6-238 Jet Pumps**, NEDE-24198, June 1979.

4. G. Hu, **Vibration Analysis for the Reactor Internals of BWR/6-238 Plants**, NEDE-23840, April 1978.

5. Recirculation System Performance Data Sheet, General Electric Document No. 383HA827AB (BWR/6-238 Plant).

Table A1

TEST HYDRAULIC CONDITIONS - PHASE I

(DAS PLAN I)

Test No.	Temp (°F)	Drive Flow (% Rated) JP 1&2	Drive Flow (% Rated) JP 3&4	M-Ratio JP1	M-Ratio JP2	M-Ratio JP3	M-Ratio JP4	Slip Joint DP JP1	Slip Joint DP JP2	Slip Joint DP JP3	Slip Joint DP JP4
NS1	68	0	0	Background noise							
NS2	68	0	0	Background noise - 100 psi - Press. Pump Off							
NS3	69	0	0	Background noise - 100 psi - Press. Pump On							
NS5	69	0	0	Background noise - 300 psi - Press. Pump On							
NS6	69	0	0	Background noise - 300 psi - Press. Pump Off							
PS0	70	0	0	100% bypass flow							
PS2	70	0.48	0.48	2.20	2.25	2.25	2.40	3.6	3.1	3.2	2.7
PS3	70	0.23	0.23	2.34	2.26	2.43	2.70	1.9	1.6	1.5	1.3
PS4	70	1.00	1.00	2.22	2.23	2.16	2.14	11.6	11.1	11.9	10.4
PS7	72	0	0	Background noise - 450 psi - Press. Pump Off							
QS0	70	1.00	0.99	2.26	2.30	2.22	2.35	8.7	8.4	9.9	8.5
QS1	70	0.52	0.51	2.23	2.32	2.22	2.47	2.5	2.4	2.7	2.4
QS2	70	0.24	0.23	2.36	2.48	2.56	3.01	0.5	0.6	0.4	0.4
QS5	124	0	0	Background noise - 450 psi - Press. Pump Off							
QS6	125	1.00	1.00	2.26	2.31	2.25	2.38	8.8	8.4	8.9	7.7
RS1	180	0	0	Background noise - 450 psi - Press. Pump Off							
RS2	180	1.00	1.01	2.22	2.29	2.27	2.40	9.5	9.0	8.2	7.0
RS3	180	0.23	0.23	2.42	2.52	2.50	2.92	0.5	0.6	0.4	0.3
RS4	179	0.52	0.50	2.23	2.27	2.23	2.45	2.0	2.0	2.4	2.0
RS5	180	0.52	0.50	2.75	2.73	2.74	2.95	-3.5	-3.7	-3.4	-3.7
RS6	182	0.99	1.01	2.39	2.43	2.40	2.54	3.5	3.2	2.4	0.8
RS7	180	0.74	0.74	2.14	2.20	2.13	2.30	7.2	7.0	7.3	6.5
RS8	181	0.77	0.76	2.76	2.77	2.71	2.88	-3.5	-3.7	-4.0	-3.7
RS9	181	0.76	0.75	2.12	2.18	2.07	2.23	8.0	7.8	8.6	7.9
SS1	180	0.76	0.75	2.00	2.07	1.93	2.14	10.8	10.5	11.6	10.7
SS2	181	0.76	0.75	1.93	2.00	1.87	2.07	12.2	11.9	13.0	12.1
SS3	180	0.76	0.74	1.85	1.91	1.79	1.98	14.3	14.1	15.1	14.3
SS4	180	0.76	0.76	1.66	1.77	1.72	1.93	17.1	16.9	17.2	16.1
SS5	180	0.50	0.50	2.71	2.80	2.82	3.03	-3.6	-3.5	-3.7	-3.8
SS6	180	0.50	0.50	2.13	2.28	2.28	2.48	2.30	2.36	2.27	1.69

Table A1 (Continued)

Test	Temp	Drive Flow (% Rated)		M-Ratio				Slip Joint DP			
No.	(°F)	JP 1&2	JP 3&4	JP1	JP2	JP3	JP4	JP1	JP2	JP3	JP4
SS7	180	0.76	0.76	1.58	1.66	1.61	1.82	19.8	19.7	20.0	19.0
SS8	180	0.75	0.75	1.50	1.60	1.53	1.73	20.7	20.7	20.9	20.0
TS1	181	0.75	1.00	2.16	2.24	2.18	2.32	11.9	11.5	11.8	10.4
TS2	181	1.01	1.01	2.72	2.75	2.71	2.87	-3.6	-3.7	-4.1	-3.7
TS3	180	1.00	1.00	2.22	2.30	2.25	2.38	9.37	9.06	9.34	7.83
TS4	180	1.00	1.00	1.96	2.08	2.01	2.16	18.9	18.4	18.7	17.3
TS5	180	1.00	1.00	1.97	2.08	2.00	2.17	19.0	18.4	19.0	17.3
TS6	181	1.00	1.01	2.14	2.25	2.17	2.29	12.1	11.6	12.0	10.8
TS7	178	1.00	1.00	1.84	1.95	1.87	2.05	23.4	23.0	23.6	22.1
TS9	180	1.00	1.00	1.70	1.79	1.72	1.90	29.7	29.4	29.7	28.2
US0	180	1.00	1.00	1.61	1.72	1.66	1.83	33.2	32.7	33.1	31.7
US1	180	1.00	1.00	1.48	1.59	1.55	1.73	38.7	38.3	38.3	36.9
US2	180	0.73	0.75	1.38	1.51	1.46	1.65	22.0	21.9	21.9	21.0
US3	180	0.74	0.75	1.31	1.44	1.38	1.58	23.5	23.5	23.5	22.6
US5	181	0.74	0.75	1.09	1.21	1.17	1.36	28.3	28.4	28.4	27.5
US6	180	0.48	0.49	1.73	1.95	1.99	2.16	5.1	5.2	4.8	4.4
US7	179	0.48	0.49	1.59	1.79	1.83	2.04	6.7	6.8	6.4	5.9
US8	179	0.48	0.49	1.35	1.57	1.63	1.87	8.9	8.9	8.5	8.1
VS0	179	0.48	0.49	1.98	2.19	2.20	2.39	3.2	3.3	2.9	2.3
VS1	180	0.75	0.75	2.07	2.19	2.14	?	7.3	7.1	7.1	6.0
VS2	180	1.00	1.01	2.33	2.41	2.23	?	5.1	4.8	5.3	3.6
VS3	178	0.48	0.49	1.18	1.43	1.41	1.69	10.6	10.7	10.5	9.9
VS4	177	0.22	0.23	2.31	2.89	2.94	3.54	-0.8	-0.6	-0.9	-1.2
VS5	176	0.23	0.23	1.26	2.17	2.26	3.30	1.1	1.3	1.1	0.7
WS2	125	0.99	1.00	2.21	2.26	2.22	2.39				
WS3	180	1.00	1.02	2.20	2.28	2.23	2.34	9.2	8.2	8.2	6.9
WS4	178	0.27	0.26	2.10	1.94	1.86	1.91	0.4	0.5	0.7	0.6
WS5	179	0.52	0.50	2.19	2.18	2.10	2.25	1.86	1.78	2.50	1.98
WS6	180	0.77	0.75	2.20	2.25	2.13	2.24	4.28	3.89	5.57	4.60
WS7	180	1.02	1.02	2.79	2.79	2.79	2.91	-3.4	-3.5	-3.9	-3.6
WT0	178	0.46	0.52	2.56	2.51	2.72	2.85	-2.0	-2.0	-3.8	-3.5
WT1	180	1.00	1.00	2.77	2.77	2.72	2.85	-3.4	-3.5	-3.9	-3.6

Table A1 (Continued)

Test	Temp	Drive Flow (% Rated)		M-Ratio				Slip Joint DP			
No.	(°F)	JP 1&2	JP 3&4	JP1	JP2	JP3	JP4	JP1	JP2	JP3	JP4
WT2	178	1.00	1.01	2.52	2.54	2.53	2.64	-2.6	-3.0	-3.4	-3.6
WT3	179	1.02	1.01	2.26	2.31	2.29	2.39	7.3	6.5	7.0	5.7
WT4	180	1.01	1.01	2.13	2.19	2.14	2.26	12.4	11.6	12.0	10.6
WT5	180	0.99	1.01	1.93	2.01	2.01	2.13	19.6	18.7	17.6	16.3
WT6	177	1.01	1.02	1.74	1.83	1.77	1.90	27.5	26.6	26.9	25.7
WZ0	180	1.02	1.02	1.53	1.58	1.50	1.64	37.4	36.8	37.5	36.3
WZ1	180	1.02	1.02	1.32	1.36	1.27	1.43	46.3	45.7	46.5	45.3
WZ2	181	1.01	1.01	2.77	2.77	2.73	2.85	-3.4	-3.5	-3.8	-3.6
WZ3	177	0.48	0.50	2.62	2.59	2.63	2.78	-2.7	-2.7	-3.1	-3.5
WZ4	179	0.76	0.76	2.71	2.70	2.66	2.76	-3.4	-3.5	-3.8	-3.6
WZ5	179	0.76	0.76	2.36	2.46	2.35	2.42	0.9	0.6	0.9	0.0
WZ6	180	0.76	0.77	2.09	2.18	2.10	2.20	7.2	6.6	7.0	6.1
WY0	182	0.77	0.77	1.87	1.91	1.88	1.99	12.5	12.1	12.3	11.5
WY1	177	0.77	0.77	1.64	1.70	1.63	1.75	17.7	17.3	17.6	16.9
WY2	180	0.76	0.77	1.58	1.61	1.56	1.68	19.5	19.2	19.4	18.6
WY3	180	0.76	0.76	1.31	1.34	1.26	1.40	26.0	25.8	26.2	25.6
WY4	179	0.76	0.76	1.17	1.20	1.11	1.25	29.2	29.0	29.4	28.8
WY5	180	0.77	0.76	0.92	0.95	0.85	0.99	34.8	34.6	34.9	34.4
WY6	179	0.76	0.76	0.74	0.74	0.65	0.74	39.2	39.2	39.5	39.1
WX0	177	0.49	0.49	2.75	2.71	2.70	2.80	-3.5	-3.4	-3.3	-3.6
WX1	178	0.50	0.50	2.45	2.42	2.43	2.55	-0.8	-0.8	-0.7	-1.2
WX3	176	0.49	0.50	2.10	2.10	2.13	2.19	2.7	2.7	2.5	2.1
WX4	175	0.49	0.50	1.83	1.90	1.85	1.90	5.3	5.2	5.1	4.8
WX5	176	0.49	0.50	1.63	1.67	1.62	1.71	7.4	7.4	7.3	6.9
WX6	176	0.49	0.50	1.44	1.49	1.44	1.55	9.0	9.0	8.9	8.5
WW0	176	0.49	0.50	1.27	1.27	1.23	1.32	11.1	11.1	11.2	10.8
WW1	177	0.49	0.50	1.02	1.02	1.00	1.08	13.4	13.4	13.5	13.1
WW2	178	0.49	0.50	0.65	0.59	0.60	0.64	17.3	17.3	12.3	17.1
WW3	176	0.24	0.24	2.88	2.67	2.57	2.57	-1.1	-1.0	-0.8	-1.0
WW4	174	0.24	0.24	2.69	2.49	2.32	2.26	-0.7	-0.6	-0.3	-0.5
XS1	180	0.125	1.27	2.86	2.86	2.89	2.94	-3.5	-3.6	-4.0	-3.7
XS2	180	0.122	1.24	2.19	2.28	2.17	2.25	16.8	15.4	16.2	14.8

Table A1 (Continued)

Test	Temp	Drive Flow (% Rated)		M-Ratio				Slip Joint DP			
No.	(°F)	JP 1&2	JP 3&4	JP1	JP2	JP3	JP4	JP1	JP2	JP3	JP4
XS3	178	0.121	1.23	2.01	2.10	1.98	2.08	26.8	25.1	26.2	24.8
SX4	178	0.120	1.22	1.78	1.89	1.80	1.90	38.7	37.0	37.6	36.3
XS5	179	0.121	1.24	1.67	1.77	1.71	1.82	44.6	43.1	42.8	41.4
XS6	177	0.120	1.21	1.58	1.70	1.59	1.72	47.9	46.1	46.9	45.5
XS7	174	0.25	0.25	2.80	2.58	2.47	2.50	-1.3	-1.1	-1.0	-1.1
XS8	173	0.25	0.25	2.38	2.26	2.09	2.09	-0.2	0.0	0.1	-0.1
XS9	173	0.25	0.25	2.10	2.00	1.85	1.83	0.5	0.6	0.8	0.6
YS0	172	0.25	0.25	1.74	1.66	1.43	1.41	1.5	1.5	1.6	1.5
YS1	171	0.25	0.25	1.57	1.48	1.22	1.17	1.9	2.0	2.1	2.0
YS2	171	0.25	0.25	1.39	1.27	1.05	0.92	2.4	2.5	2.7	2.5
YS3	170	0.25	0.25	1.20	1.01	0.77	0.67	2.9	3.1	3.2	3.0
YS4	169	0.25	0.25	0.94	0.69	0.45	0.31	3.7	3.7	3.9	3.7
YS5	180	0.95	0.95	M-ratio sweep							
YS6	180	0.07	1.01	27.25	23.54	1.99	2.49	23.1	25.4	14.3	8.0
YS7	178	0.08	1.02	22.64	19.83	2.11	2.72	18.6	19.9	6.0	-2.5
YS8	177	0	0	Background - 396 psi - Press. Pump Off							

Table A2

TEST HYDRAULIC CONDITIONS - PHASE II

(DAS PLAN II)

Test No.	Temp (°F)	Drive Flow (% Rated) JP 1&2	Drive Flow (% Rated) JP 3&4	M-Ratio JP1	M-Ratio JP2	M-Ratio JP3	M-Ratio JP4	Slip Joint DP (psi) JP1	Slip Joint DP (psi) JP2	Slip Joint DP (psi) JP3	Slip Joint DP (psi) JP4
AA1	69	0.10	0.12	Background noise - 450 psi - Press. Pump Off							
AA2	70	0.98	1.01	2.78	2.72	2.63	2.77	-3.5	-3.6	-4.1	-3.7
AA3	71	0.98	1.01	2.51	2.50	2.38	2.52	-1.7	-1.6	-1.4	-3.2
AA4	70	0.99	1.03	2.32	2.33	1.97	2.11	6.0	5.8	8.8	7.2
AA5	69	0.98	1.04	1.94	1.98	1.78	1.92	21.0	20.5	20.7	19.4
AA6	73	0.98	1.09	2.03	2.07	1.64	1.78	17.4	16.9	18.5	16.9
AA7	71	0.98	1.12	1.55	1.59	1.27	1.41	36.5	35.9	35.8	34.5
AA8	70	0.96	0.99	1.22	1.24	1.20	1.34	48.9	48.5	48.2	47.3
AA9	69	0.99	0.99	1.69	1.73	1.64	1.80	32.4	31.8	32.5	31.2
AA0	68	0.99	0.99	M-ratio sweep : 2.7 - 1.3							
AB0	176	0.97	1.00	2.80	2.78	2.75	2.88	-3.5	-3.6	-4.1	-3.7
AB1	180	1.00	1.01	2.46	2.49	2.41	2.52	0.4	-0.2	0.7	-0.8
AB2	179	1.00	1.00	2.19	2.26	2.17	2.28	11.1	10.2	10.9	9.7
AB3	178	1.00	1.00	2.07	2.14	2.07	2.21	16.1	15.2	15.8	14.2
AB4	180	1.00	1.01	1.84	1.93	1.85	1.96	24.1	23.1	23.6	22.5
AB5	180	1.00	1.01	1.75	1.82	1.74	1.85	28.4	27.4	28.0	26.9
AB6	180	1.00	1.01	1.77	1.83	1.75	1.88	28.0	27.1	27.7	26.5
AB7	179	1.00	1.01	1.62	1.69	1.61	1.76	33.7	32.8	33.3	31.9
AB9	180	1.00	1.01	1.44	1.48	1.37	1.52	42.0	41.3	42.0	40.8
AC0	178	1.00	1.01	1.51	1.57	1.55	1.67	39.2	38.3	38.3	37.3
AC1	177	1.00	1.01	M-ratio sweep : 1.4 - 2.7							
AC2	176	1.23	1.23	2.19	2.28	2.16	2.17	17.0	15.2	17.2	17.1
AC3	176	1.25	1.25	Pump Trip							

APPENDIX B
DATA ACQUISITION PLAN

Table B-1

DATA ACQUISITION PLAN - PHASE I

EMR Channel No.	Sensor Name	Type	Model No.	Serial No.	Sensitivity (Units/ Volt)	Units
1	AREA1X	Accelerometer	EGA3-S125-500 GE7	18B7-4X	1.86 E7	g
2	AREA1Y		EGA3-S125-500 GE7	18B7-4Y	1.83 E3	
3	AREA1Z		EGA3-S125-500 GE7	18B7-4Z	1.74 E3	
4	ARMA1		EGA-S125H-200D GE9	21I7J-J4-13	1.99 E3	
5	ARMA2		EGA-S125H-200D GE9	21I7J-J6-12	1.96 E3	
6	ARMA3			15I7J-J2-11	2.02 E3	
7	ARMA4			15I7J-J8-5	1.98 E3	
8	ARMA5			16I7J-J4-4	2.07 E3	
9	ARMA6			23I7J-J2-3	1.97 E3	
10	ARMA7			16I7J-J11-2	2.06 E3	
11	ARDA1			18J7J-J1-1	2.01 E3	
12	ARDA3			0.6I7J-J4-26	2.09 E3	
13	ARDA4			28I7J-J5-24	1.97 E3	
14	ARTA1			26J7J-J1-22	2.00 E3	
15	ARDA2			28I7J-J18-28	1.96 E3	
16	ARTA2			15I7J-J3-30	2.07 E3	
17	AREP1	Pressure transducer	112M106	1803	2.14 E1	psi
18	AREP1			1805	2.15 E1	
19	ARMP1			1807	2.33 E1	
20	ARMP2			1840	2.26 E1	
21	ARMP3			1850	2.33 E1	
22	ARMP4			1832	2.35 E1	
23	ARMP5			1806	2.15 E1	
24	ARMP6			1811	2.22 E1	
25	ARMP7			1851	2.25 E1	
26	ARMP8			1834	2.11 E1	
27	ARMP9			1808	2.07 E1	
28	ARMP10			1810	2.07 E1	
29	ARMP11			1809	2.05 E1	
30	ARMP12			1835	2.28 E1	

Table B-1 (Continued)

EMR Channel No.	Sensor Name	Type	Model No.	Serial No.	Sensitivity (Units/ Volt)	Units
31	ARMP13	Pressure transducer	112M106	1827	2.33 E1	psi
32	ARMP14	↓	↓	1836	2.26 E1	↓
33	ARMP15			1852	2.14 E1	
34	ARMP16			1831	2.39 E1	
35	ARMP17			1829	2.22 E1	
36	ARMP18			1833	2.41 E1	
37	ARMP19			1853	2.19 E1	
38	ARMP20			18.41	2.09 E1	
39	ARMP21			18.38	2.38 E1	
40	ARMP22			1854	2.13 E1	
41	ARMP23			18.55	2.45 E1	
42	ARMP24			1830	2.25 E1	
43	ARDP1			1738	2.38 E1	
44	ARDP2			1739	2.28 E1	
45	ARDP3			1740	2.24 E1	
46	ARDP4			1741	2.09 E1	
47	ARDP5			1742	2.16 E1	
48	ARDP6			1743	2.58 E1	
49	ARDP7			1764	2.45 E1	
50	ARDP8			1765	2.25 E1	
51	ARDP9			1766	2.17 E1	
52	ARDP10			1767	2.14 E1	
53	ARDP11			1768	2.19 E1	
54	ARDP12			1769	2.04 E1	
55	ARTP1			1770	2.28 E1	
56	ARTP2			1771	2.40 E1	
57	ARTP3			1772	2.43 E1	
58	ARTP4	↓	↓	1773	2.34 E1	↓
59	ARTS3	Strain gage	MG238-09H-20	4229-1	4.21 E-1	in./in.
60	ARTS1	Strain gage	MG238-09H-20	4229-4	4.21 E-1	in./
61	BLMA1	Accelerometer	EGA-S125H-200D GE9	7J7K-J3-50	2.02 E3	g

Table B-1 (Continued)

EMR Channel No.	Sensor Name	Type	Model No.	Serial No.	Sensitivity (Units/ Volt)	Units
62	ARTS4	Strain gage	MG128-09H-20	4229-3	4.21 E-1	in./in.
63	BLMA2	Accelerometer	EGA-S125H-200D GE9	28I7K-39-48	2.00 E3	g
64	BLDA1	↓	EGA-S125H-200D GE9	16I7J-38-16	2.02 E3	↓
65	ARBA6	↓	EGA-S125-500 GE7	7L6C7-E13-13	2.13 E3	↓
66	ARBA7	↓	EGA-S125-500 GE7	7L6C7-E13-13	1.90 E3	↓
67	ARBA8	↓	EGA-S12S-500 GE7	8D7D-J1-1	2.00 E3	↓
68	ARBA1X	↓	EGA-S125-500 GE7	18B7-SX	2.00 E3	↓
69	ARABA1Y	↓	EGA-S125-500 GE7	7L6C7-E13-13	1.90 E3	↓
70	ARBA1Z	↓	EGA-S12S-500 GE7			↓
71	ARA1	↓	EGA-S125H-200D GE9	14I7J-J18-19	2.00 E3	↓
72	BRMA1	↓	EGA-S12%H-200D GE9	7J7K-J17-94	1.98 E3	↓
73	ARA3	↓	EGA-S125H-200D GE9	28I7J-J4-21	2.00 E3	↓
74	ARA4	↓	EGA-S125H-200D GE9	14I7J-J3-10	2.01 E3	↓
75	ARA5	↓	EGA-S125-500 GE7	7L6CZ-E2-2	2.12 E3	↓
76	BRMA2	↓	EGA-S125H-200D GE9	7J7K-J10-53	2.05 E3	↓
77	ARA7	↓	EGA-S125-500 GE7	7L6C7-E7-7	2.01 E3	↓
78	ARBA2	↓	EGA-S125H-200D GE9	18J7J-J2-7	1.84 E3	↓
79	ARBA3	↓	↓	14I7J-J5-6	1.90 E3	↓
80	ARBA4	↓	↓	7J7K-J8-58	2.01 E3	↓
81	ARBA5	↓	↓	16I7K-J3-56	2.00 E3	↓
82	ARP1	Pressure transducer	122M106	1774	2.22 E1	psi
83	ARP2	↓	↓	1775	2.16 E1	↓
84	ARP3	↓	↓	1776	2.08 E1	↓
85	ARP4	↓	↓	1777	2.13 E1	↓
86	ARP5	↓	↓	1778	2.60 E1	↓
87	ARP6	↓	↓	1779	2.40 E1	↓
88	ARP7	↓	↓	1780	2.21 E1	↓
89	ARP8	↓	↓	1781	2.22 E1	↓
90	ARS1	Strain gage	SG 128-01-30	4726-37	4.82 E-1	in./in.
91	ARS3	↓	↓	4726-39	4.82 E-1	↓
92	ARS4	↓	↓	4726-40	4.82 E-1	↓

Table B-1 (Continued)

EMR Channel No.	Sensor Name	Type	Model No.	Serial No.	Sensitivity (Units/ Volt)	Units
93	ARS2	Strain gage	SG128-01-30	4726-42	4.82 E-1	in./in.
94	ARABS17			4776-17	4.82 E-1	
95	ARBS23			4726-18	4.82 E-1	
96	ARBS19			4726-19	4.82 E-1	
97	ARBS21			4726-20	4.82 E-1	
98	ARBS31			4726-21	4.82 E-1	
99	ARBS25			4726-22	4.82 E-1	
100	ARBS29			4726-23	4.82 E-1	
101	ARBS27			4776-24	4.82 E-1	
102	ARBS1			4726-25	4.82 E-1	
103	ARBS7			4726-30	4.82 E-1	
104	ARBS3			4726-31	4.82 E-1	
105	ARBS5			4726-32	4.82 E-1	
106	ARBS15			4726-33	4.82 E-1	
				16I7J-J9-9		
107	BRDA1	Accelerometer	EGA-S125H-200D GE9	4726-34	2.02 E3	g
108	ARBS13	Strain gage	SG128-01-30	4726-35	4.82 E-1	in./in.
109	ARBS11		SG128-01-30	4726-36	4.82 E-1	
110	ARBS2		MG128-09H-20	4229-30	4.21 E-1	
111	ARBS8			4229-13	4.21 E-1	
112	ARBS4			4229-12	4.21 E-1	
113	ARBS6			4229-14	4.21 E-1	
114	ARBS16			4229-15	4.21 E-1	
115	ARBS10			4229-17	4.21 E-1	
116	ARBS14			4229-16	4.21 E-1	
117	ARBS12			4229-18	4.21 E-1	
118	ARBS18			4229-19	4.21 E-1	
119	ARBS24			4229-20	4.21 E-1	
120	ARBS20			4229-21	4.21 E-1	
121	ARBS22			4229-22	4.21 E-1	
122	ARBS32			4229-23	4.21 E-1	
123	ARBS26			4229-24	4.21 E-1	

Table B-1 (Continued)

EMR Channel No.	Sensor Name	Type	Model No.	Serial No.	Sensitivity (Units/ Volt)	Units
124	ARBS30	Strain gage	MG128-09H-20	4229-11	4.21 E-1	in./in
125	ARBS28	↓	↓	4229-25	4.21 E-1	↓
126	ARBS33			4229-7	4.21 E-1	
127	ARBS34			4229-26	4.21 E-1	
128		↓	↓			↓
129	ALEA1X	Accelerometer	EGA2-S125-500 GE7	18B7-1X	1.81 E3	g
130	ALEA1Y	↓	EGA2-S125-500 GE7	18B7-1Y	1.97 E3	↓
131	ALEA2		EGA-S125H-200D GE9	16I7J-J10-31	2.09 E3	
132	BLDA2		↓	21I7J-J7-17	1.99 E3	
133	ALMA1			28I7K-J1-41	1.94 E3	
134	ALMA3			16Ij&-J2-35	2.03 E3	
135	ALMA4			28I7J-J2-25	2.07 E3	
136	ALMA5			15I7J-J7-14	2.00 E3	
137	ALMA6			29I7J-J1-27	2.05 E3	
138	ALMA7			14I7J-J2-29	2.08 E3	
139	BRDAZ			14I73-J6-4	2.00 E3	
140	ALDA2			28I7J-J6-34	2.04 E3	
141	ALDA3			28I7J-J16-36	2.15 E3	
142	ALDA4			28I7J-J14-38	2.01 E3	
143	ALTA1			21I7J-J5-32	1.98 E3	
144	ALDA1		↓	26J75-32-23	2.08 E3	
145	ALTA4		EGA-S125H-200D GE9	7J7K-J14-60	2.08 E3	
146	SSPA1		EGA-S125-500 GE7	7L6C7-E9-9	2.10 E3	
147	SSPA2	↓	EGA-S125-500 GE7	7L6C7-E12-12	2.21 E3	↓
148	ALEP1	Pressure transducer	112M106	1799	2.39 E1	psi
149	ALEP2	↓	↓	1800	2.37 E1	↓
150	ALMP1			1802	2.19 E1	
151	ALDP1			1735	2.32 E1	
152	ALDP2			1736	2.30 E1	
153	ALDP3	↓	↓	1737	2.29 E1	↓
154	ALTS1	Strain gage	MG128-09H-20	4229-5	4.21 E-1	in./in.

Table B-1 (Continued)

EMR Channel No.	Sensor Name	Type	Model No.	Serial No.	Sensitivity (Units/ Volt)	Units
155	ALTS3	Strain gage	MG218-009H-20	4229-6	4.21 E-1	in./in
156	ALTS2	↓		4229-9	4.21 E-1	↓
157	ALTS4			4229-10	4.21 E-1	
158	BLEA1X	Accelerometer	EGAZ-S125-500 GE7	18B7-3X	1.95 E3	g
159	BLEA1Y	↓	EGA-S125-500 GE7	1887-3Y	2.07 E3	↓
160	BLEA2		EGA-S125H-200D GE9	7J7K-J2-47	2.01 E3	

Table B-2

DATA ACQUISITION PLAN - PHASE 2

EMR Channel No.	Sensor Name	Type	Model No.	Serial No.	Sensitivity (Units/ Volt)	Units
1	AREA1X	Accelerometer	EGA3-S125-500 GE7	18B7-4X	1.86 E3	g
2	AREA1Y		EGA3-S125-500 GE7	18B7-4Y	1.83 E3	
3	AREA1Z		EGA3-S125-500 GE7	18B7-4Z	1.74 E3	
4	ARMA1		EGA-S125H-200D GE9	21I7J-J4-13	1.99 E3	
5	ARMA2			21I7J-J6-12	1.96 E3	
6	ARMA3			15I7J-J2-11	2.02 E3	
7	ARMA4			15I7J-J8-5	1.98 E3	
8	ARMA5			16I7J-J4-4	2.07 E3	
9	ARMA6			23I7J-J2-3	1.97 E3	
10	ARMA7			16I7J-J11-2	2.06 E3	
11	ARDA1			18J7J-J1-1	2.01 E3	
12	ARDA3			16I7J-39-26	1.96 E3	
13	ARDA4			28I7J-35-24	2.09 E3	
14	ARDA1			26J7J-J1-22	1.97 E3	
15	ARDA2			28I7J-J18-28	2.00 E3	
16	ARTA2			15I7J-J3-30	2.07 E3	
17	AREP1	Pressure transducer	112M106	1803	2.19 E1	psi
18	AREP2			1805	2.15 E1	
19	ARMP1			1807	2.33 E1	
20	ARMP2			1840	2.26 E1	
21	ARMP3			1850	2.33 E1	
22	ARMP4			1832	2.35 E1	
23	ARMP5			1806	2.15 E1	
24	ARMP6			1811	2.22 E1	
25	ARMP7			1851	2.25 E1	
26	ARMP8			1834	2.11 E1	
27	ARMP9			1808	2.07 E1	
28	ARMP10			1810	2.07 E1	
29	ARMP11			1809	2.05 E1	

Table B-2 (Continued)

EMR Channel No.	Sensor Name	Type	Model No.	Serial No.	Sensitivity (Units/ Volt)	Units
30	ARMP12			1835	2.28 E1	
31	ARMP13	Pressure				
		transducer	112M106	1837	2.33 E1	psi
32	ARMP14			1836	2.26 E1	
33	ARMP15			1852	2.14 E1	
34	ARMP16			1831	2.39 E1	
35	ARMP17			1839	2.22 E1	
36	ARMP18			1833	2.41 E1	
37	ARMP19			1853	2.19 E1	
38	ARMP20			18.41	2.09 E1	
39	ARMP21			18.38	2.38 E1	
40	ARMP22			1854	2.13 E1	
41	ARMP23			18.55	2.45 E1	
42	ARMP24			1830	2.25 E1	
43	ARDP1			1738	2.38 E1	
44	ARDP2			1739	2.28 E1	
45	ARDP3			1740	2.24 E1	
46	ARDP4			1741	2.09 E1	
47	ARDP5			1742	2.16 E1	
48	ARDP6			1743	2.58 E1	
49	ARDP7			1764	2.45 E1	
50	ARDP8			1765	2.25 E1	
51	ARDP9			1766	2.17 E1	
52	ARDP10			1767	2.14 E1	
53	ARDP11			1768	2.19 E1	
54	ARDP12			1769	2.04 E1	
55	ARTP1			1770	2.28 E1	
56	ARTP2			1771	2.40 E1	
57	ARTP3			1772	2.43 E1	
58	ARTP4			1773	2.34 E1	
59	ARTS1&3	Strain gage	MG128-09H-20	4229-1	4.21 E-1	in./in.
60	ARTS2	Strain gage	MG128-09H-20	4229-4	4.21 E-1	in./in.

Table B-2 (Continued)

EMR Channel No.	Sensor Name	Type	Model No.	Serial No.	Sensitivity (Units/ Volt)	Units
61						
62						
63						
64						
65	BLEA1X	Accelerometer	EGA2-S125-500 GE7	1887-3X	1.95 E3	g
66	BLEA1Y		EGA2-S125-500 GE7	1887-3Y	2.07 E3	
67	BLEA2		EGA-S125H-200D GE9	7J7K-J2-47	2.01 E3	
68	BLMA1			7J7K-J3-50	2.00 E3	
69	BLMA2			28I7K-J9-483	2.00 E3	
70	BLDA1			16I7I-J8-16	2.02 E3	
71	BLDA2			21I7J-J7-199	1.99 E3	
72	BLMP1	Pressure transducer	112M106	1782	2.08 E1	psi
73	BLMP2			1783	2.28 E1	
74	BLMP3			1784	2.20 E1	
75	BLMP4			1785	2.48 E1	
76	BLMP5			1786	2.34 E1	
77	BLMP6			1795	2.16 E1	
78	ARBA2			1796	2.11 E1	
79	BLMP8			1797	2.19 E1	
80	BLMP9			1798	2.23 E1	
81	BLOP1			1701	2.27 E1	
82	BLOP2			1702	2.24 E1	
83	BLOP3			1699	2.13 E1	
84	BLDP4			1727	2.09 E1	
85	BLDP5			1728	2.23 E1	
86	BLDP6			1729	2.36 E1	
87	BLDP7			1730	2.11 E1	
88	BLDP8			1731	2.14 E1	
89	BLDP9			1732	2.14 E1	
90	BLDP10			1734	2.34 E1	
91	BLDP11			1734	2.37 E1	

Table B-2 (Continued)

EMR Channel No.	Sensor Name	Type	Model No.	Serial No.	Sensitivity (Units/ Volt)	Units
92	BLTS1&3	in./in.	SG128-01-30	4726-5&8	2.41 E-1	in./in.
93	BLTS2&4	in./in.	SG128-01-30	4726-6&7	2.41 E-1	in./in.
94	BREA1X	Accelerometer	EGA2-S125-500 GE7	18B7-2X	2.12 E3	g
95	BREA1Y	↓	EGA2-S125-500 GE7	18B7-24	1.88 E3	↓
96	BREA2	↓	EGA-S125H-200D GE7	7J7K-J16-57	2.03 E3	↓
97	BRMA1	↓	↓	7J7K-J17-44	1.98 E3	↓
98	BRMA2	↓	↓	7J7K-J10-53	2.05 E3	↓
99	BRMA3	↓	↓	7J7K-J6-46	1.98 E3	↓
100	BRDA1	↓	↓	16I7J-J9-9	2.03 E3	↓
101	BRDA27	↓	↓	14I7J-J6-2	2.00 E3	↓
102	BRTS1&2	Strain gage	SG128-01-30	4726-1&3	2.41 E-1	in./in
103	BRTS2&4	↓	↓	4726-2&4	4.82 E-1	↓
104	BRBS6&8	↓	↓	4726-9&14	2.41 E-1	↓
105	BRBS 10&12	↓	↓	4726-29&27	2.41 E-1	↓
106	BARBA1	Accelerometer	EGA-S125H-200D GE7	17I75-J4-18	1.98 E3	g
107	BRBA2	↓	EGA-S125H-200D GE7	14I7J-J4-15	2.05 E3	↓
108	BRBA3	↓	ED1005	BBN-002	1.04 E2	↓
109	ARP1	Pressure transducer	112M106	1774-36	2.22 E1	psi
110	ARP22	↓	↓	1775-30	2.16 E1	↓
111	ARBS8	↓	↓	1776-13	2.08 E1	↓
112	ARP4	↓	↓	1777-12	2.13 E1	↓
113	ARP56	↓	↓	1778-14	2.60 E1	↓
114	ARP616	↓	↓	1779-15	2.40 E1	↓
115	ARP710	↓	↓	1780-17	2.21 E1	↓
116	ARP814	↓	↓	1781-16	2.22 E1	↓
117	ARBS2&8	Strain gage	MG128-09H-20	4229-30&13	2.22 E-1	in./in.
118	ARBS 16&10	↓	↓	4229-19&20	2.11 E-1	↓

Table B-2 (Continued)

EMR Channel No.	Sensor Name	Type	Model No.	Serial No.	Sensitivity (Units/ Volt)	Units
119	ARBS 18&24			4229-19&20	4.21 E-1	in./in
120	ARBS 26&32	Strain gage	MG128-09H-20	4229-24&23	2.41 E-1	
121	ARBS1&3		SG128-01-30	4726-37&39	2.41 E-1	
122	ARS2&4		SG128-01-30	4726-42&40	2.41 E-1	
123						
124						
125						
126						
127						
128						
129	ALEA1X	Accelerometer	EGA2-S125-500 GE7	18B7-1X	1.81 E3	g
130	ALEA1Y		EGA2-S125-500 GE7	18B7-1Y	1.97 E3	
131	ALEA2		EGA-S125H-200D GE9	16I7J-J10-31	2.09 E3	
132	ALMA2			16I7J-J7-37	2.04 E3	
133	ALMA1			28I7K-J1-41	1.93 E3	
134	ALMA3			16I7J-J2-35	2.03 E3	
135	ALMA4			28I7J-J2-25	2.07 E3	
136	ALMA5			15I7J-J7-14	2.00 E3	
137	ALMA6			29I7J-J1-27	2.05 E3	
138	ALMA7			14I7J-J2-29	2.08 E3	
139						
140	ALDA2			28I7J-J6-34	2.04 E3	
141	ALDA3			28I7J-J16-36	2.15 E3	
142	ALDA4			28I7J-J14-38	2.01 E3	
143	ALTA1			28I7J-J8-32	1.98 E3	
144	ALDA1			26J75-J2-23	1.88 E3	
145	ALJA4		EGA-S125H-200D GE9	7J7K-J14-60	2.08 E3	
146	SSPA1		EGA-S125-500 GE7	7L6C7-E9-9	2.10 E3	
147	SSPA2		EGA-S125-500 GE7	7L6C7-E12-12	2.21 E3	

Table B-2 (Continued)

EMR Channel No.	Sensor Name	Type	Model No.	Serial No.	Sensitivity (Units/ Volt)	Units
148	ALEP1	Pressure transducer	112M106	1799	2.39 E1	psi
149	ALEP2	↓		1800	2.37 E1	↓
150	ALMP1		112M106	1802	2.19 E1	
151	ALDP1		↓	1735	2.32 E1	
152	ALDP2			1736	2.30 E1	
153	ALDP3	↓		1737	2.29 E1	
154	ALTS3&1	Strain gage	MG128-09H-20	4229-6&5	2.11 E-1	in./in.
155	ALTS4&2	Strain gage	MG128-09H-20	4229-10&9	2.21 E-1	in./in.
156						
157						
158						
159						
160						